AUSTRALIA

Report 286

Rig Seismic research cruises 10 & 11: geology of the Central Great Australian Bight region

J.B. Wilcox, H.M.J. Stagg, H.L. Davies & others

Bureau of Mineral Resources, Geology & Geophysics

Department of Primary Industries and Energy
BUREAU OF MINERAL RESOURCES, GEOLOGY & GEOPHYSICS

REPORT 286

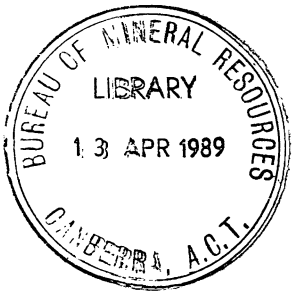

RIG SEISMIC RESEARCH CRUISES 10 & 11:

GEOLOGY OF THE CENTRAL GREAT AUSTRALIAN BIGHT REGION

Principal Investigators:
J.B. Willcox, H.M.J. Stagg, & H.L. Davies

Division of Marine Geosciences & Petroleum Geology

Scientific Staff (Leg 1):
B. Willcox, H. Stagg, H. Davies, P. Hill, N. Johnston, Liu Zhong-chen,

Technical Support Staff (Leg 1):
J. Bedford, R. Curtis-Nuthall, P. Harris, B. Jones, J. Kossatz, C. Lawson, B. Maplestone, I. Roach, G. Saunders, P. Walker

Scientific Staff (Leg 2):
H. Davies, H. Stagg, C. Conor, D. Choi, J. Clarke, T. Graham, P. Haines, M. Joshima, M. Walton

Technical Support Staff (Leg 2):
N. Clarke, D. Holdway, J. Kossatz, R. McMahon, L. Miller, M. O'Connor, D. Pryce, K. Revill, J. Stuart, R. Schuler

AUSTRALIAN GOVERNMENT PUBLISHING SERVICE
CANBERRA, 1988

DEPARTMENT OF PRIMARY INDUSTRIES & ENERGY
Minister: Senator the Hon. Peter Cook
Secretary: G.M. Miller

BUREAU OF MINERAL RESOURCES, GEOLOGY & GEOPHYSICS
Director: R.W.R. Rutland

Published for the Bureau of Mineral Resources, Geology and Geophysics
by the Australian Government Publishing Service

ISBN 0 644 08719 6
ISSN 0084-7100

Edited by H.L. Davies
Figures by Divisional cartographic unit
Word processing by H.M.J. Stagg

Printed in Australia by Watson Ferguson and Co., Brisbane

CONTENTS

TABLES

FIGURE CAPTIONS

ABSTRACT

The 10th and 11th cruises of the research vessel *Rig Seismic*, BMR Surveys 65 and 66, gathered geophysical and geological data in the region of the Eyre and Ceduna Terraces in the Great Australian Bight. The region was selected for study because it provides the best opportunity to test new concepts of margin and basin development on the southern margin of Australia, and because most of the margin has been previously subject to only reconnaissance investigation. In an interval of eight weeks in October-December 1986 we collected more than 12500 km line km of geophysical data, including 3500 line km of multichannel seismic reflection data, principally over the Great Australian Bight Basin, Eyre Sub-basin, and Polda Trough, made 11 heatflow determinations, and collected 14 dredge hauls and 20 cores.

The magnetic data confirm that Late Cretaceous spreading between Australia and Antarctica was directed N-S. However, there is tentative evidence in the seismic data of NW-SE strike-slip faulting in the Cretaceous, beneath the outer margin of the Ceduna Terrace, suggesting that the early continental extension direction may have been in a NW-SE direction.

The Eyre Sub-basin is bounded to the south by a ridge of Precambrian basement which, from the geometry of rotated fault blocks within the basin, probably rests upon a S-dipping primary detachment surface. This basement ridge is at least partly composed of sheared granite, as shown by dredging. The southern flank of the basement ridge, in turn, is a 30 degree S-dipping detachment surface upon which rest rotated blocks of sedimentary rock beneath the continental rise. Sediments in this 'rise basin', south of the Eyre Sub-basin, are 4-6 km thick, and are probably Cretaceous and Tertiary (from tentative correlation with the Otway Basin). They comprise at least nine unconformable seismic sequences, some of which clearly prograde southward.

Sediments beneath the Ceduna Terrace include a thick prograded sequence characterized by large-scale foreset beds. This unit probably is bounded by Cenomanian and Maastrichtian unconformities (Tilbury & Fraser, 1979), and thus provides a datum for interpretation of seismic stratigraphy. The thick sediments of the Ceduna Terrace extend as much as 15 km landward of the shelf break in at least one location and are thus accessible to shelf-depth offshore drilling.

Heatflow values on the Ceduna Terrace are higher than the worldwide average, at around 75 mW/m2, and include some anomalously high values which may be related to ?Tertiary volcanism. Probable intrusive and volcanic rocks are apparent in seismic profiles, and sodic phonotephrite lava (undersaturated alkali basalt) was encountered in two dredge hauls. Dredged sediments indicate marginal marine terrigenous sedimentation from Late Cretaceous through to Early Eocene, and pelagic carbonate sedimentation (limestone and nanno and foram ooze) from Middle Eocene onwards. The youngest sediments dredged were Late Miocene nanno and foram ooze and red-brown mudstone. Cores from the shelf and terraces are mostly pelagic ooze, but those from submarine canyons show an earlier phase of vigorous sediment transport.

INTRODUCTION

The continental shelf of the southern margin of the Australian continent is broadest in the Great Australian Bight (as much as 200 km in width), and narrows to about 25 km width to the east and the west. The generally arcuate outline of the continental slope is broken by a major terrace (Ceduna Terrace) and two minor terraces (Eyre and Beachport Terraces).

The margin includes two major sedimentary basins (the Great Australian Bight and Otway Basins; Figure 1) and a number of sub-basins. Exploration effort has culminated in the drilling of 14 offshore wells in the Otway Basin, four wells in the Duntroon Embayment (or Basin), two wells in the Polda Trough, and one well in each of the Great Australian Bight Basin and Eyre Sub-basin. Only five wells - Potoroo-1, Jerboa-1, Apollo-1, Mercury-1, and Gemini-1 - have been drilled along the 1300 km of margin between the Duntroon Embayment and Cape Leeuwin. In addition, little or no bottom sampling, either by coring of soft sediments or dredging of submarine outcrops, has been attempted in this region. Regional structure has been determined by seismic surveys of moderate quality but modern seismic reflection methods have been applied only to restricted areas, principally on the central Eyre and Ceduna Terraces, and across the Polda Trough.

Given the considerable thickness (up to 12 km) of sediment in the Great Australian Bight Basin (GAB Basin), the patchy distribution of existing high-quality seismic data, and the paucity of geological data, the basin presents an obvious target for a framework geological-geophysical study.

Apart from the considerations noted above, the structure and prospectivity of this part of the margin warrants re-evaluation in the light of new concepts of margin breakup history, notably

1. that the separation of Antarctica from Australia was not a simple Palaeogene event, but started with an interval of slow spreading in the mid-Cretaceous (Cande & Mutter, 1982; Veevers, 1986); and

2. that separation was not initially north-south, and was not simultaneous at all points along the margin (in-house unpublished data).

These concepts are discussed later in this report.

The Eyre Terrace-Ceduna Terrace sector of the GAB Basin was selected as the focus of the proposed investigation primarily because it is the sector most likely to provide key data on the tectonic evolution of the region, while offering a sedimentary section comparable with most other parts of the GAB Basin. A study of the Polda Trough was added to the program because of a need to test a newly-installed airgun array in an area close to the port of Ceduna.

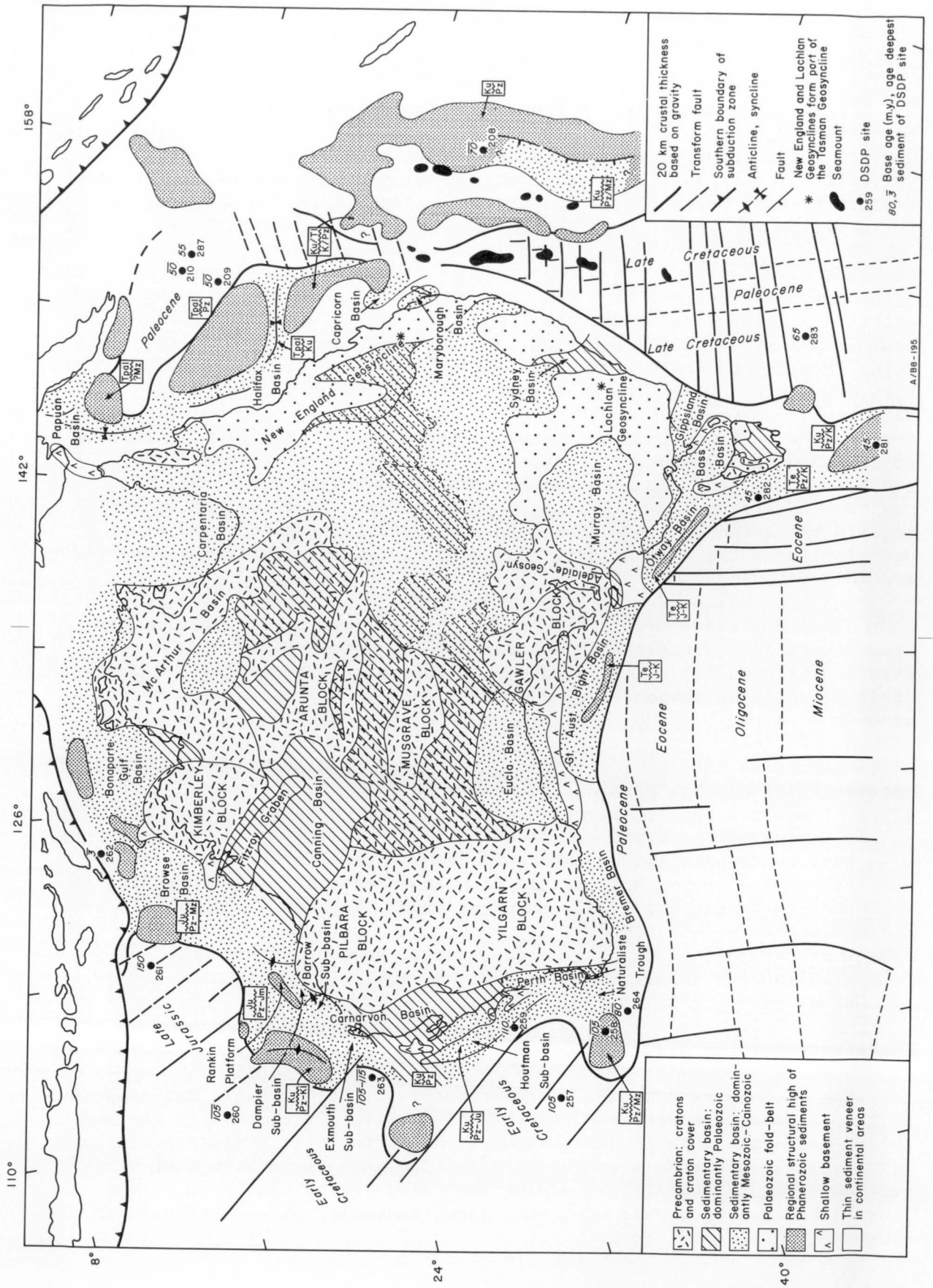

Figure 1: Structural elements in and around Australia (after Willcox, 1981), showing the location of the sedimentary basins along the southern margin. Note that the age of the oceanic crust adjacent to the southern margin has been revised to Late Cretaceous.

ACKNOWLEDGEMENTS

The success of the two Southern Margin cruises is due in no small part to the skill and professionalism of Dave Harvey, Master of the *Rig Seismic*, and his crew, who gave every assistance possible to the scientific crew (Appendix A). We also wish to acknowledge the prompt assistance given by Geophysical Service International (GSI) during the early stages of the first cruise when gun array teething problems plagued the program and, in particular, the assistance given by Mr Ken Bakewell, senior GSI gun mechanic.

GEOLOGICAL BACKGROUND

PREVIOUS STUDIES

Regional studies of the southern margin include those by Boeuf & Doust (1975), Deighton & others (1976), and Willcox (1978). Willcox (1981), in his review of the petroleum prospectivity of the marginal plateaus of Australia, also looked at selected parts of the southern margin. A number of authors have examined the crustal structure of the margin in varying degrees of detail, notably Konig and Talwani (1977), Mutter (1978), Talwani & others (1979), and Konig (1980). On a more restricted geographical basis, Whyte (1978), Fraser & Tilbury (1979), and Tilbury & Fraser (1981) have studied the Ceduna Terrace, while Bein & Taylor (1981) have studied the Eyre Terrace, and Nelson & others (1986) have reviewed the Polda Trough. The history of sea-floor spreading between Australia and Antarctica was initially studied by Weissel & Hayes (1972) with a subsequent major revision by Cande & Mutter (1982) that was further refined by Veevers (1986).

BATHYMETRY

The bathymetry of the great Australian Bight region has been described by Conolly & Von der Borch (1967), Conolly & others (1970), and Willcox (1978), while a detailed bathymetry map of the Ceduna Terrace was compiled by Tilbury & Fraser (1981). In this section, we summarise the findings of the latter two of these reports with reference to the bathymetry map in Figure 2.

Continental Shelf

The continental shelf is almost featureless, forming a gently sloping plain out to the shelf break at about 125-165 m depth. Minor changes in slope also occur at about 25 and 90 m depth. In the west of the GAB, near Esperance, the shelf is about 60 km wide, and the seabed falls away sharply below the shelf edge. Between the Archipelago of the Recherche and the Eyre Peninsula, the shelf forms a large arcuate plain with a maximum width of 300 km to the east of Eucla. Farther eastwards, the width of the shelf varies from 50 to 200 km, while in the extreme southeast it narrows to about 20 km. The shelf on the eastern side of the GAB has been extensively modified by the Pleistocene outlets of the Murray River.

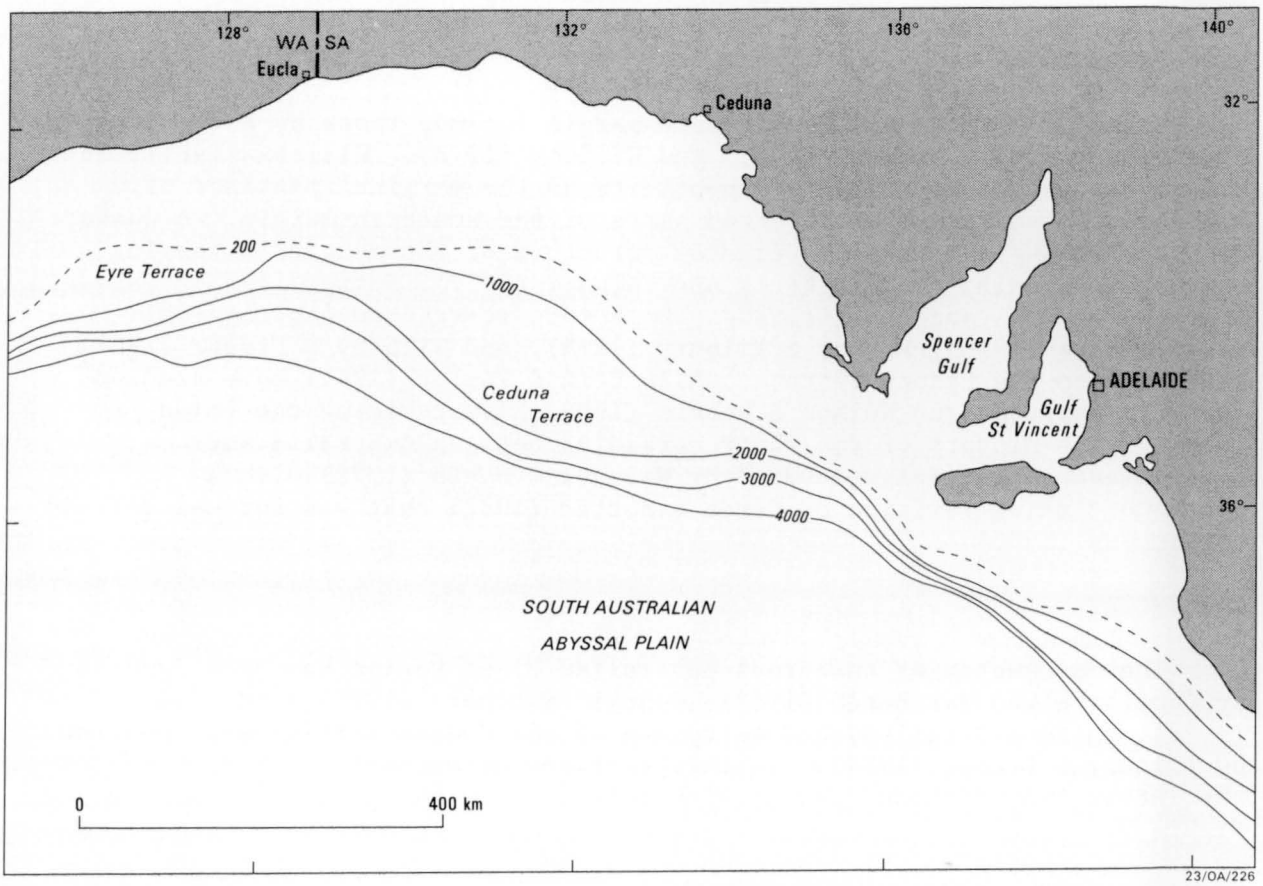

Figure 2: Bathymetry of the Great Australian Bight region, showing the principal bathymetric features; simple conic projection; contours in metres.

Continental Slope and Marginal Terraces

The continental slope is highly variable in width and gradient and is broken by several terraces. In the west, gradients are up to 6 degrees. Inflections in the contours plotted by Willcox (1978) suggests canyon development perpendicular to the slope, although individual canyons are poorly defined due to the sparsity of lines parallel to the slope. The base of the slope in the west is at about 3600 m.

The major part of the slope between Eyre and Ceduna is occupied by the Eyre and Ceduna Terraces. Offshore from Eyre, the continental slope dips at about 2 degrees south-southeastwards from the shelf edge at about 200 m. At 400 m depth, it flattens out to about 1 degree to form the Eyre Terrace, an oval feature about 60 km wide and 300 km long. The outer limit of the terrace lies at about the 1600 m isobath. Below the outer margin, the slope steepens to 5 degrees and merges with the rise at about 3500 m. The southeasterly-trending Eyre canyon extends from near the middle of the terrace onto the continental slope along its southern edge. The Eucla canyon has cut several hundred meters into the continental slope at about 129 E, at the junction of the Eyre and Ceduna Terraces.

The Ceduna Terrace is a sigmoidal-shaped feature, some 70000 km2 in area, up to 130 km in width and 600 km in length. It is bounded to the north by an upper slope between the shelf break at 150-200 m and the 500 m isobath, and to the south by a lower slope between the 2500 and 4000 m isobaths. The surface of the terrace slopes gently to the southwest with an average gradient of 0.6 degree, compared with an average of 2 degrees for the continental slope. The lower slope merges with the continental rise at about 4000 m.

The most striking features of the bathymetry of the Ceduna terrace are the numerous submarine valleys which dissect its surface (Tilbury & Fraser, 1981). They are mostly broad and shallow and form a dendritic tributary system feeding steeper walled canyons on the lower slope. The valleys originate on the upper slope as small channels; these coalesce to form valleys 5-10 km wide in the upper part of the terrace; these in turn converge on the lower part of the terrace to form valleys about 20 km wide, that eventually feed the canyons of the lower slope.

To the east of the Ceduna Terrace, the continental slope off Kangaroo Island is similar to that on the western side of the GAB, having gradients of up to 8 degrees, and showing extensive canyon development. The slope here extends down to about 4600 m. It is deeply incised by the numerous channels of the Murray River system of canyons, and Von der Borch and others (1970) have recorded the depth of the main canyon as about 1800 m below the adjecent seabed. Many canyons in this area are almost parallel to the slope, deepening westwards.

Continental Rise and Abyssal Plain

The continental rise is composed of a smooth apron of sediments lying between the continental slope and the abyssal plain. The upper boundary of the rise progressively deepens eastwards, from about 3000 m off Esperance to as much as 5000 m in the extreme southeast. South of the Eyre Terrace, the rise is abnormally broad, in excess of 200 km, with a gradient of about 0.5 degree. By contrast, south of the Ceduna terrace, the rise is only

about 50 km wide.

The South Australian Abyssal Plain, in excess of 5500 m deep, is a relatively small area of smooth level ocean floor occupying the area between the rise, the Diamantine Zone, and the rugged northern flank of the Southeast Indian Ridge.

SPREADING HISTORY

While the southern margin of Australia has been recognised as a type area for studying the development of rifted continental margins (Sproll & Dietz, 1969), it has become apparent in recent years that the spreading history of this part of the Southern Ocean is far more complex than first thought.

Magnetic lineations in the Southern Ocean were first identified and mapped by Weissel & Hayes (1972) on the basis of data recorded by the *Eltanin*. Weissel & Hayes concluded that the oldest magnetic anomaly that could be identified was anomaly 22 (Fig. 3), and that breakup between Australia and Antarctica occurred at about 55 Ma in the Early Eocene. In addition to the basic lineation pattern, Weissel & Hayes also identified several large-scale anomalous magnetic or morphologic features that have always been difficult to explain. These features include -

1. The Australia-Antarctic Discordance, a region of subdued yet confused magnetic anomalies and deeper than expected crust astride the Southeast Indian Ridge south of the GAB (see also Weissel & Hayes, 1974, and Vogt & others, 1983).

2. The Diamantina Zone, a latitudinal band of very rough topography south of southwest Australia. The Diamantina Zone is most pronounced west of 125 E, while to the east it gradually becomes buried by sediments. The eastward extent of the Diamantina Zone is ill-defined.

3. A broad Magnetic Quiet Zone (MQZ) along the southern margin of Australia extending from the west of the continent (where it is relatively disturbed) to the eastern side of the GAB where it encompasses the oldest magnetic anomalies. The crust beneath the MQZ has variously been interpreted as continental (Falvey, 1974; Boeuf & Doust, 1975; Deighton & others, 1976) or as a hybrid "rift-valley" crust (Talwani & others, 1979).

In a major re-interpretation of the oldest part of the magnetic anomaly series, Cande & Mutter (1982) suggested that the anomalies originally identified as 19-22 could be better modelled as anomalies 20-34, with spreading during this period being at a very slow rate (~0.45 cm/yr). Cande & Mutter estimated breakup of Antarctica and Australia at some time in the interval 110-90 Ma. This revised identification, which is now broadly accepted, accounts for the roughness of the Diamantina Zone (attributed to slow spreading), the previous difficulties in identifying the older magnetic anomalies, and the period of rapid basin subsidence prior to 90 Ma on the southern margin of Australia (Falvey & Mutter, 1981).

More recently, Veevers (1986) has refined the estimate of breakup age to 95 +/-5 Ma (Cenomanian-Turonian) by proposing that Cande & Mutter's

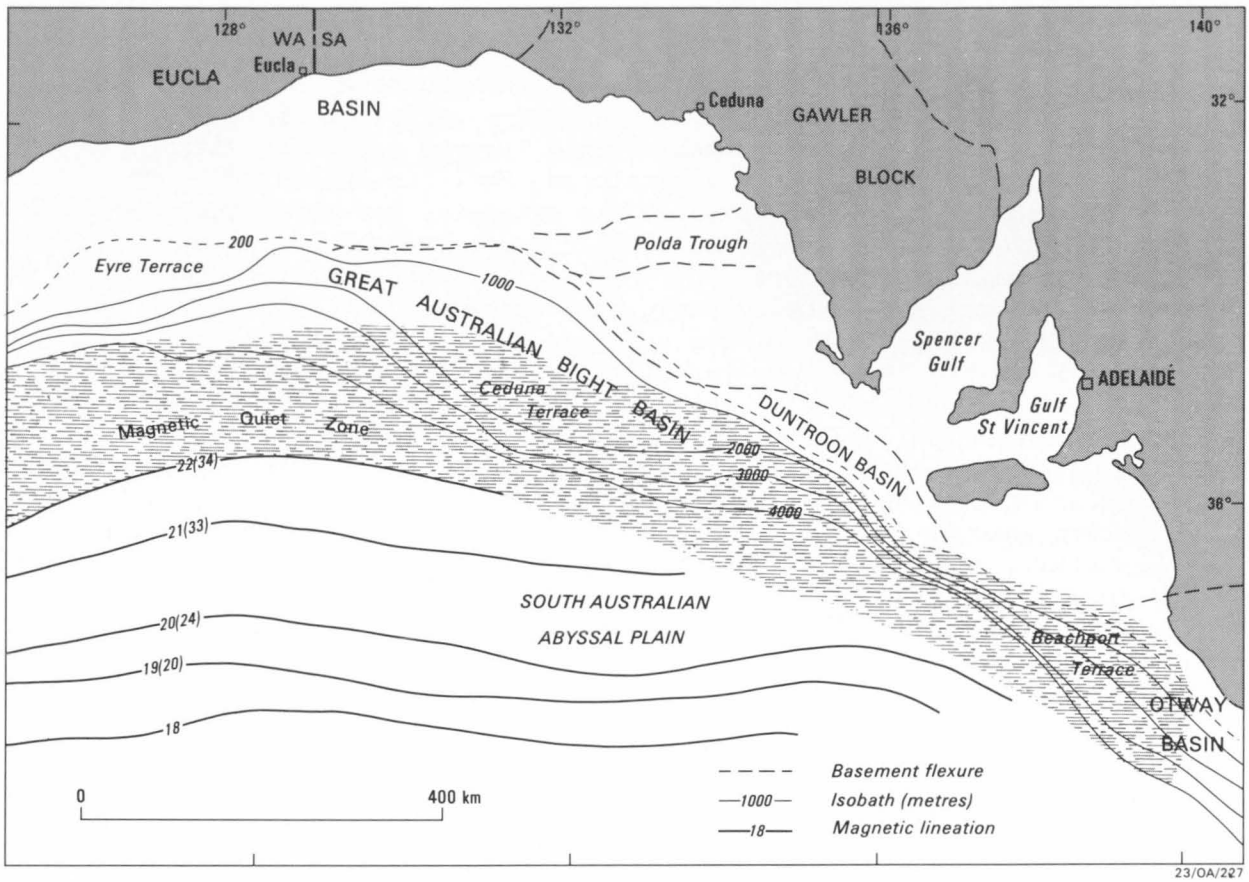

Figure 3: Structural elements of the southern margin (after Fraser & Tilbury, 1979). Original magnetic lineation identifications and revised identifications (in parentheses) are shown.

anomaly 34 is in fact the continent-ocean boundary (COB) edge-effect anomaly and by extrapolating the 0.45 cm/yr spreading rate.

All reconstructions of the southern margin regional and local geology and evolution published prior to 1981 now need to be reviewed and revised in light of the now generally accepted Cenomanian-Turonian breakup age.

STRUCTURE

The geology of the southern margin is dominated by three sedimentary basins of varying importance - namely the Bremer Basin south of the Yilgarn Block, the GAB Basin with the associated Eyre Sub-basin, Polda Trough, and Duntroon Embayment, and the Otway Basin on the eastern flank of the GAB adjacent to Bass Strait (Fig. 1).

Formation of a major rift valley along the southern margin probably began in the Jurassic with the development of a series of isolated rift grabens, of which the Polda and Robe-Penola Troughs may be surviving examples (Willcox, 1981). Late Jurassic and Early Cretaceous block-faulting led to the formation of an extensive and more continuous rift valley that extended from the western margin of the Australia-Antarctic proto-continent, parallel to the present southern margin as far east as the Otway Basin. Development of this rift valley probably allowed the influx of the sea from the young Indian Ocean (Deighton & others, 1976). Mutter (1978) has suggested that the margins of the rift valley were controlled by major boundary faults that extend to the deep crust and which appear to have remained fixed during the rifting process. Deposition within the rift valley continued through the Late Jurassic and Cretaceous; variations in the amount of influx along the valley axis account for the present distribution of the basins. Fraser & Tilbury (1979) suggest that deposition was probably predominantly continental at this time with some marine influences, as recorded at Potoroo-1; these marine influences may have been more pronounced nearer the axis of the rift valley.

Fraser and Tilbury (1979) further proposed that deposition on the Ceduna Terrace was interrupted by two phases of uplift and erosion - one at the end of the Early Cretaceous and the other in the early Tertiary; however, they saw little evidence for the earlier unconformity in the deeper parts of the GAB Basin. In line with the prevailing interpretation of breakup in the Palaeocene/Eocene, they interpreted the resultant unconformities as an intra-rift event and breakup. In light of Cande & Mutter's (1982) revision of the breakup age, it appears that the Early Cretaceous event probably coincides with breakup, while the Early Tertiary unconformity is perhaps due to a eustatic sea-level change as Cande and Mutter suggest. To the west, on the Eyre Terrace, data from Jerboa-1 (Bein & Taylor, 1981; Figs 4 & 5) show a hiatus from the end of the Cenomanian (~95 Ma) until the Early Eocene (~50 Ma) - that is, the two erosional events appear as one. The seismic data presented by Bein & Taylor suggest that this major hiatus may extend over much of the Eyre Sub-basin (Figs 6 & 7).

In the remainder of this section we outline the structure of the southern margin basins, concentrating on the less well known Bremer and GAB Basins and the Polda Trough.

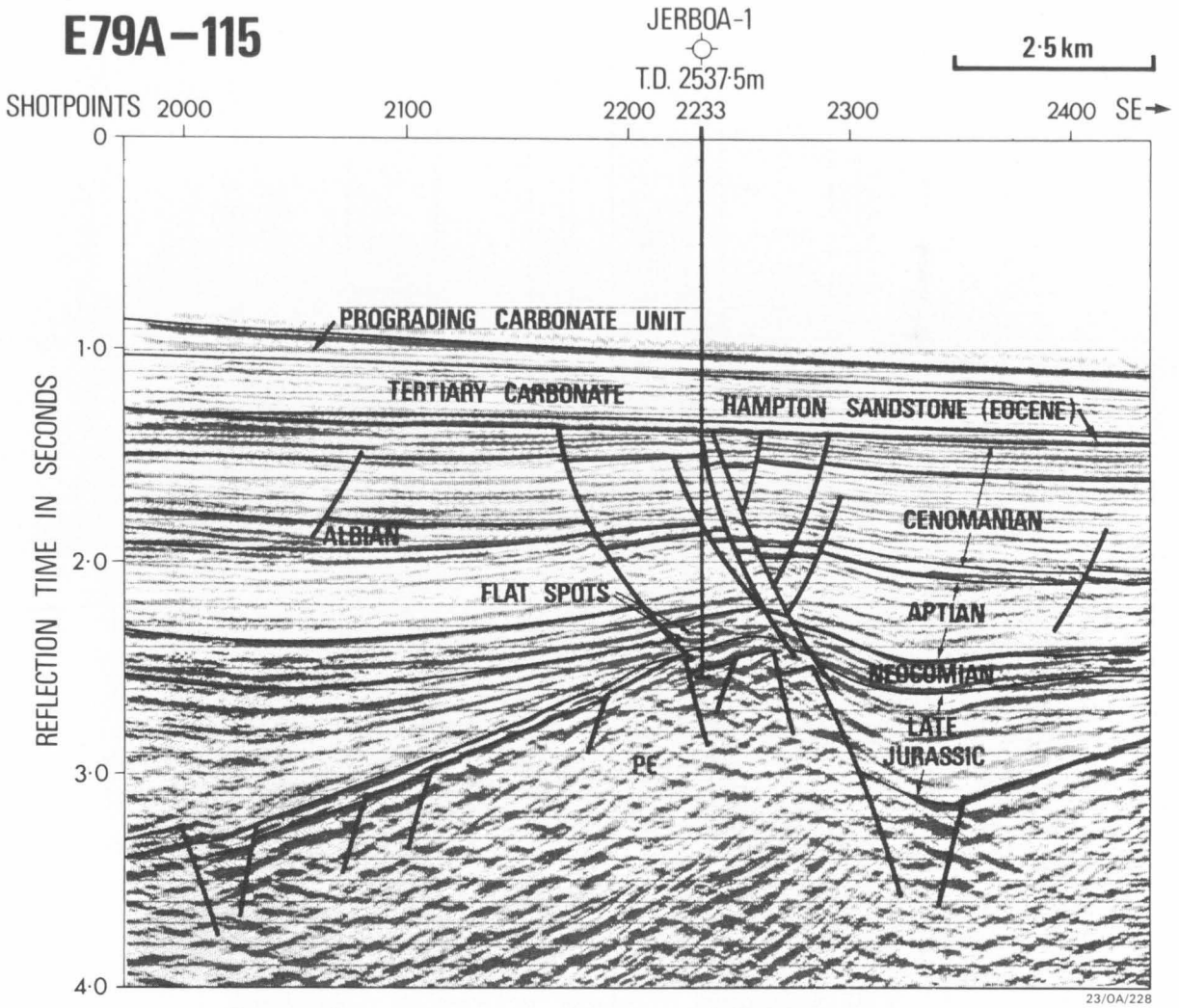

Figure 4: Seismic profile through Jerboa-1 (after Bein & Taylor, 1981).

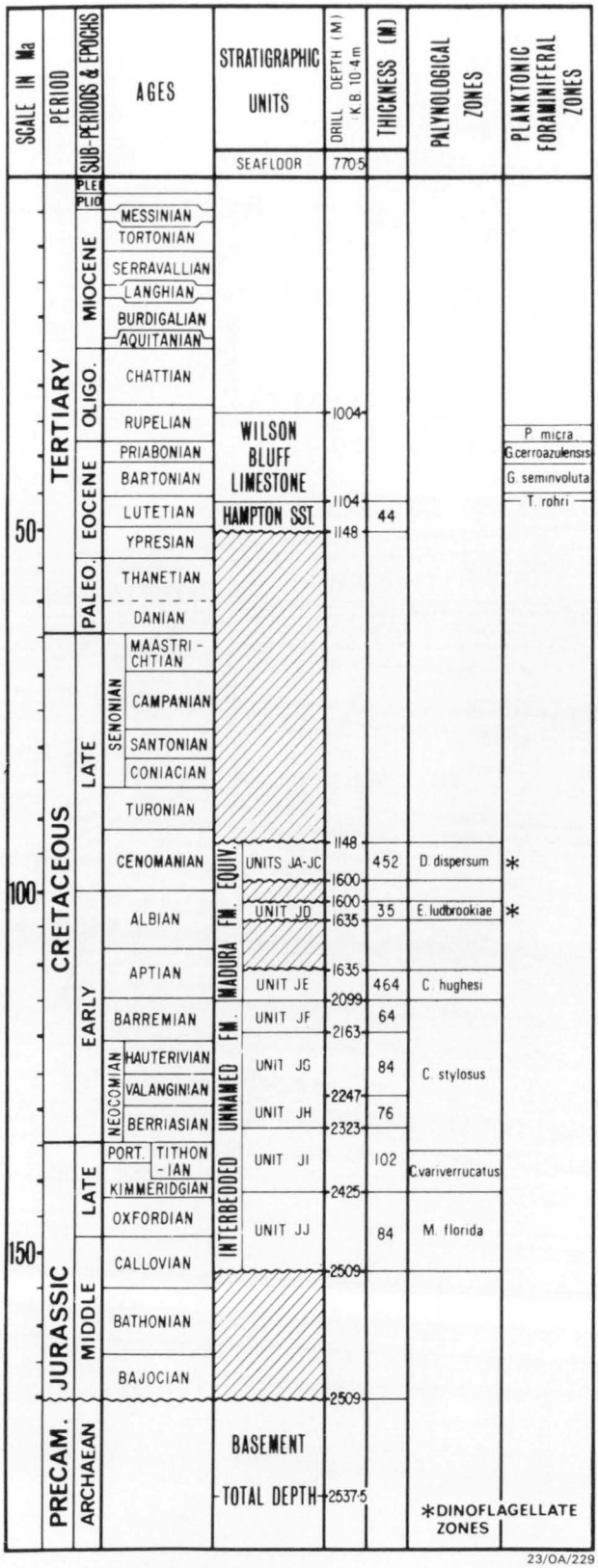

Figure 5: Stratigraphic chart for Jerboa-1 (after Bein & Taylor, 1981).

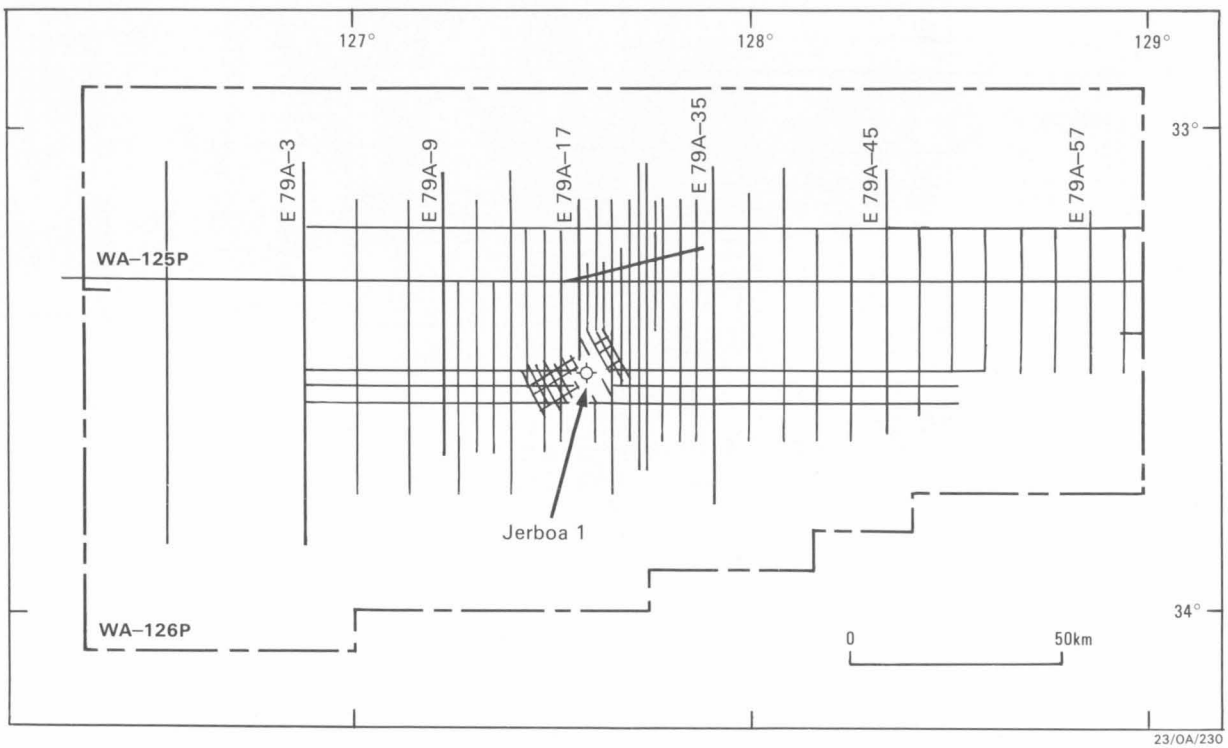

Figure 6: Esso-Hematite tracks in permits WA-125P and WA-126P in the Eyre Sub-basin, and location of Jerboa-1 (after Bein & Taylor, 1981).

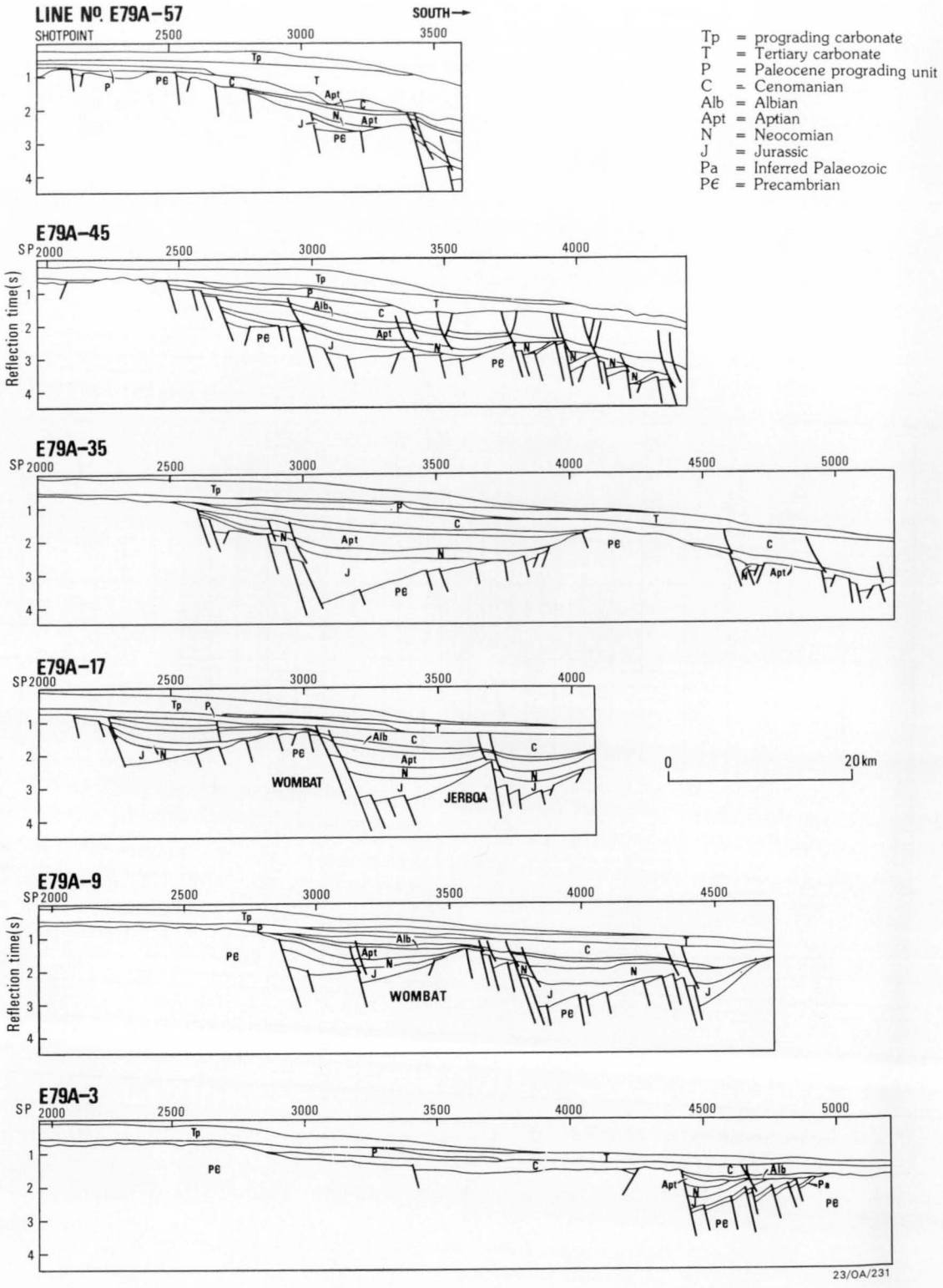

Figure 7: Seismic interpretation for six lines across the Eyre Sub-basin (after Bein & Taylor, 1981). Location of profiles shown in Fig. 6.

The main part of the Bremer Basin lies offshore. There is no offshore well control and the tectonic history can only be inferred from geophysical data. Seismic data suggest that Precambrian basement on the continental shelf is overlain by a thin veneer of Tertiary sediments. Cooney & others (1974) presented seismic data from the continental slope which indicate a thicker section. They interpreted a thick Lower Cretaceous block-faulted unit, overlain by Upper Cretaceous and Lower and Upper Tertiary sediments. Each unit has been structured and eroded by lateral movements and breached anticlines are evident within the Lower Cretaceous unit (Willcox, 1981).

The Polda Trough (also referred to as the Polda Basin or the Elliston Graben) is a sediment filled linear depression in the Gawler Block. Its axis strikes along 33 30'S, oblique to the shelf edge, and it extends from the western side of the Eyre Peninsula as far as the continental slope at the western end of the Ceduna Terrace. The structural relationship between the GAB Basin and the Polda Trough is unclear, with the trough appearing to splay off from the larger basin. The trough was originally located by aeromagnetic survey (Hammons, 1966) and has been further delineated by seismic surveys since then (Smith & Kamerling, 1969). The only stratigraphic control is provided onshore by Polda-1 bore, which intersected Quaternary, middle Eocene, and Upper Jurassic sediments with a total thickness of 160 m, and offshore by Gemini-1, which intersected about 285 m of (?)Tertiary Wilson Bluff limestone and 571.5 m of Upper Jurassic fluvial and lacustrine sediments, before reaching TD in granitic material. Seismic data interpreted by Smith & Kamerling (1969) indicate that the northern edge of the Polda Trough is fault-bounded, whereas the southern edge is formed by a flexure in the basement. Downfaulted basement thus forms a tilted block which shallows towards the southern edge (Willcox, 1978).

The GAB Basin is somewhat ill-defined except for its northern margin. Setting aside the relatively minor Polda and Robe-Penola Troughs, the basin consists of a major depocentre underlying the Ceduna Terrace (which is generally referred to as the GAB Basin), an easterly extension underlying the continental shelf and upper slope (the Duntroon Embayment), and the Eyre Sub-basin to the west which underlies the Eyre Terrace and the broad continental rise (Fig. 3).

The GAB Basin proper underlies the Ceduna Terrace principally in water depths of 200-2500 m. The greatest thickness of sediments - possibly up to 10 km - is found along a depositional axis that roughly coincides with the 1200 m isobath on the terrace (Figs 3, 8, & 9). The sedimentary section thins abruptly across the northern margin where the shallow basement of the Gawler Craton is down-faulted southwards by as much as 6 km into the GAB Basin (Fig. 9). The trend of this basement scarp changes from easterly in the western half of the basin to southeasterly in the east (Fraser & Tilbury, 1979; Fig. 10); the scarp is also much steeper in the west and southeast (>20 degrees) than it is in the central area (<10 degrees). The southern margin of the basin cannot be as precisely defined. While the basin thins rapidly beneath the lower slope of the Ceduna Terrace, there is still 4-5 km of sediment present beneath the continental rise (Willcox, 1981).

In addition to the prominent northern margin scarp, Fraser & Tilbury

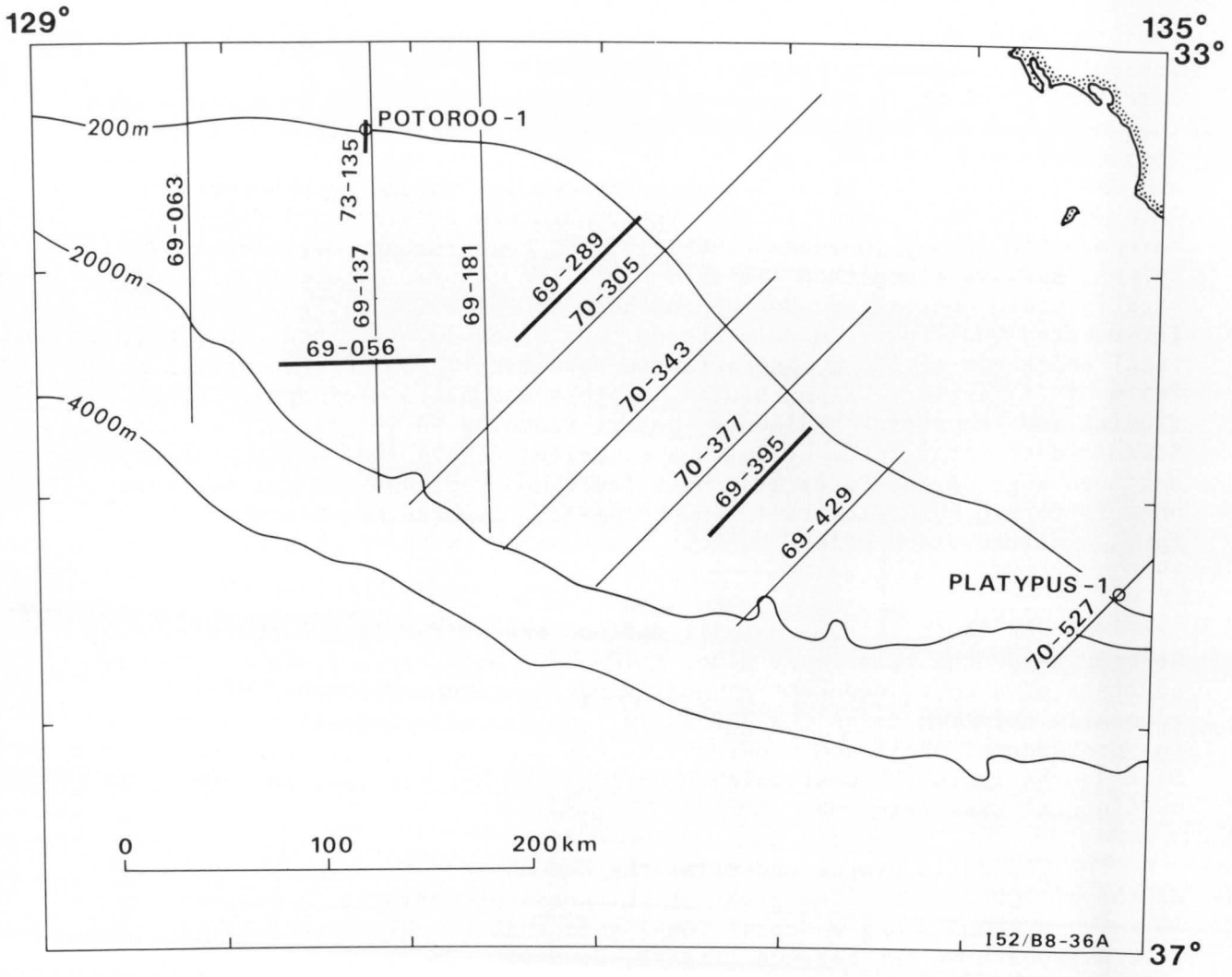

Figure 8: Location of Ceduna Terrace seismic profiles shown in Fig. 9 (after Fraser & Tilbury, 1979).

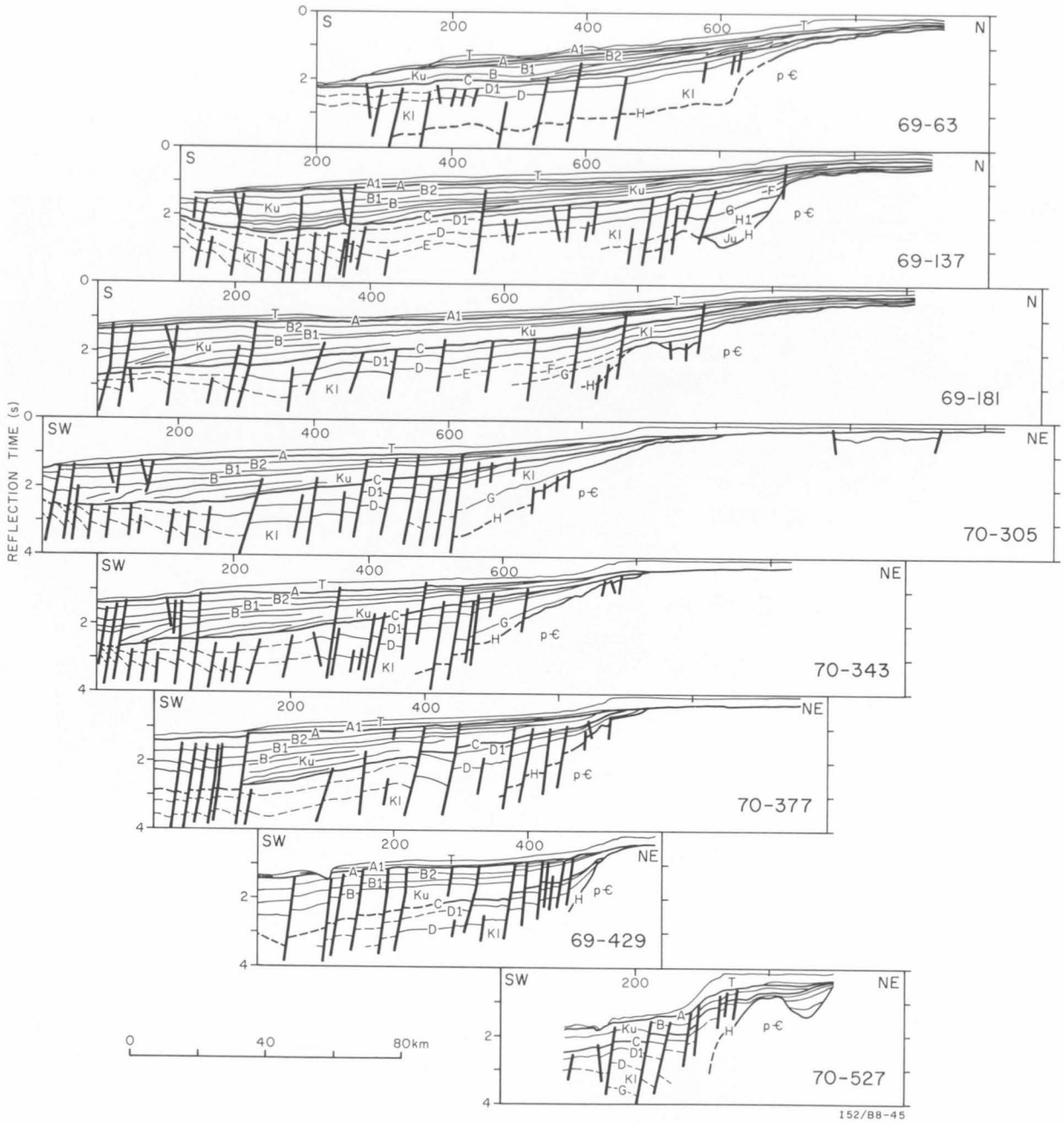

Figure 9: Line drawings of selected seismic sections across the Ceduna Terrace (after Fraser & Tilbury, 1979). Locations of profiles shown in Figure 8.

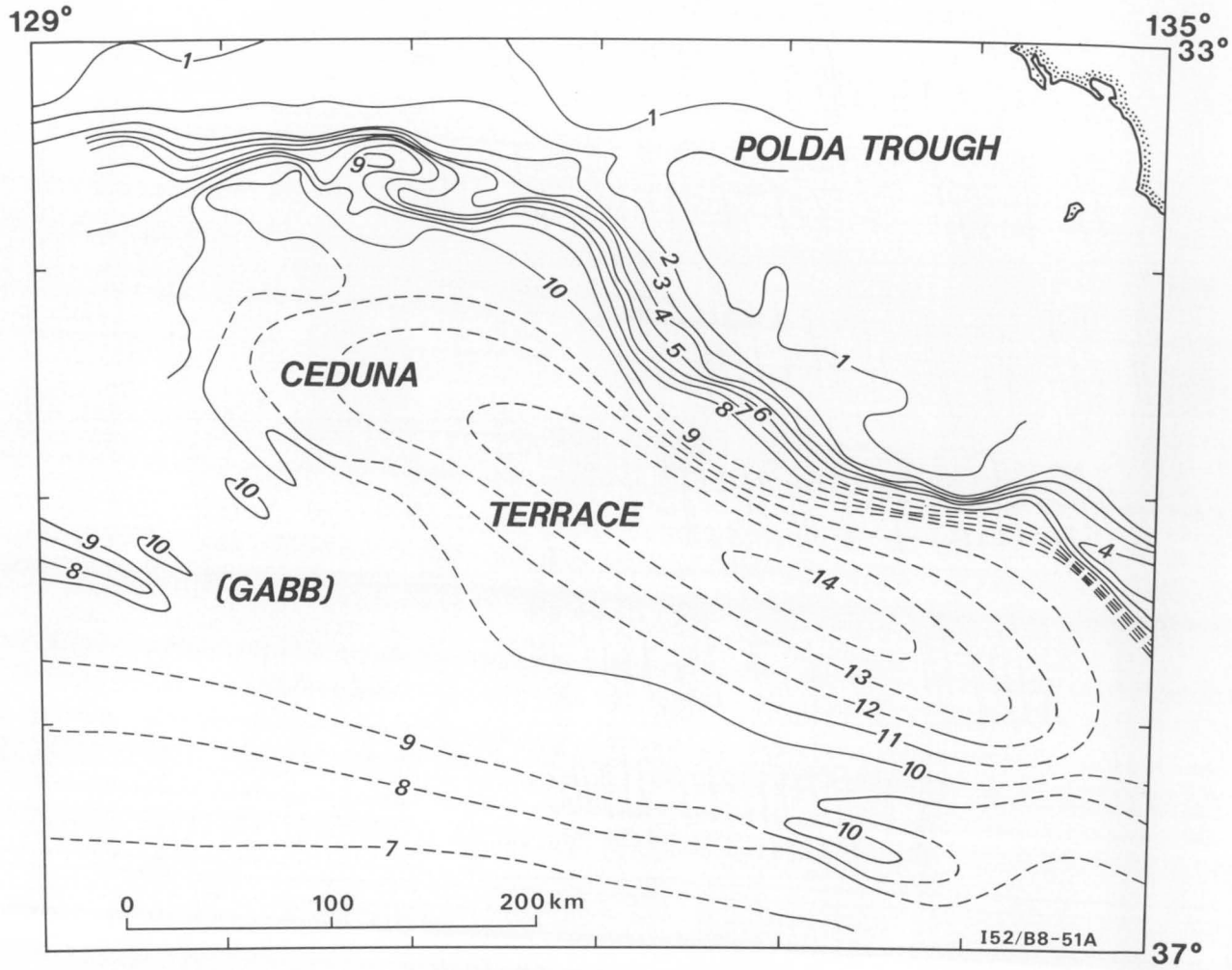

Figure 10: Basement contours, in km, beneath the Ceduna Terrace (after Fraser & Tilbury, 1979). Continuous lines are contours based on seismic data. Broken lines are generalised contours inferred from magnetic depth estimates, sonobuoy refraction results (Mutter, 1978), and structural considerations.

(1979) recognised two other prominent sets of faults within the GAB Basin, which they referred to as "intra-basin" faults and "outer-margin" faults. The intra-basin faults are most prominent in the inner, seaward-thickening part of the basin (Fig. 11) and commonly result in narrow, landward-tilted fault blocks. Most are east- to southeast-trending growth faults, slightly curved at depth, and in some cases showing roll-over of the deeper beds into the fault plane on the downthrown side of the fault. As with the boundary faults, Fraser & Tilbury (1979) note that the intra-basin faults appear to have been active much later in the east of the basin, where they extend well into the upper part of the section. The outer-margin faults (Fraser & Tilbury, 1979; Fig. 12) have a general easterly trend and are concentrated in the southeast. These faults are usually of Tertiary age and exhibit little growth; Fraser & Tilbury (1979) and Mutter (1978) suggested that these faults formed in response to the onset of seafloor spreading. In light of the now generally accepted mid-Cretaceous age of margin breakup, it may be that they developed as a result of a change of margin subsidence rate when the spreading rate accelerated in the Eocene.

The Duntroon Embayment is the strongly-faulted part of the GAB Basin lying west of Kangaroo Island and south of Eyre Peninsula. Robertson & others (1979) suggest that the embayment was close to a triple-point junction with the postulated failed-arm of the junction perhaps developed along the pre-existing strongly-developed structural grain of the Adelaide Fold Belt to produce the South Australian Rift Valley. Within the Duntroon Embayment, three main structural provinces have been recognised (Whyte, 1978; Fig. 13). The first of these provinces is referred to as the "inner basin" and lies in the northern part of the embayment between the northern boundary fault and the "central high". The inner basin is a graben or half-graben which is extensively normal-faulted in the deep section. The central high is characterised by upthrown and downthrown basement blocks which give rise to three distinct anticlinal structures with intervening synclines; Echidna-1 tested one of these anticlines. The central high is considered to have formed during the Late Cretaceous to Early Tertiary, at which time variable amounts of the Upper Cretaceous section were removed by erosion. The third zone, the "outer growth fault belt", is separated from the central high to the north by one or more basement faults. In structural style, this zone is similar to the GAB Basin proper. Despite the name, there is little evidence of synsedimentary faulting and the faults are considered to be the result of movements in deep basement (Robertson & others, 1979).

The Eyre Sub-basin, underlying the Eyre Terrace and adjacent continental rise, is separated from the main GAB Basin by a zone of narrow continental slope at the head of the Great Australian Bight (Fig. 3). The sub-basin consists of two major half-grabens (Figs 7 & 14) with associated smaller fault blocks (Bein & Taylor, 1981), and is bounded to the north, west, and south by shallow Precambrian basement, and to the southeast by the GAB Basin. The northern boundary is formed by an EW-trending fault zone, and the principal half-grabens are separated by an ENE-trending rotated basement block, the Wombat feature. The northern half-graben closes to the east as the Wombat feature converges on the basement of the northern margin. The southern half-graben, which trends parallel to the Wombat feature, contains the greatest thickness of sediments - up to 6 km. The southern margin of the half-graben is formed by a broad high-standing basement block. East of 128 E, the basement high becomes longitudinally dissected into many smaller rotated basement blocks by mainly

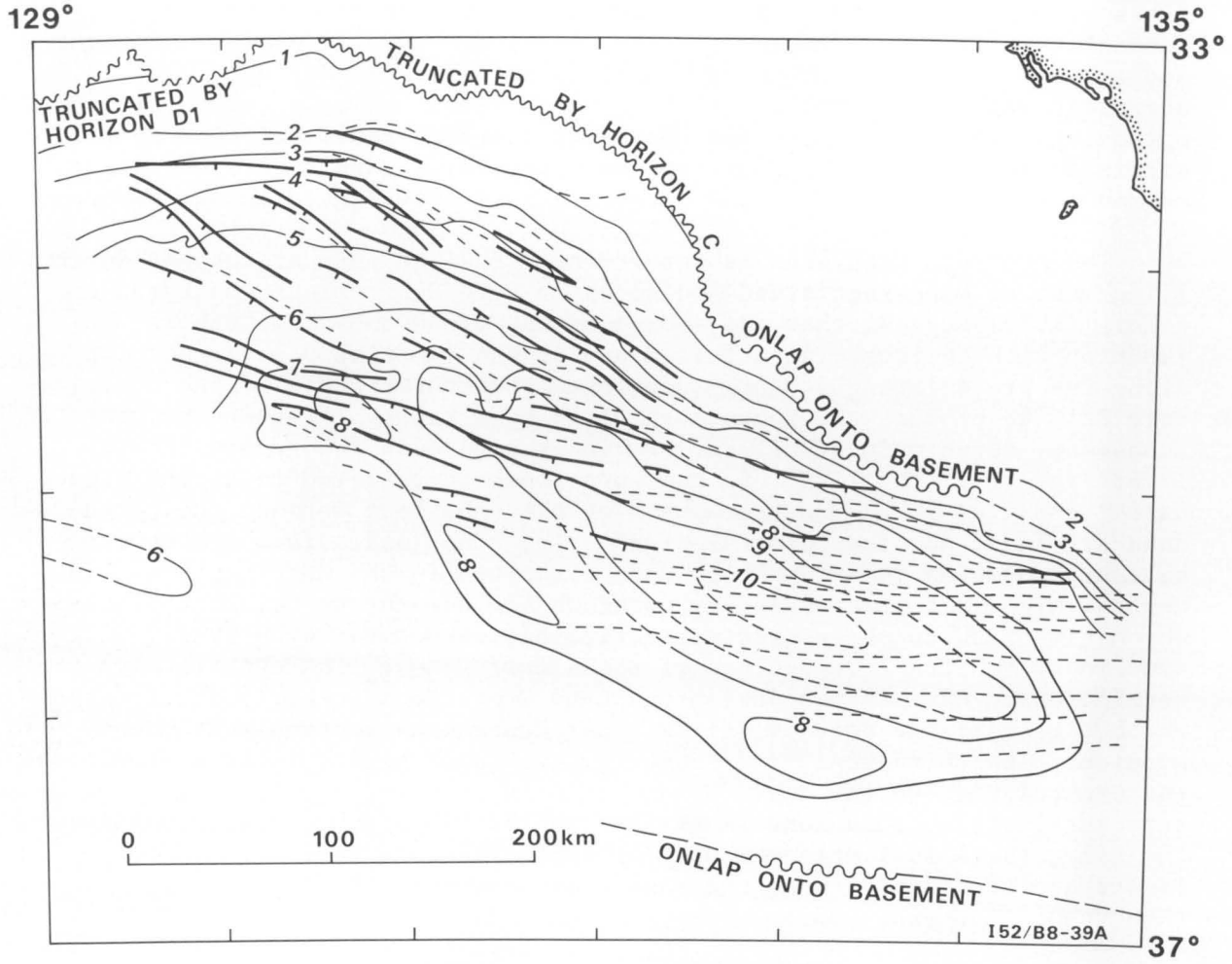

Figure 11: Generalised structure contours of the Cenomanian horizon beneath the Ceduna Terrace, in km (after Fraser & Tilbury, 1979). Intra-basin faults shown as solid lines; outer margin faults shown as dashed lines.

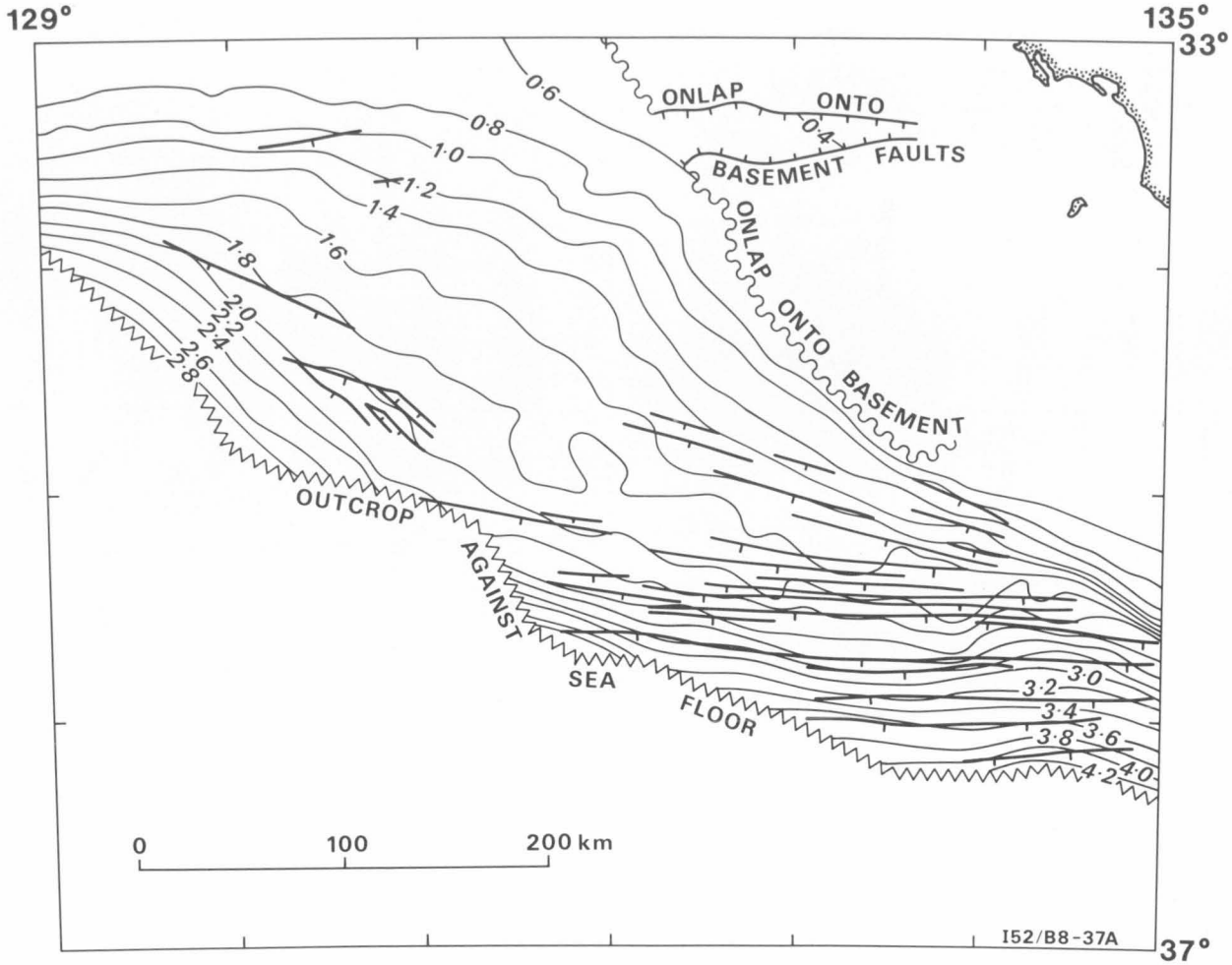

Figure 12: Generalised structure contours of the Palaeocene horizon beneath the Ceduna Terrace, in km (after Fraser & Tilbury, 1979). Outer margin faults shown as solid lines.

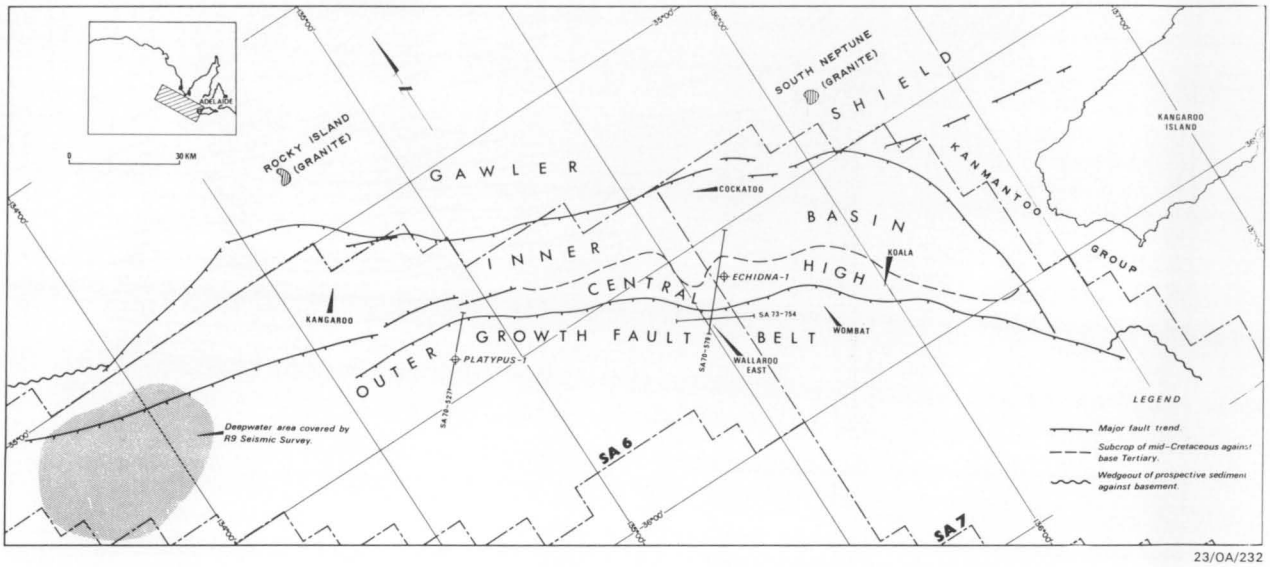

23/OA/232

Figure 13: Structural elements of the Duntroon Embayment (after Whyte, 1978).

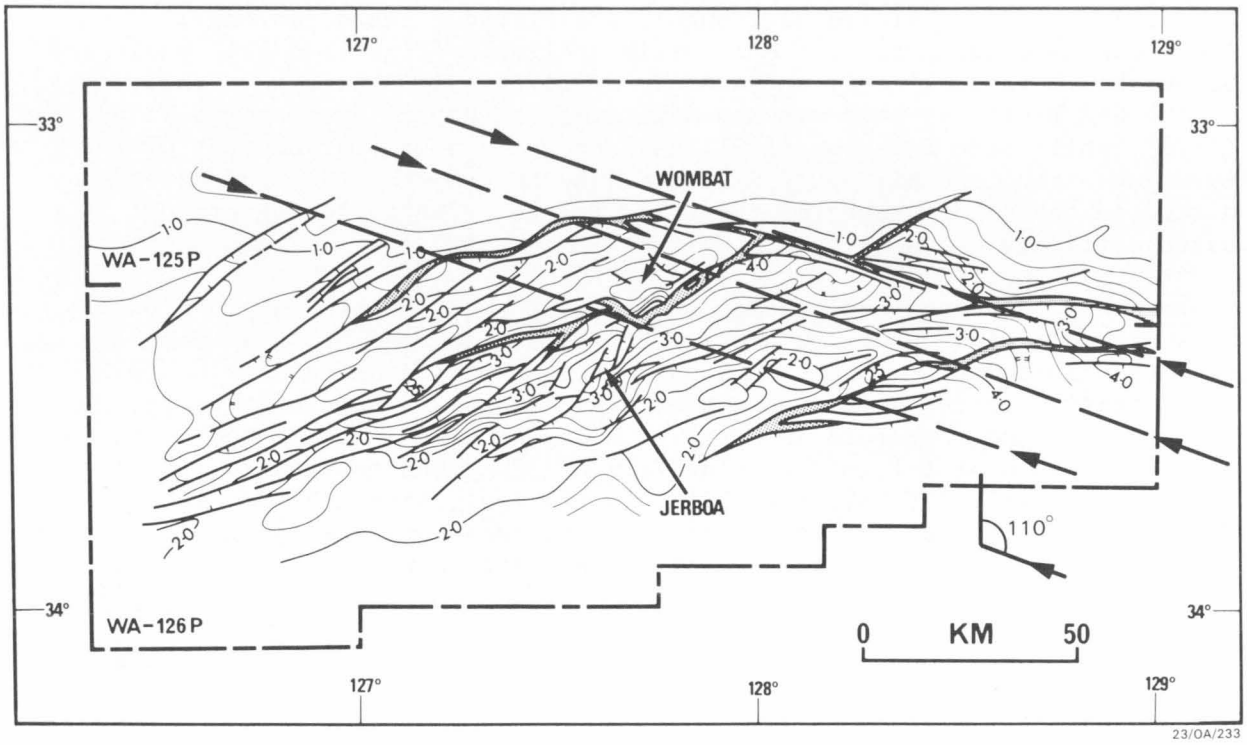

Figure 14: Time structure map on basement in the Eyre Sub-basin (after Bein & Taylor, 1981). Contour interval 0.25 s two-way reflection time.

down-to-the-south normal faults. These faults generally trend E-W, replacing the SW-NE faulting of the western sub-basin as the major structural orientation. Further eastwards, basement drops away rapidly to the south and the greatest thickness of sediment is probably found on the continental rise. Within the southern half-graben, many smaller basement fault blocks are found, and Jerboa-1 was drilled on one of these. Bein & Taylor (1981) suggested that the anomalously high features, such as the Jerboa block, may have been re-activated by fault rejuvenation in the Late Cretaceous.

STRATIGRAPHY

Well control of the stratigraphy of the southern margin basins is limited - Jerboa-1 (Eyre Sub-basin), Potoroo-1 (GAB Basin), Apollo-1, Gemini-1,and Mercury-1 (Polda Trough), and Platypus-1 and Echidna-1 (Duntroon Embayment) are the only wells available (Figs 15 & 16), while the Bremer Basin is completely untested by drilling. To date, the stratigraphy of the GAB Basin has been discussed in greatest detail by Fraser & Tilbury (1979), while Bein & Taylor (1981) have provided a similar account of the Eyre Sub-basin, and Willcox (1978) and Robertson & others (1979) have discussed the stratigraphy of the Polda Trough. The following account is based primarily on these papers.

As has been previously noted, rifting of the southern margin probably began at some time in the Jurassic. Fraser & Tilbury (1979) reported a depression between the northern margin escarpment of the GAB Basin and a basement rise to the south which they suggested was a continuation of the Polda Trough and therefore inferred to contain Upper Jurassic sediments as were found in Gemini-1 in the Polda Trough. Such sediments were also inferred by Willcox (1981; Fig. 17). To the west, Bein & Taylor (1981) reported Middle-Upper Jurassic poorly-sorted sandstone overlying Precambrian basement in Jerboa-1. These sandstones were interpreted to be weathering products and debris derived locally from basement, which split off the high blocks shortly after basin initiation. Depositional environments were probably lacustrine. Seismic data elsewhere in the Eyre Sub-basin indicate thick wedges of largely shale-prone Upper Jurassic sediments with some interbedded sandstone.

Deposition through to the Neocomian probably continued to be dominantly continental. The Loongana Sandstone was laid down in the GAB Basin while in the Eyre Sub-basin a sand-prone sequence with excellent reservoir characteristics was deposited by the outbuilding of deltas into a deep lake. Non-marine conditions persisted into the Aptian in the Eyre Sub-basin with the deposition of a thick sequence of claystones and shales. In the GAB Basin, the first indication of marine conditions comes in the Aptian and Albian with the deposition of fine-grained shales, siltstones, and minor sandstones in a restricted marine environment resulting from the transgression of a shallow sea from the northeast (Veevers & Evans, 1975). More fully marine conditions probably developed in topographically lower areas south of Potoroo-1. The earliest marine influence recorded in Jerboa-1 occurred in the Albian when a thin shale-prone prograding unit was deposited unconformably over the Aptian non-marine claystones. Marine deposition in the Eyre Sub-basin continued into the Cenomanian with a thick sequence of interbedded shales, claystones, and sandstones. This depositional episode may have continued later into the Cretaceous in the thicker parts of the sub-basin, although there is a major hiatus in

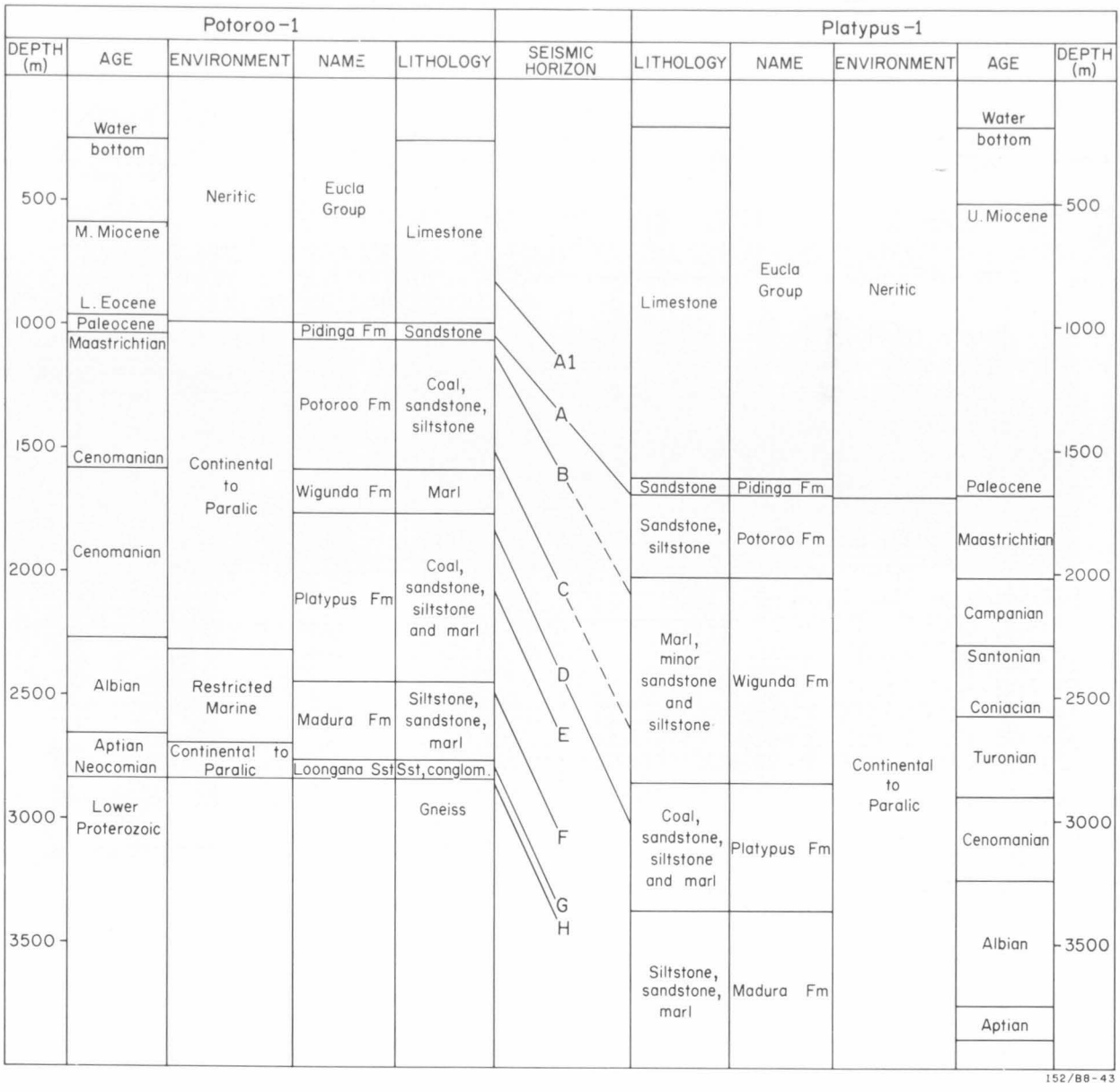

Figure 15: Stratigraphic tables for Potoroo-1 and Platypus-1 wells (after Fraser & Tilbury, 1979). Correlation of seismic intervals between the two wells is shown, with tentative correlations indicated by dashed lines.

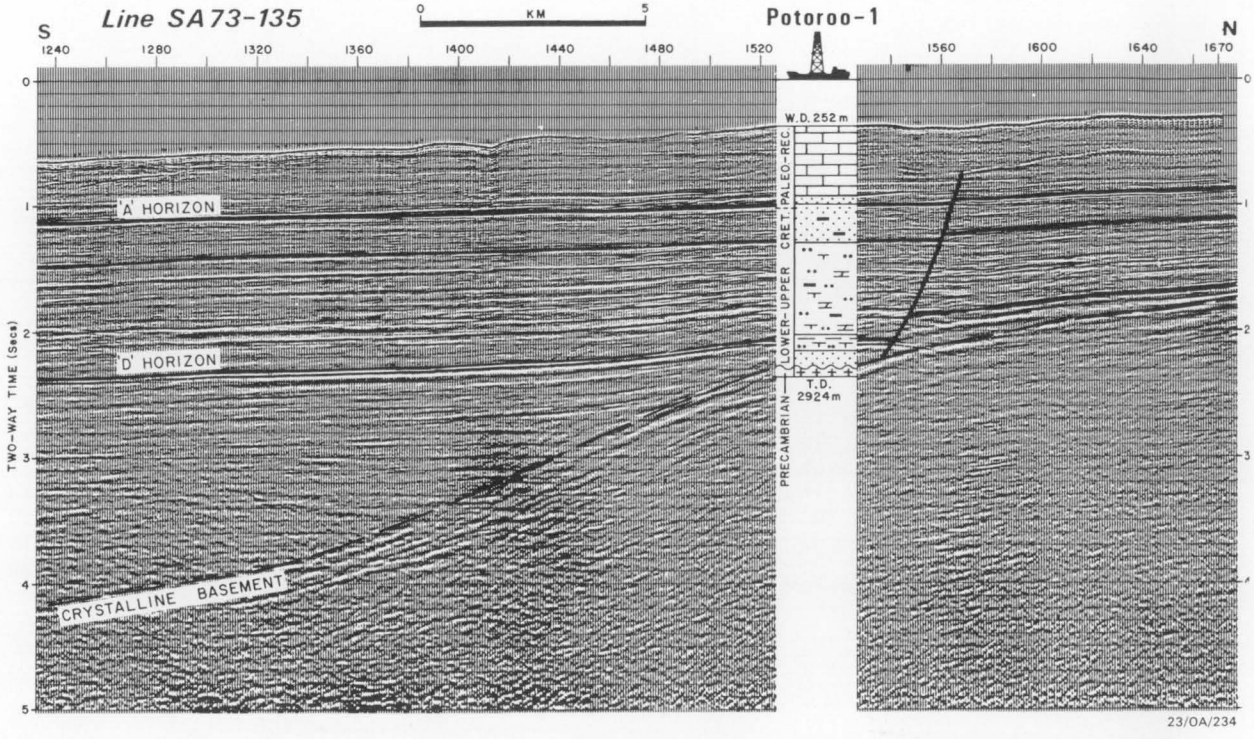

Figure 16: Seismic section through Potoroo-1 showing the well stratigraphy (after Whyte, 1978).

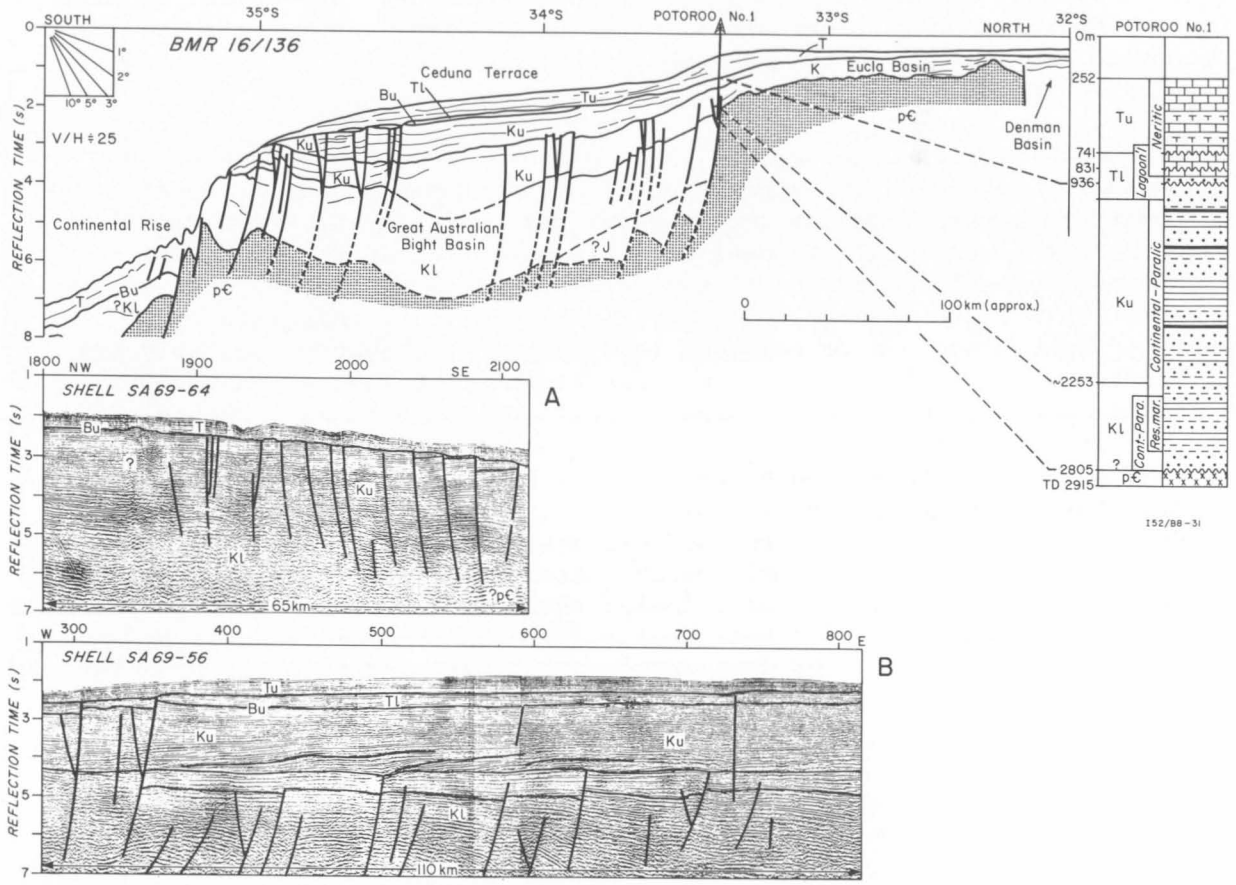

Figure 17: Interpretation of BMR seismic profile across the Ceduna Terrace tied to Potoroo-1 on the northern flank of the GAB Basin (after Willcox, 1981). Dashed horizons are schematic and based on Boeuf and Doust (1975, figure 8). Depositional environments in Potoroo-1 are indicated. Profile a shows fault blocks on the seaward margin of the terrace; profile B shows prograding in an Upper Cretaceous unit.

Jerboa-1 between the Cenomanian and the Middle Eocene.

In the GAB Basin, the Aptian-Albian marine incursion was followed by a major Cenomanian regression that produced a paralic environment with coal deposition being prominent; shallow marine conditions were probably preserved in the southwest of the basin. Seismic sequence analysis suggests that there was probably a return to stable marine conditions in the Late Cenomanian with the deposition of predominantly fine-grained sediments, contemporaneous with the restricted marine Belfast Mudstone in the Otway Basin. Deighton & others (1976) and Fraser & Tilbury (1979) interpret this change to probably signify an easternwards encroachment of the sea along the floor of the rift valley. Fraser & Tilbury suggested that the incursion may have been related to a global rise of sea level (Vail & others, 1977) rather than tectonic subsidence. Given that breakup is now thought to have taken place in the Cenomanian-Turonian, it is likely that both tectonic (post-breakup subsidence) and global sea level effects are responsible.

Marine sedimentation continued in the GAB Basin from the Cenomanian into the Maastrichtian with the deposition of abundant sandstones at least along the northern margin. In the southwest of the basin, a thick prograded sequence with large-scale foreset beds was deposited at the same time. Significant upbuilding of the topset beds indicates a relative rise of sea level at this time. Fraser & Tilbury (1979) attribute this rise to tectonic subsidence due to sediment loading rather than to a eustatic sea level rise. Again, it appears that post-breakup subsidence can be invoked as the responsible mechanism. Depositional environments were probably paralic in the north of the basin and perhaps as deep as bathyal in the south. A seismic facies change in the late Upper Cretaceous in the upper part of the prograded sequence indicates a change from shallow marine sandstones and shales to interbedded discontinuous sands and coals deposited in a delta plain environment. Fraser & Tilbury (1979) propose a high rate of terrigenous influx as being the main cause of this regression. The seismic data further indicate that the regression was followed by a transgression which seems to have resulted in a seaward-thinning wedge of paralic facies sediments cutting across the top of the prograded sequence and extending over most of the Ceduna Terrace.

On both flanks of the GAB, the Tertiary sequences are somewhat similar, as might be expected. The Ceduna Terrace is characterised by transgressive marine sands of the Palaeocene Pidinga Formation unconformably overlain by Eocene and younger Eucla group open marine carbonates. In the Eyre Sub-basin, sedimentation commences again in the Early Eocene with the Hampton Sandstone which is, in turn, conformably overlain by open marine carbonates. Fraser & Tilbury (1979) noted the presence of small mounds above the Palaeocene unconformity which they attributed to volcanic breakups, extruded at about the time of breakup. Given the revision of breakup age, this explanation is perhaps less likely.

GREAT AUSTRALIAN BIGHT (CEDUNA TERRACE AREA)

Only one well has been drilled in the GAB Basin (Potoroo-1 on the northern margin), despite a relatively comprehensive regional seismic coverage, and the basin can be considered barely explored for hydrocarbons. Fraser & Tilbury (1979) rated the basin as having fair or good hydrocarbon potential on the basis of the presence of at least 10 km of Mesozoic sediment which they interpreted to include widespread marine deposits in the western part of the basin in both Lower and Upper Cretaceous sequences. Furthermore, the apparent dearth of erosional unconformities in the centre of the basin and the almost continuous and often rapid deposition would have tended to favour the anaerobic conditions which are required for the generation of hydrocarbons and reduced the likelihood of escape of hydrocarbons from potential traps. However, Willcox (1981) notes that while source rocks are likely to be found in most of the Cretaceous sequences, they may be expected to be mainly humic and hence gas-prone, except possibly for the marginal marine shales and mudstones of Aptian-Albian age.

Fraser & Tilbury (1979) recognised two main possibilities in the GAB Basin that may be favourable for hydrocarbon generation, migration, and entrapment. These possibilities were -

1. The top part of the faulted Lower to mid-Cretaceous sequence where structural entrapment may exist in tilted blocks by a combination of dip closure and faulting. While source and seal may be present in the form of marine beds within the blocks and fine-grained sediments of the Wigunda Formation respectively, Potoroo-1 was not encouraging for the presence of reservoirs.

2. Juxtaposition of a thick Upper Cretaceous deltaic sequence, interpreted to contain interbedded sands and shales, directly above a probable fine-grained, shallow-marine sequence. Sourcing could be from the deeper marine sequence, with any generated hydrocarbons having a simple migration path into stratigraphic traps in the form of sand bodies within the delta. However, Willcox (1981) suggests that the deltaic sequence may be too shallow for maturity, and further points out that the delta shows no proximal downwarping or closure.

EYRE SUB-BASIN

Although the sole wildcat well drilled in the Eyre Sub-basin was unsuccessful in finding hydrocarbons, it was sited in the centre of the sub-basin and thus provided good stratigraphic control. Bein & Taylor (1981) considered the main exploration target to be two sand-prone sequences of Neocomian age that proved to have porosities of 20% and 17%, respectively. All sediments penetrated by Jerboa-1 were immature for oil generation, although the sediments near the well total depth were approaching maturity. Given the large amount of structuring seen in the seismic data and the interpreted presence of possibly suitable marine source beds, the Eyre Sub-basin cannot be discounted as a potential hydrocarbon source.

POLDA TROUGH

To date, only Robertson & others (1979) have published an assessment of the hydrocarbon potential of the Polda Trough - and that assessment was brief. Gemini-1 was drilled on a seismically-defined prospect where the data indicated the presence of at least 2000 m of sediments. These were interpreted to consist of a thick marine Lower cretaceous section overlying Jurassic lacustrine and fluviatile sediments. No Cretaceous sediments were sampled at all, and the well was abandoned in igneous rocks at a depth of 894 m. While the results of Gemini-1 have seriously down-graded the prospectivity of the Polda Trough, doubt remains as to whether the igneous material represents basement or whether it may be underlain by prospective sediments.

PALAEOTEMPERATURES

The only two marine heat-flow determinations on the southern margin are prior to this program are values of 48.2 mW/m2 in the South Australian Abyssal Plain and 58 mW/m2 from the continental slope south of the Duntroon Embayment. Bein & Taylor (1981) stated that palaeotemperature results from Jerboa-1 indicate that none of the sediments in that well have been heated above 100 C and that basement rocks have not been heated above 200-300 C since the Proterozoic. Bein & Taylor used these palaeotemperatures to support their thesis that the complex basement fault pattern of the Eyre Sub-basin is the result of brittle fracture in a tensional stress field.

Willcox (1981) states that the temperature gradients in Echidna-1, Platypus-1, and Potoroo-1 indicate a heat-flow of about 80 mW/m2 on the Ceduna Terrace. However, recent heat-flow data from a similar marginal feature, the Exmouth Plateau (Choi, Stagg, & others, 1987), shows a large variation in heatflow (~100%) across the structure, and it is probably unreasonable to extrapolate scattered heat-flow values from the margin of a basin across the basin depocentre.

PREVIOUS DATA BASE

We briefly summarise here the major sources of geophysical data for the area in terms of quality, geographical location, and availability between the western end of the Great Australian Bight and the western end of the Otway Basin. These are the data that have been used in the following summary of the regional geology and spreading history of the southern margin.

REGIONAL SURVEYS

1. *BMR Continental Margins Survey*: N-S and E-W lines extending from the shoreward side of the continental shelf out to the abyssal plain at an average separation of about 35 km (Fig. 18). The seismic data were recorded 6-fold analogue with a sparker energy source and vary in quality from poor to moderate. Digital magnetic, gravity, bathymetry, and navigation data are also available.

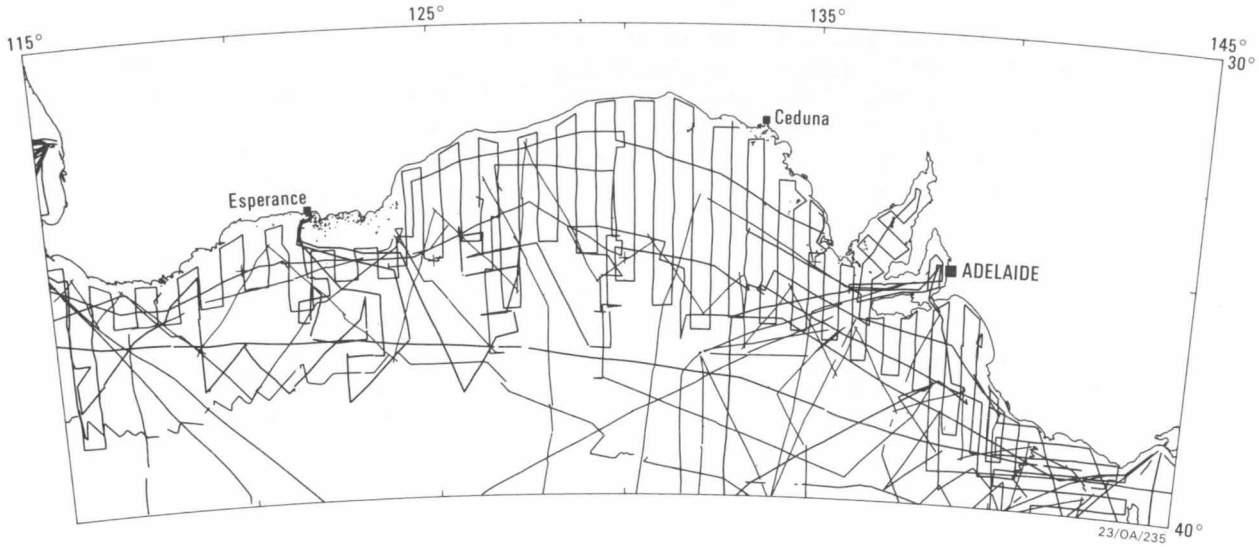

Figure 18: Ships tracks of the BMR Continental Margin Survey, Shell *Petrel*, and Lamont-Doherty Geological Observatory (*Vema*, *Eltanin*) along the southern margin of Australia.

2. *Petrel (Shell Development Australia Pty Ltd)*: zig-zag lines extending across the margin from the continental shelf out to the abyssal plain, with an average separation of about 100 km between the centre points of adjacent lines (Fig. 18). Seismic data were recorded 24-fold digital with an airgun array sound source and vary in quality from moderate to good. Seismic data have not been stacked (other than a two-fold optical stack produced on-board) although copies of the field tapes are available for this purpose. Digital non-seismic data are also available.

LOCAL SURVEYS

1. *Eyre Terrace (Esso)*: 3151 km of stacked 48-fold airgun array seismic data of high quality are available along lines with variable separation (Fig. 6). Digital navigation data are available.

2. *Ceduna Terrace (Shell)*: 24546 km of stacked digital seismic data (variable fold) of fair to good quality recorded from 1966-76 are available (Appendix F; Fig. 19). Lines are generally oriented N-S/E-W or NE-SW/NW-SE and the line separation is highly variable. Coverage of the plateau margins is extremely limited. Digital navigation data are also available.

OTHER DATA

A considerable quantity of other company seismic data, principally on the eastern side of the GAB, are available in BMR, but are not pertinent to the studies proposed here. Determination of the spreading history has primarily been made from magnetic data acquired on the surveys referred to above and also by the Lamont-Doherty Geological Observatory vessels *Conrad*, *Eltanin*, and *Vema* (Figs 3 & 18). The locations of wells in the Great Australian Bight region are given in Appendix G.

CRUISE OBJECTIVES

The marine geoscience program on the southern margin was designed to address the following questions, as outlined in the original cruise proposal (Appendix B):

1. What is the relationship between the structure and stratigraphy of the Eyre Sub-basin, the western GAB Basin underlying the Ceduna Terrace, and the thick sediments of the continental rise? (Fraser & Tilbury (1979) implied that the western GAB Basin had the higher hydrocarbon potential, due to postulated greater thickness of marine sediments.)

2. What was the direction of initial opening between Australia and Antarctica? Examination of available data suggests it may have been NW-SE rather than the commonly accepted N-S. If it was NW-SE, then existing interpretations of the deep basin structures will need to be re-cast to accommodate possible wrench faulting. In the case of the Ceduna Terrace, the deep structures may have a significant wrenching component, particularly along the SW margin.

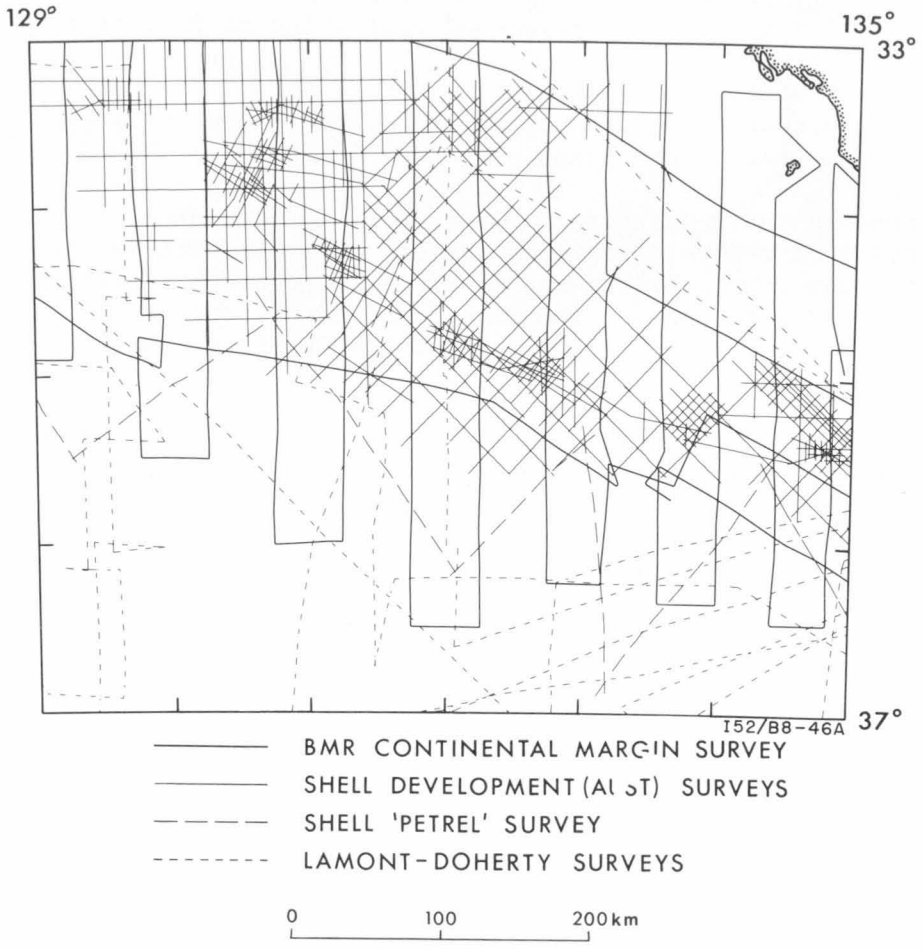

Figure 19: Ships tracks across the Ceduna Terrace (after Fraser & Tilbury, 1979).

3. What is the distribution of seismic facies, particularly in relation to the various Cretaceous marine incursions? It is these incursions which have the best potential for providing suitable hydrocarbon source rocks.

4. What is the relationship of continental extension to margin structure, the Diamantina Zone, and the Australian-Antarctic Discordance?

6. What is the relationship of the margin and basin development to the following aspects of hydrocarbon prospectivity:
   - age of structuring of GAB Basin?
   - indications of Cretaceous deltas and marine source rocks?
   - heat-flow and maturity?
   - breaching of Cretaceous traps during the Tertiary?
   - migration paths and potential entrapment?

7. What are the sedimentary rock types, organic contents, environments of deposition, and physical properties of sediments that may be exposed on the outer continental margin? Present knowledge stems from only one drill hole in each of the Eyre Sub-basin (Jerboa-1) and the GAB Basin (Potoroo-1), and in the case of the GAB Basin the well was sited on the basin margin.

8. What is the heat-flow regime and its history over the Ceduna Terrace, Eyre Terrace, and continental rise? In particular, what are the imprints of the various and complex episodes of structuring and tectonism on the regional heat-flow, and what is the level of heat-flow, and hence maturity, in those areas that can be considered hydrocarbon-prospective

CRUISE PLAN

The southern margin program was split between two cruises, starting in Fremantle in mid-October, 1986 and ending in Adelaide in mid-December, with a crew change in Port Lincoln. At a transit speed of 10 knots, a total of about 7 days were allowed for transit time on the first leg and 3 days for the second leg, leaving 21 and 25 days respectively for work. The following program was devised to address the points raised in the previous section.

LEG 1

The first leg was to be devoted entirely to 48-channel, 24-fold multichannel seismic profiling along the planned tracks shown in Figure 20. Data were to be shot with the new 26.2 litre (1600 cu in) GSI airgun array. A total of 3600 km of seismic data was proposed with the tracks oriented primarily NW-SE and NE-SW at a variable spacing. At 5.5 knots, this was estimated to take about 17 days. The remaining time was set aside for streamer deployment, bad weather standby, and further detailed seismic work as required. In the event, bad weather and gun array problems used up all the slack time.

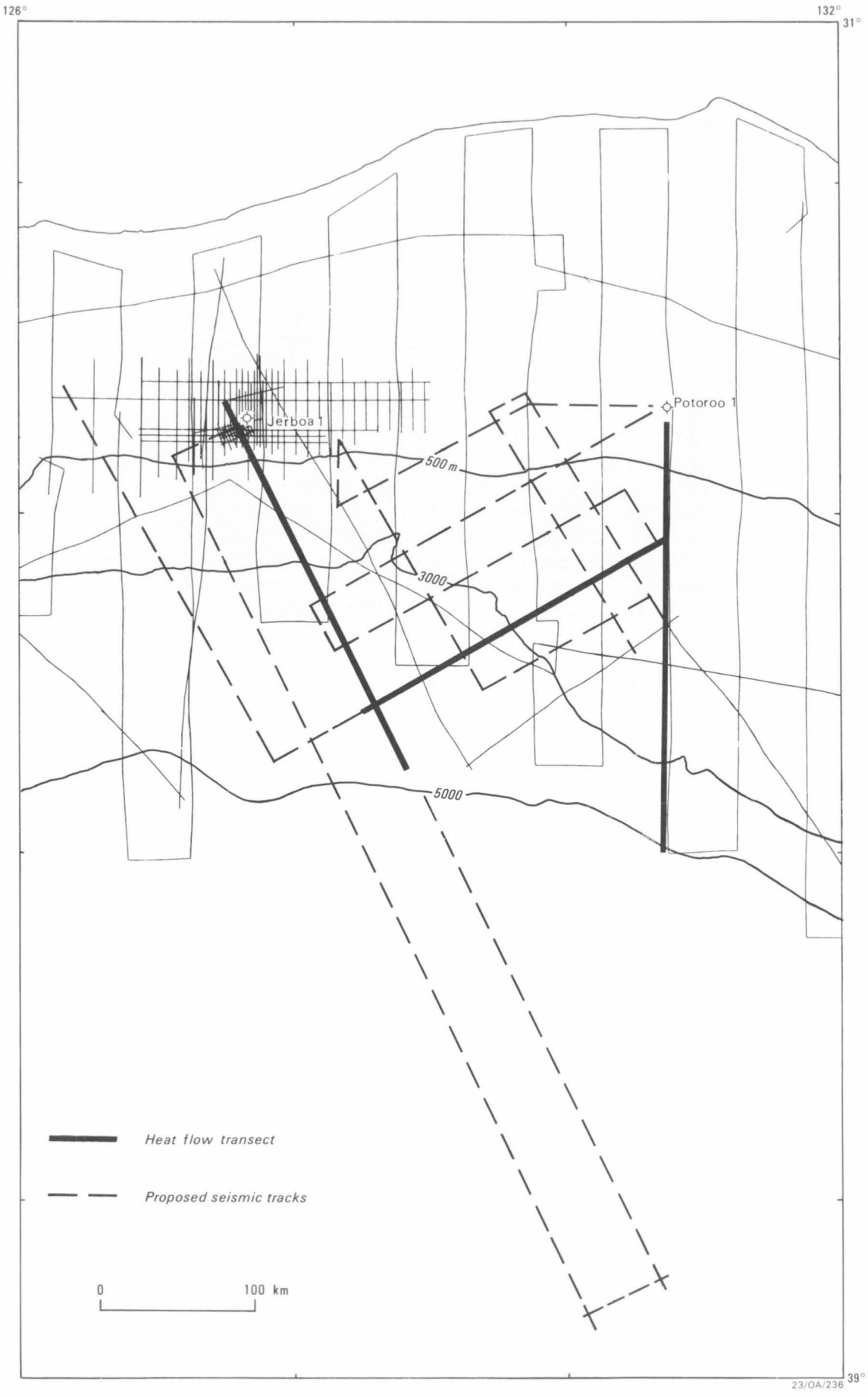

Figure 20: map showing location of multichannel seismic lines proposed for Leg 1 (Survey 65).

The lines shown in Figure 20 were designed:

1. to be perpendicular to the main trends on the Eyre Terrace;

2. to be perpendicular to the main trends on the southwestern and southern Ceduna Terrace;

3. to compromise on the apparently conflicting trends at the Ceduna/Eyre Terrace junction; and

4. to complement existing high-quality lines on the Ceduna Terrace (Shell), Eyre Terrace (Esso), and in deep water (Shell *Petrel*).

LEG 2

The second leg was to be entirely given over to sampling and heat-flow studies, with a minor amount of magnetic work (approximately 2 days), time permitting. It was intended to do the heat-flow work at the start of the leg, so that any failed stations could be identified during the cruise and re-occupied late in the cruise if sufficient time remained. As a number of sediment cores would be collected for the heat-flow program, the sampling program of 18 days would concentrate primarily on dredging the outer margins of both the Eyre and Ceduna Terraces. The general locations of the planned sampling areas are shown in Figure 21; specific site location would depend on detailed analysis both of existing data and also of the seismic data acquired during Leg 1. Given the rather gentle slopes (and the likely surficial sediment cover) on the southern margin of the Ceduna Terrace, it was expected that a considerable number of attempts would be required to obtain representative samples from this area.

If both the heat-flow and sampling programs were successfully completed, it was intended to finish Leg 2 with a maximum of 2 days high-speed magnetic profiling along two tracks spaced equidistantly between the two long seismic lines that were to extend across the South Australian Abyssal Plain. These four lines of magnetic data, spaced about 12 km apart, would then give good control on the trend and age of the magnetic lineations during the first phase of Southern Ocean spreading.

ACTUAL PROGRAM COMPLETED

The tracks of the actual program completed are shown in Figures 22 and 23. The major variations to the proposed program were as follows -

LEG 1 (SURVEY 65)

1. Due to time lost early in the cruise to airgun array trials, the two long lines extending to about 38.5 S were deleted, and a single oceanic crust to continental shelf transect across the Ceduna Terrace was substituted (Line 15). Minor adjustments were made to other tracks to fit in with time constraints and the vagaries of the weather.

2. A previously unplanned program of approximately 480 km of reflection seismic was completed over the Polda Trough (Lines 101-106), of which about

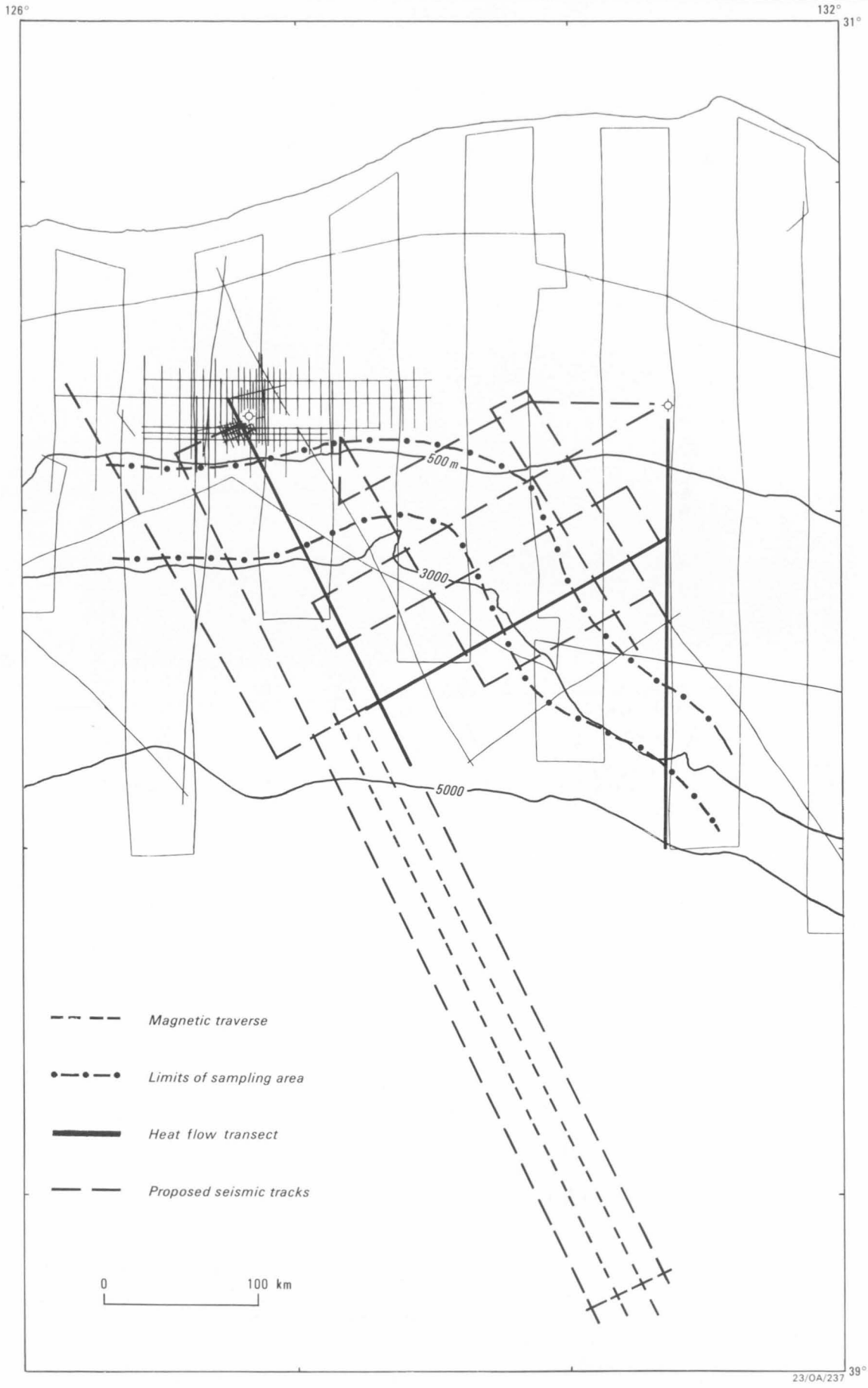

Figure 21: Map showing location of proposed sampling, heatflow, and magnetic work for Leg 2 (Survey 66).

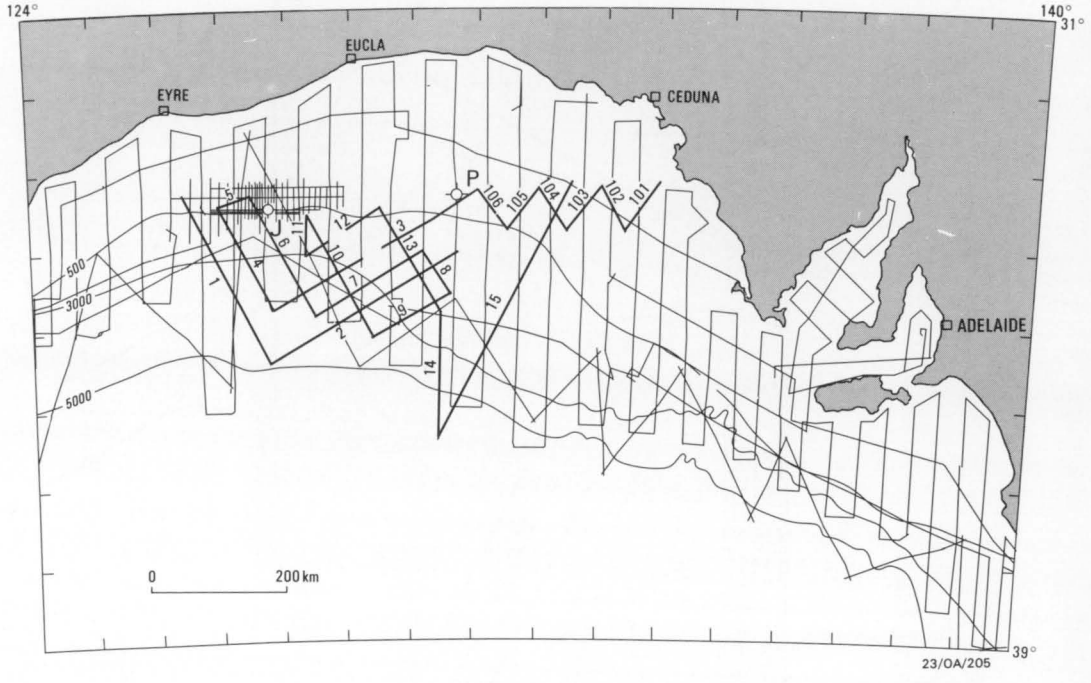

Figure 22: Map showing actual multichannel seismic lines completed during Leg 1.

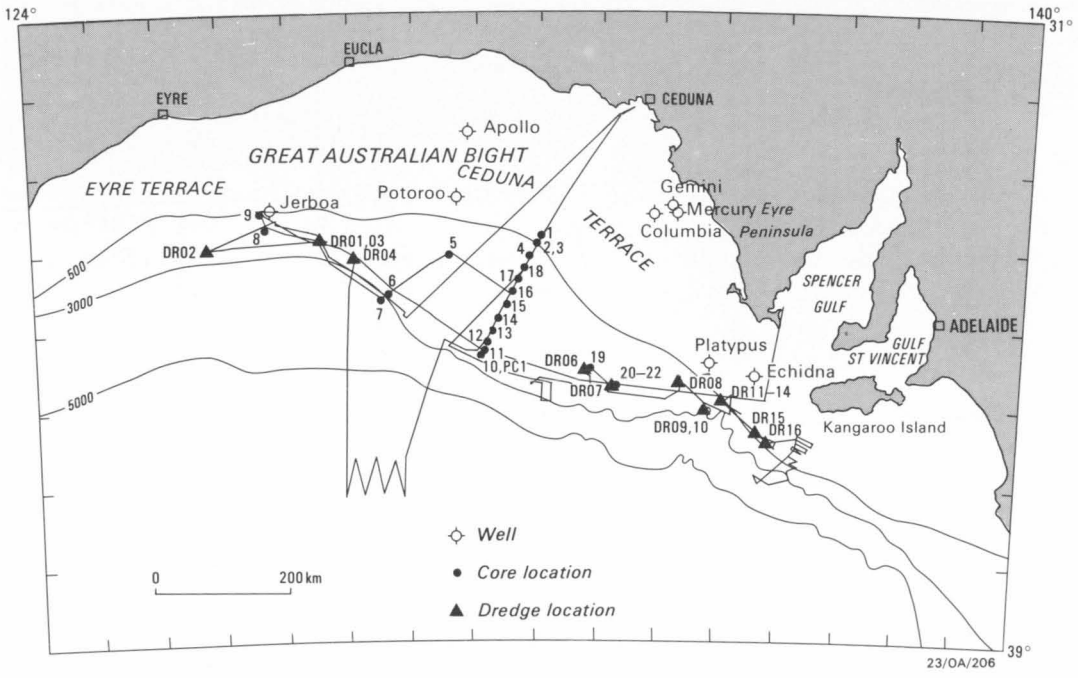

Figure 23: Map showing tracks completed and sites occupied during Leg 2.

370 km was shot 12-fold with a 600 m streamer. This program was instigated primarily to complete trials of the airgun array, which until then had proved troublesome. In the event, a useful additional investigation was completed.

LEG 2 (SURVEY 66)

1. Leg 2 was extensively modified from the projected program because of the loss of more than half the wire on the main coring winch, prior to Leg 1. Only 4200 m of wire remained, which restricted operations to water depths of less than 3500 m. This ruled out all the deep-water dredging and coring targets and radically curtailed the heatflow program.

2. The heatflow program was also restricted by the hard seabed, and successful heatflow operations were confined to the Ceduna Terrace.

3. Prior to the cruise, it was anticipated that there would be problems in finding suitable dredging targets on the western Ceduna Terrace, due to the rather gentle and apparently sediment-covered slopes, and the paucity of canyon development. This proved to be the case. Consequently, the main dredging effort was directed to the eastern half of the Ceduna Terrace, where submarine canyons are extensively developed.

The way-points for the seismic reflection lines (Survey 65), together with shooting fold and source type are given in Appendix C. A listing of the sampling and heatflow stations is given in Appendix D. Appendix E is an operational diary for Leg 1 of the Southern Margin Program.

PRELIMINARY INTERPRETATION OF ON-LINE GEOPHYSICAL DATA

The Great Australian Bight Basin (GABB) in this region may be considered in terms of three components: the Eyre Sub-basin, the sedimentary sequences beneath the Ceduna Terrace, and the thick sequences which lie beneath the continental rise south of the Eyre Terrace and southwest of the Ceduna Terrace, which we will refer to as the 'rise basin'. A fourth component, arguably not a part of the GABB, is the Polda Trough, which lies beneath the continental shelf, north of the Ceduna Terrace.

EYRE SUB-BASIN

The north-northwesterly trending lines 65/1, 65/4, and 65/6 (Fig. 22) extend across the Eyre Sub-basin. Stratigraphic correlation is provided by 65/6 which passes over the Jerboa-1 well site (Survey time = 304.1804, Figs 4, 5, & 24).

The seismic data tend to confirm the gross easterly strike of the basin; however, the dominant east-northeasterly structural grain, and northwesterly cross-trends (Fig. 14), indicate that the basin margins may form an *en echelon* arrangement of normal and strike-slip (?transfer)

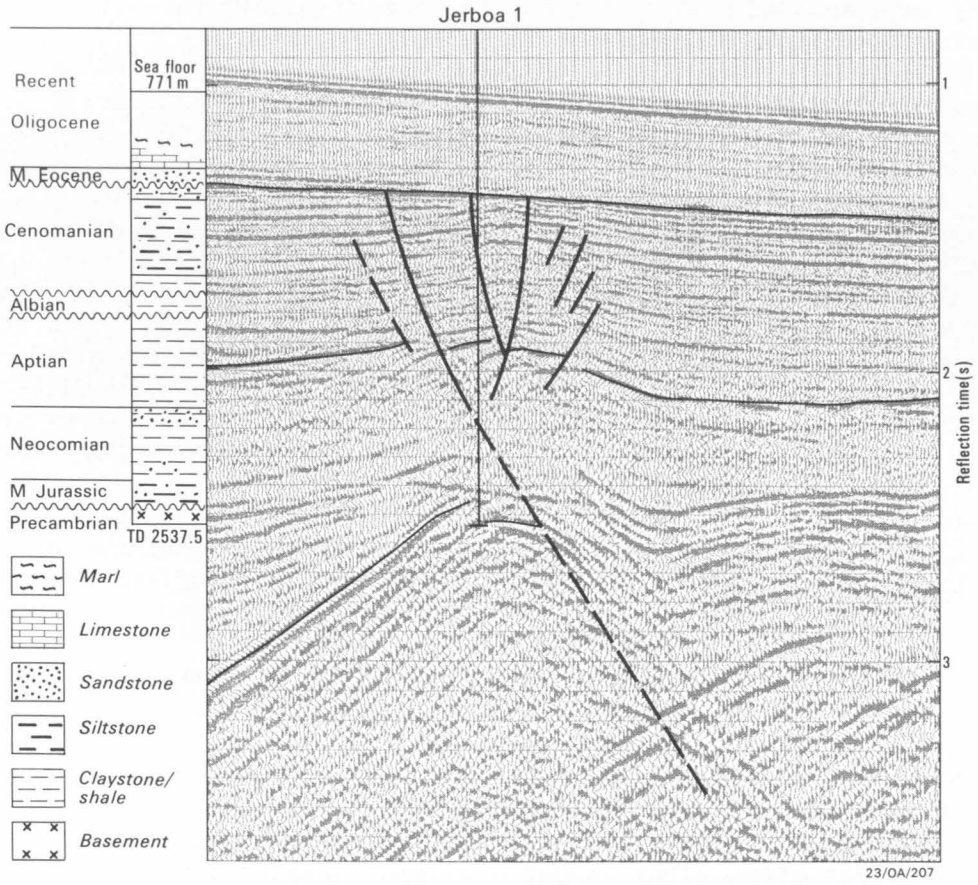

Figure 24: A portion of stacked seismic data for line 65/6, showing the correlation with Jerboa-1 stratigraphic/lithologic column.

faults. The basin appears to terminate in the west (at about 126 30 E) at a major fault. In the east it has the form of a single half-graben extending under the junction between the Eyre and Ceduna Terraces. The basin lies beneath the upper continental slope and the landward 50-60 percent of the Eyre Terrace.

The Eyre Sub-basin has developed over an extensional terrain, in which infra-rift fault-blocks are composed largely of crystalline Precambrian basement rocks of the flanking shield areas. This Precambrian basement was strongly planated prior to basin formation. The basin is underlain by two major rotated fault-blocks - the Wombat and Jerboa structures of Bein & Taylor (1981; Fig. 7). The bounding normal faults, which have southerly throws as much as 3000m, dip at about 35 degrees within the visible part of the section, but probably sole-out at depth.

Elevated Precambrian basement, which underlies the outermost 40 percent of the Eyre Terrace, lies adjacent to the southern edge of the fault-block complex at Jerboa. The relationship of the fault-blocks to the basement indicates that the basement must be underlain at depth by a detachment surface (soles of the fault-blocks) or that the basment surface is itself a detachment fault (Fig. 25).

The seismic characteristics of the fault-blocks around Jerboa are "softer" than for those on the Wombat structure and on the elevated basement area south of the basin. If it were not for the fact that Precambrian was penetrated at the well-site it would be reasonable to postulate that the "Jerboa blocks" are composed of Palaeozoic or early Jurassic sedimentary units. A similar situation exists on ESSO line E79A-3 where Bein & Taylor (1981) postulate the presence of Palaeozoic infra-rift sediments. However, it is possible that the soft seismic characteristic is created by the overlapping multiple events on this part of the monitor section.

The fault-blocks in the deepest part of the basin (that is around Jerboa) give rise to a complex of overlapping seismic events, many of which are not eliminated by migration processing. This phenomenon is probably created by the occurance of strike-slip faults (or possibly transfer faults) running almost parallel to the plane of the section. The basement structure map presented by Bein & Taylor (1981) shows a right-lateral structural offset between the Wombat and Jerboa features which could be due to a north-northwesterly striking transfer fault.

The sedimentary section in the deepest part of the Eyre Sub-basin exceeds 3 seconds record time (4000-5000 m). On the basis of the well tie, seven major sequences can be dated (Table 1), comprising infrarift, synrift, and post breakup units. It is evident that the elevated basement area along the southern margin of the basin was first transgressed in late Albian or Cenomanian time, but it is not clear if the older (underlying) sequences to the north and south of the basement area are of similar age and facies.

The presence of Upper Jurassic synrift sediments at the Jerboa well-site is especially significant, as it provides a minimum date for the onset of rifting on this portion of the margin. The only other proven occurrence of Jurassic sediments is further east, within the Polda Trough.

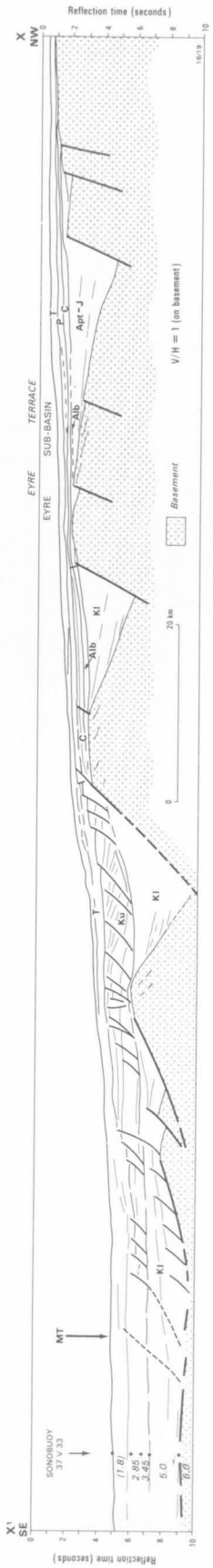

Figure 25: Line drawing of a Shell *Petrel* seismic line across the Eyre Sub-basin and continental rise (after Lister & others, in press).

Upper Boundary	Lower Boundary	Internal Configuration	Age	Facies	Comment
Seabed	Onlap – concordant	Continuous wedge; high amplitude	Tertiary; post-Early Oligocene	Carbonate	
Toplap – concordant	Downlap – concordant (onlap)	Prograding wedge	Paleocene – Eocene	Shelfal	Includes Eocene Hampton Sst; extends South to continental rise.
Concordant (some erosional trunc.)	Onlap	Continuous high amplitude	Albian – Cenomanian	Marine transgression	Onlaps & transgresses southern basement block; position on rise depocentre uncertain facies change under lower slope.
Concordant	Onlap	Discontinuous mixed amplitude	Neocomian – Aptian	Continental ?deltaic	Synrift sediments
Concordant – erosional truncation	Onlap	Low frequency wedge	Probably Late Jurassic	Continental	Synrift sediments
Boundaries obscured by multiples			Late Jurassic	?alluvial fans	Synrift sediments
Erosional truncation	Not evident	Low frequency parallel-bed.– complex	Precambrian ?some Palaeozoic	Crystallised sediments	Infra-rift

23/OA/266

Table 1: Seismic sequences, Eyre Sub-basin

The preliminary results indicate several problems which will need to be addressed:

1. The Eyre Sub-basin sequences are not necessarily a part of the Great Australian Bight Basin, nor are they necessarily related to the continental rise section to the south.

2. Rift-onset occurred in the pre-Late Jurassic in the Eyre Sub-basin, but the precise age of rift-onset in the Great Australian Bight Basin has yet to be proven. In the Otway Basin, the first stage of rift-onset is believed to be Early Cretaceous.

3. Structural trends in the Eyre Sub-basin are east-northeast, whereas in the Otway Basin area they are west-northwest. What is the direction of continental extension in the GAB Basin?

4. Both the Polda Trough and the Eyre Sub-basin are complex half-grabens which strike east-west and apparently join end to end, and both are separated from the Great Australian Bight Basin by an elevated area of crystalline basement. However, the Polda Trough contains older Permo-Carboniferous or even Cambro-Ordovician sediments. Are these features structurally related, with the Polda Trough Palaeozoic sediments being preserved within a Mesozoic graben, or was the Polda Trough an old line of weakness which extended westwards to forma a foundation for the Eyre Sub-basin (ie infra-rift)?

SEDIMENTS BENEATH THE SOUTHWESTERN CEDUNA TERRACE

A regional grid of lines was located on the southwestern part of the Ceduna Terrace (65/2, 3, 7, 8, 9, 12, and 13; Fig. 22) with line 65/3 providing a tie through Potoroo-1. In addition, a transect line, with up to 10 seconds sub-seabed recording, was run from the abyssal plain, across the Great Australian Bight Basin, to the northern edge of the Polda Trough (65/15). The transect was on an azimuth of 027 degrees, which is parallel to the measured direction of extension in the Bass and Gippsland Basins, and the surmised direction of extension in the Otway Basin. One of its objectives was to test for a similar extension direction in the Great Australian Bight Basin.

The thick sub-parallel bedded section on the Ceduna Terrace, and the presence of a strong multiple event on the seismic monitors, prevent any worthwhile analysis of the seismic stratigraphy in this preliminary interpretation. However, the Ceduna Terrace lines (*eg* 65/7) show several features which are of significance to our understanding of the tectonics of the region:

1. Figure 26 shows a thick prograded sequence with large scale forset beds which has been discussed by Fraser and Tilbury (1979). This sequence thins to the southwest and passes into a deep-water (prodeltaic) facies just beyond the outer edge of the Ceduna Terrace. The prograded sequence is bounded by unconformities of Cenomanian and Maastrichtian age (Horizons B and C of Fraser & Tilbury) and this provides a reference for the ages of other features on the lower continental slope.

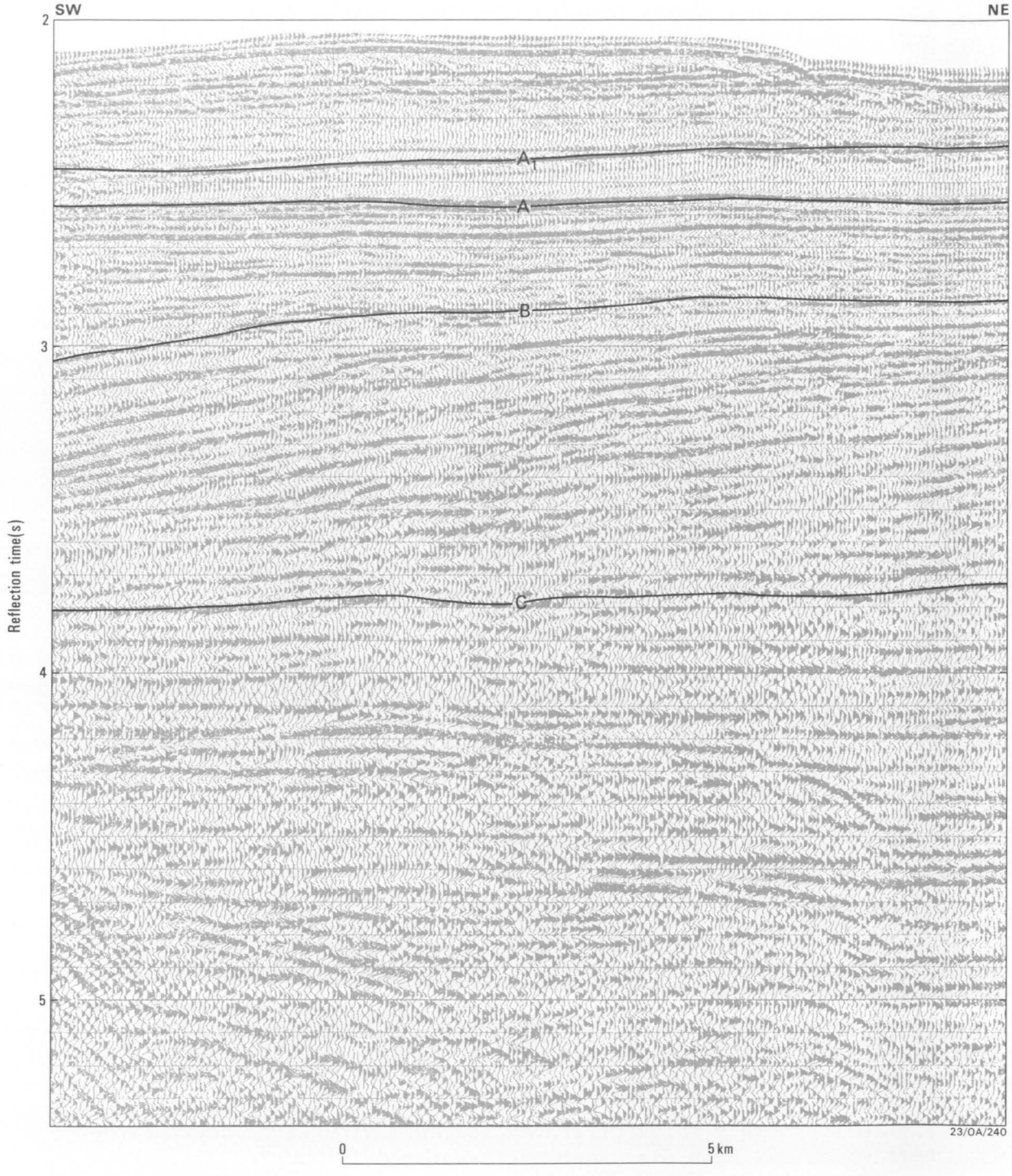

Figure 26: A portion of stacked seismic data for line 65/7, showing a prograding deltaic sequence (B-C) bounded by Maastrichtian and Cenomanian unconformities (as discussed by Fraser & Tilbury, 1979).

2. Figures 27 and 28 show faulted anticlines which underlie the lower continental slope along the southwestern margin of the Ceduna Terrace. The anticlinal crests are fractured and the entire structures appear to have been overthrust. They are considered to have formed in a "transpressional" environment in the pre-Cenomanian, probably shortly after the Albian marine transgression. These features may reflect movement on a transfer fault, trending north-northwest, and separating the Great Australian Bight Basin proper from the deep-seated rise basin to its southwest.

3. Figure 29 shows several cuspate features and diffractions which are considered to form a positive flower structure. Such features are usually indicative of wrench zones. Their location along the continental rise/lower continental slope boundary, southwest of the Ceduna Terrace, is further evidence for a strike-slip fault.

SEDIMENTS BENEATH THE CONTINENTAL RISE

A regional network of four NNW-trending lines (65/1, 4, 6, 10; Fig. 22) and four ENE-trending lines (65/2, 3, 7, 9) was designed to investigate the continental rise south of the Eyre Terrace. A further two lines (65/14, 15) extended across the rise to the south of the Ceduna Terrace.

The continental rise south of the Eyre Terrace is underlain by an abnormally thick sedimentary section (about 4000-6000 m) which appears to be a deep-seated part of the Great Australian Bight Basin. A tentative stratigraphic correlation can be made from this area, across the southwest margin of the Ceduna Terrace, to Potoroo-1 well. However, the well is situated in an unfavourable location, being on the very northern extremity of the Great Australian Bight Basin, where the sedimentary section is attenuated. There is no direct correlation between the rise sequences and Jerboa-1 well, except for the uppermost Cretaceous and Tertiary strata. An extensive area of elevated Precambrian basement, and a steep continental slope, separates the "rise basin" from the Eyre Sub-basin. Although the two basins are usually considered to be genetically related, there is no obvious evidence for this in the seismic data. As discussed above, the Eyre Sub-basin may be an older feature that connects with the Polda Trough. The structural trends within the rise basin will require detailed mapping to test this hypothesis.

South of the Eyre Terrace, the rise basin extends for more than 150 km, from the steep continental slope to a basement hummock which marks the continent/ocean boundary (COB) at about 36 S. The Precambrian surface at the northern boundary dips southwards at 30 degrees, and is interpreted as a major detachment fault. This fault underlies several rotated fault-blocks near the basin margin, but these disappear from view further south, due to the thick sediment cover. The seismic data support the concept that the rise basin is underlain by a highly extended continental terrain. The basin extends eastwards to south of the Ceduna Terrace, where it is much narrower (<50 km); the COB, which also marks the southern limit of the rise, strikes more or less east-west. The northern boundary fault, separating the rise from the thick section beneath the Ceduna Terrace,

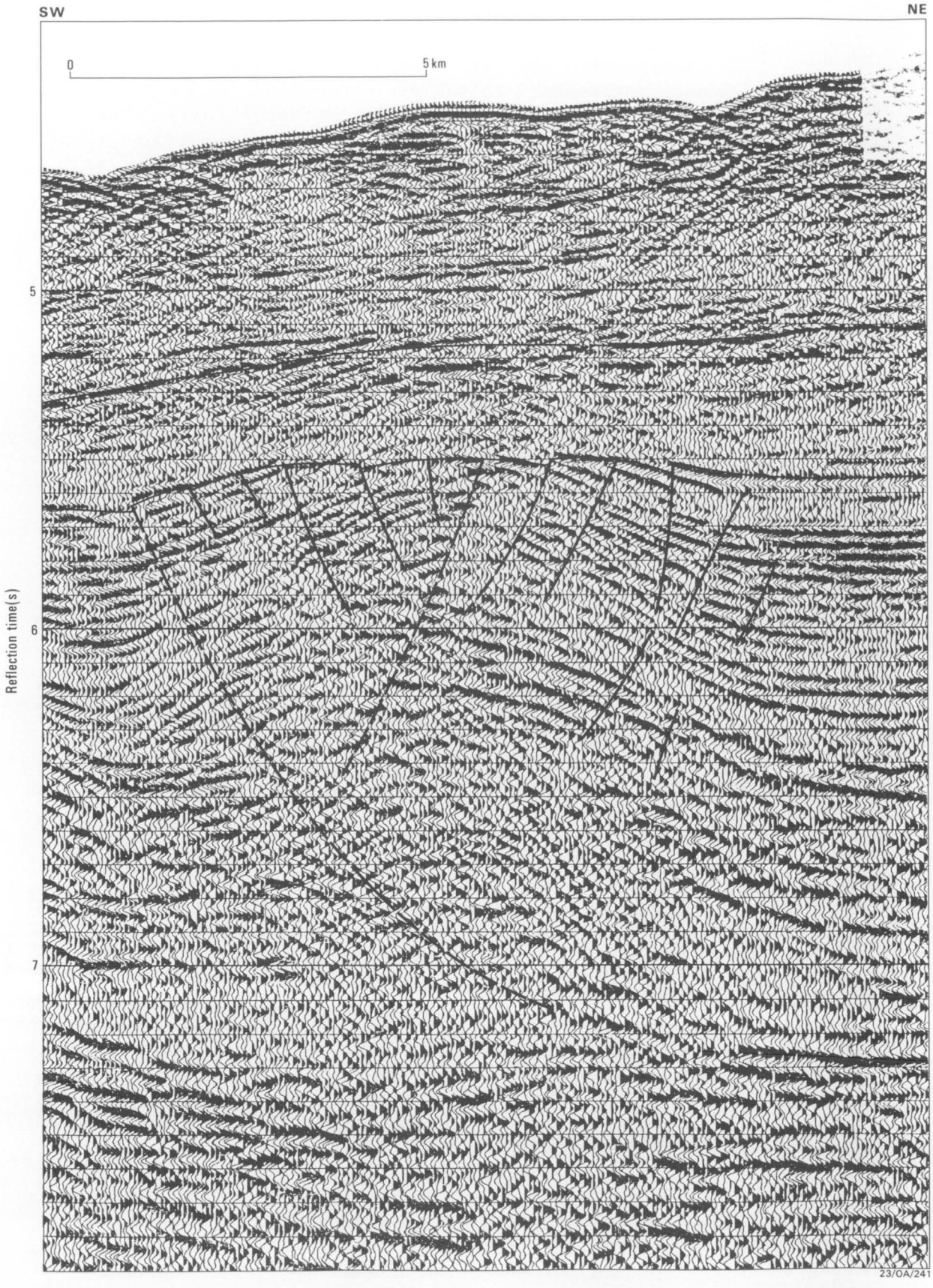

Figure 27: A portion of stacked seismic data for line 65/7, across the southwest flank of the Ceduna Terrace, showing a faulted anticline and thrust plane possibly generated by transpressional tectonism.

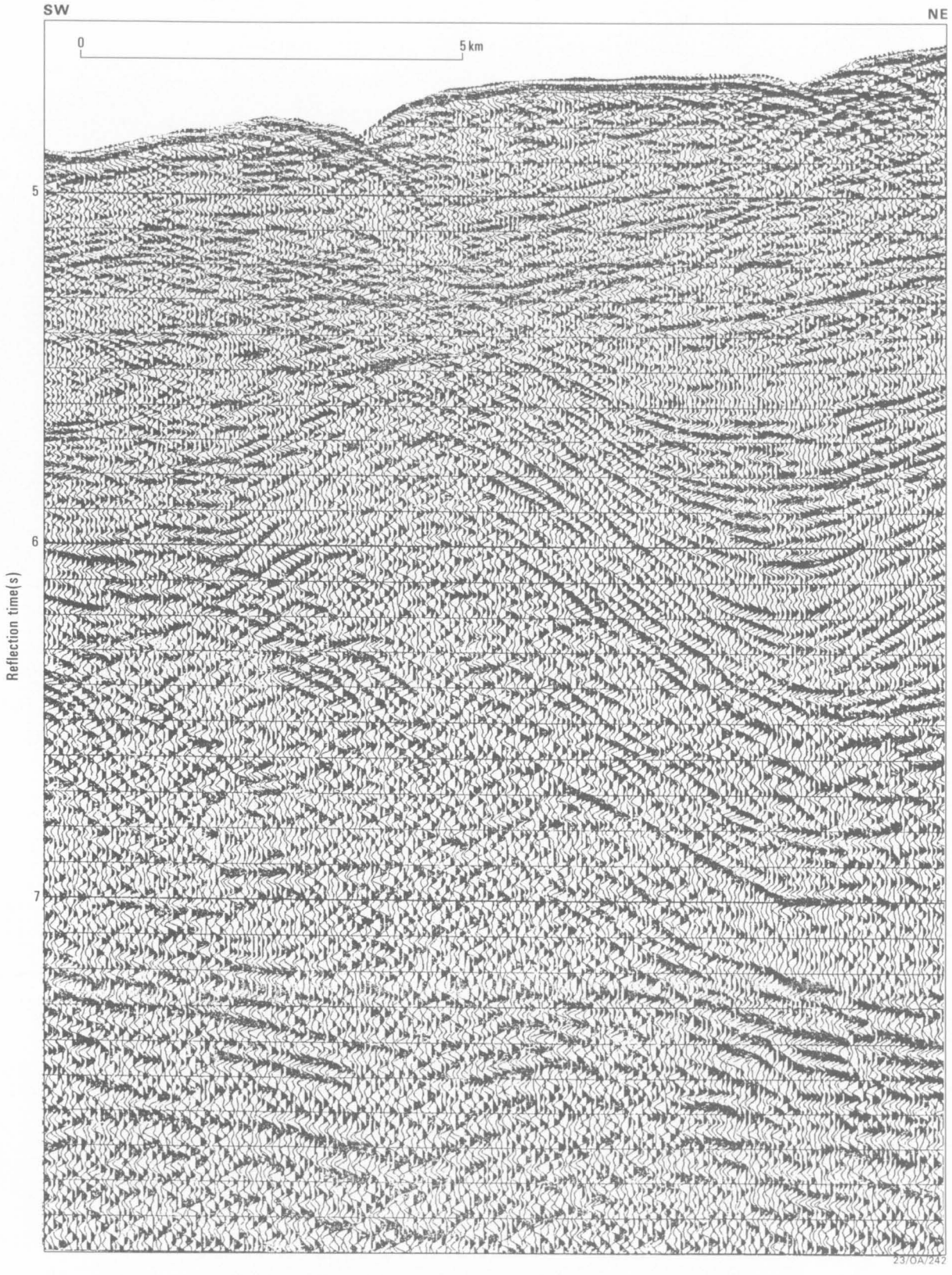

Figure 28: Possible transpressional structure on the southwest flank of the Ceduna Terrace (see also Fig. 27); stacked seismic data line 65/7.

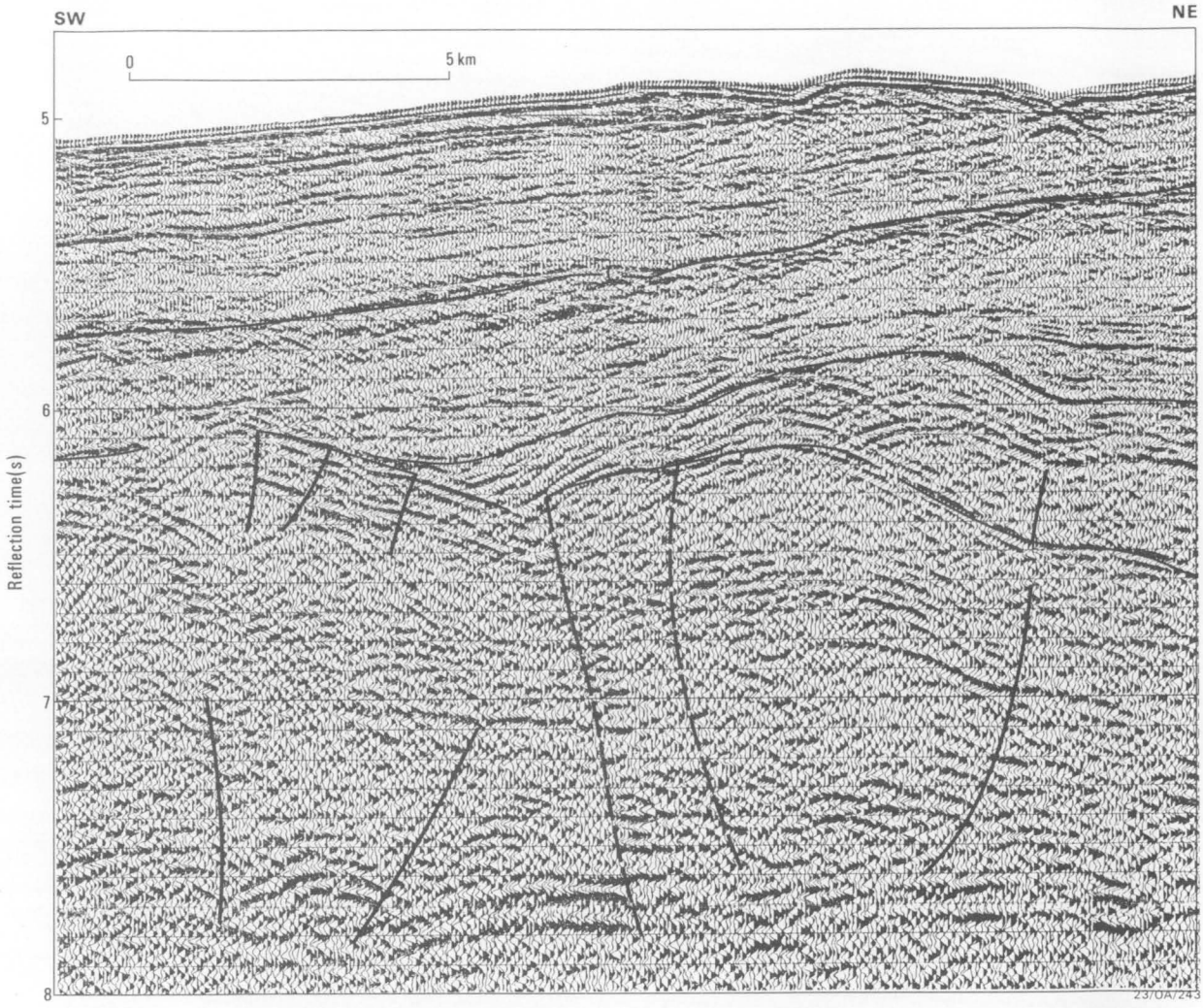

Figure 29: Part of a positive flower structure overlying a probable wrench zone beneath the southwest flank of the Ceduna Terrace; stacked seismic data from line 65/7.

appears to be Early Cretaceous, and in this area the southern boundary is also a basement hummock.

Seismic sections across the continental rise show many unconformities in the upper 2-2.5 s (2000-3000 m) of section below sea floor (b.s.f.) and faint low frequency reflectors down to about 5 s b.s.f. The lowermost unconformities (in most places two unconformities, J and K; Figs 30 & 31) are affected by draping and minor faulting which is probably caused by reactivation of deep-seated fault-blocks. The upper unconformities (in most places 9 can be identified, A - I; Figs 30 & 31) divide the sedimentary section into wedges, some of which prograde from near the northern boundary of the basin. The wedges grade into near horizontal layers about 50 km further south.

Precise dating of the unconformities cannot be attempted from the monitor records; however, previous studies (Boeuf & Doust, 1975; Willcox, 1978) indicate that, on the basis of the gross seismic character, both Cretaceous and Tertiary sequences are to be expected under the rise. From the stratigraphic position of unconformity J (Fig. 30), and the clearly recognisable onlap of the overlying sequence (I - J), it is plausible that unconformity J is at the base of the Albian marine transgressive sequence identified at the well-sites.

The relatively strong unconformity E, and onlap of the overlying sequence D-E, may define renewed subsidence of the continental margin at the start of the present episode of normal spreading in the mid-Eocene (42 Ma, Anomaly 18). This would be consistant with observations from the continental slope in the Otway Basin where Hinz and others (1987) recognise a mid-Eocene unconformity as the fifth below the seabed (Figs. 32 & 33).

On the basis of the Otway interpretation, unconformity C should relate to the Early Oligocene onset of full oceanic circulation, which followed clearance of the Australian and Antarctic Plates (35 Ma, Anomaly 13). This unconformity is widespread in the Southern Ocean, but is not as well defined in the rise basin as in the Otway Basin/South Tasman Rise region.

The unconformities F, G and H appear to separate progradational sequences at the northern edge of the rise basin (Fig. 31). Similar unconformities, of Paleocene to middle Eocene age, are associated with prograding in the Otway and West Tasmanian margin.

POLDA TROUGH

Because the greater part of the Polda Trough is located on the continental shelf in water depths of 80-100 m, the seismic monitor records are severely degraded by water-bottom multiples, ringing, and refracted arrivals from shallow high-velocity basement. It is anticipated that post-cruise processing will produce significantly enhanced data, so at this stage only a brief description of the more obvious and significant features is given.

The seismic monitor records from this cruise suggest that the Polda Trough is a rift graben, 20 km wide, trending close to east-west, with a sedimentary fill of at least 2.5 s. The structure can readily be traced from east to west on lines 65/101 to 65/104 and also line 65/15, but the westward extension of the trough through lines 65/105 and 65/106 is not

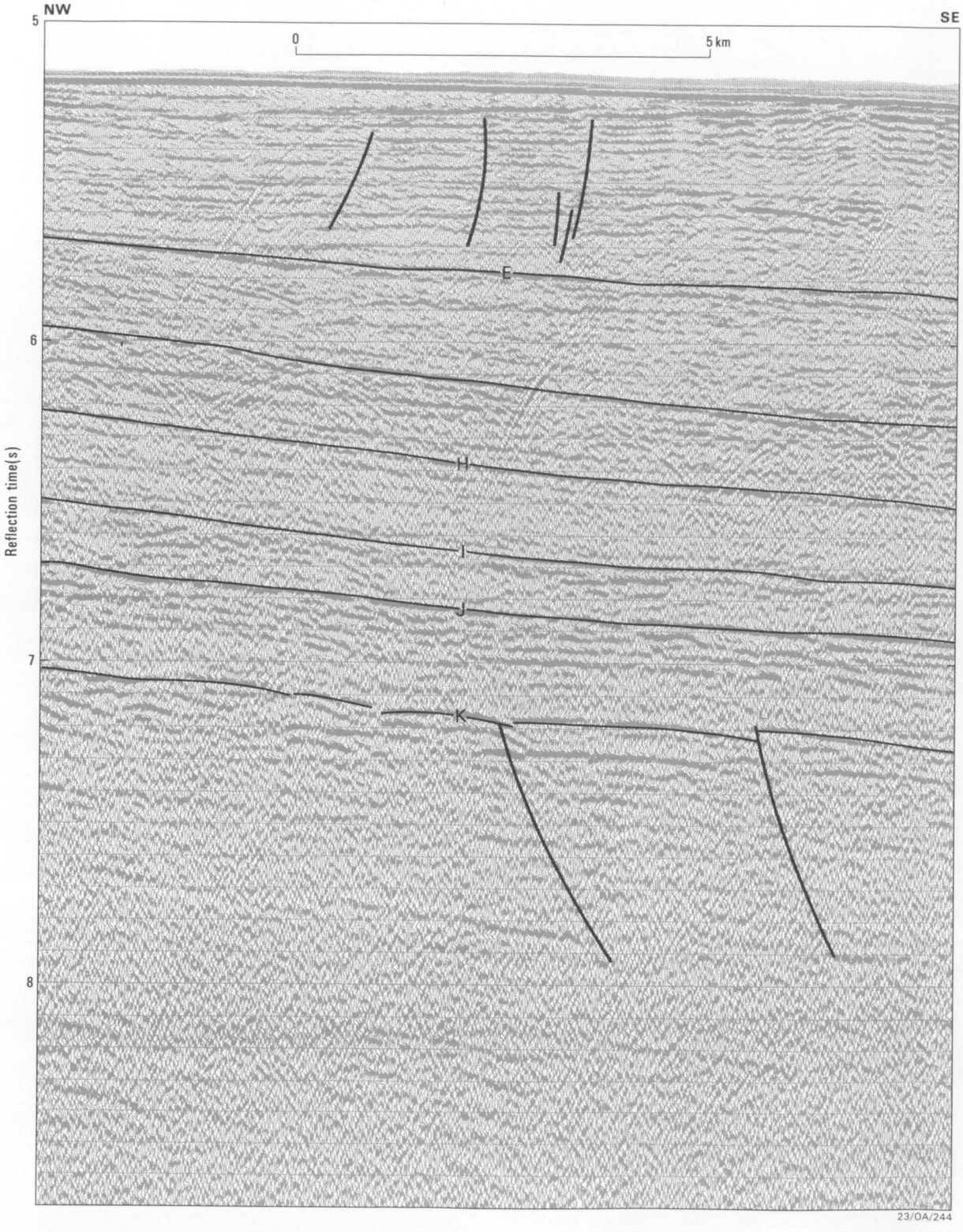

Figure 30: Unconformities beneath the continental rise south of the Eyre Terrace; stacked seismic data from line 65/4.

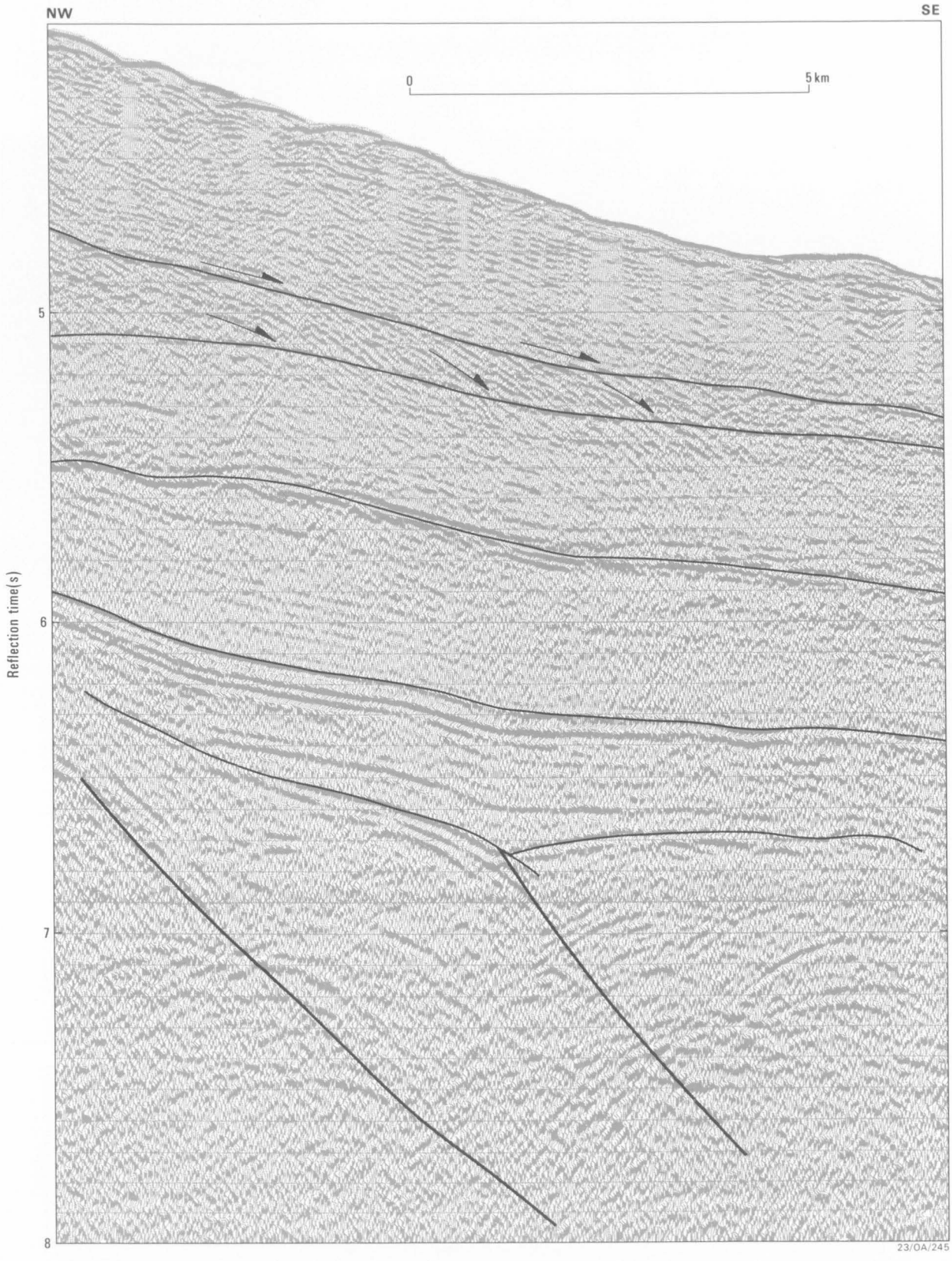

Figure 31: Unconformities beneath the inner continental rise, south of the Eyre terrace, bounding sediment wedges, some of which show progradation; stacked seismic data from line 65/4.

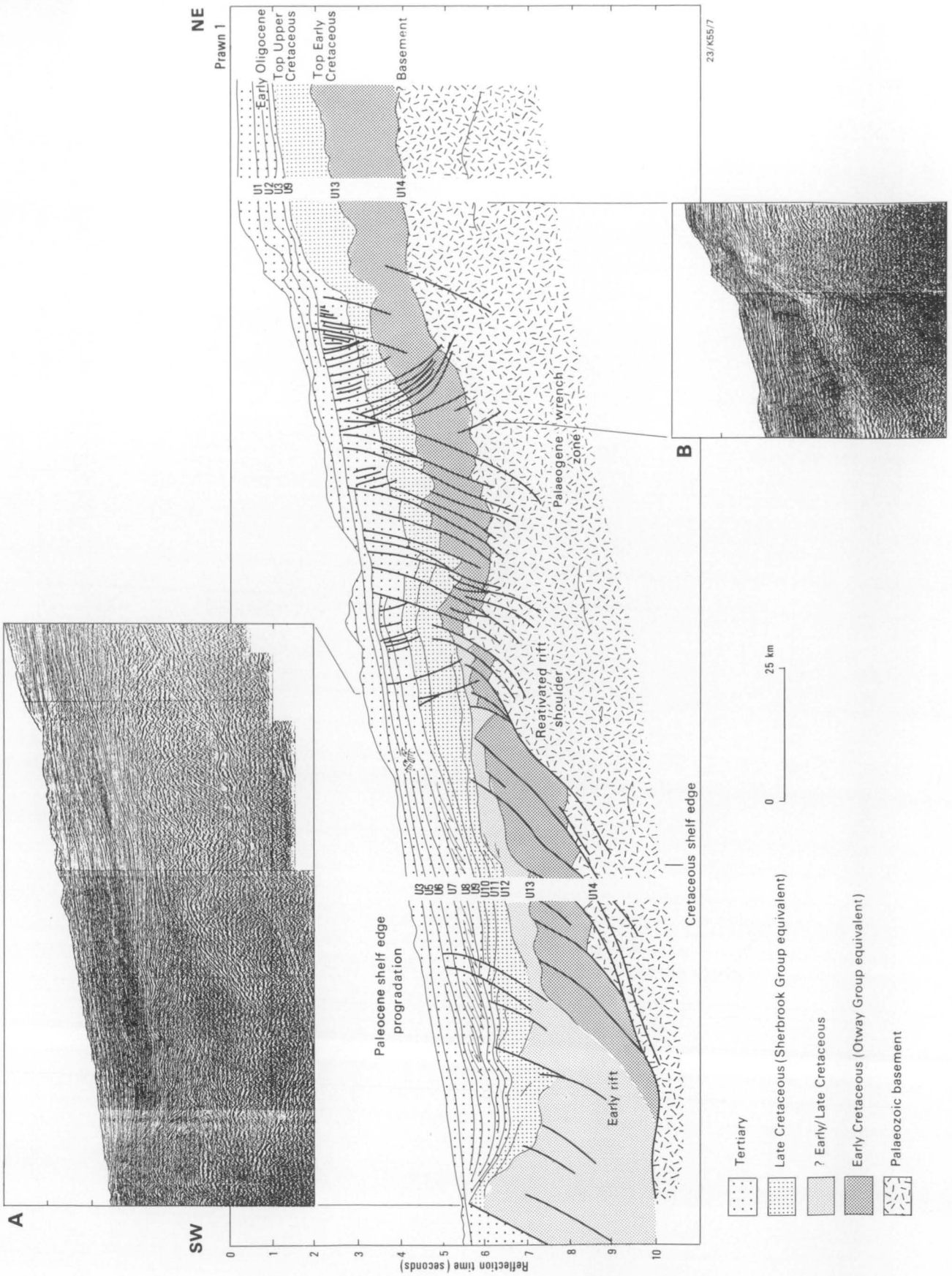

Figure 32: Interpretation of seismic profiles 40-22/23, tied tentatively to Prawn-3 (after Hinz & others, 1987). Unconformities U1 to U14 are described in Figure 33. A. Seismic detail of Palaeocene-earliest Eocene shelf edge progradation. B. Seismic detail showing uncertainties in shelf to slope correlation.

Unconform (Sequence)	Characteristics	Tectonic Significance	Facies Interpretation	Approx Thickness (m)	Proposed Age Identification			Otway Basin Shelf Equivalent and Unconformities	Comment
					Stratigraphic	m.y.	Equivalent Mag Anom		
	Low frequency, stratified and folded Floors Jurassic or Early Cretaceous rift beneath the lower continental slope	Pre–rift Tasman Geosyncline Crustal extension and first stage rifting at about U14 time	Varied metasediments and volcanics	Unknown	Palaeozoic and ? Precambrian				"Basement"
U14						? 140			
S(13–14)	Low frequency, stratified on rift shoulder		Continental–? fluvial, lacustrine	1000	Jurassic and Early Cretaceous		M Series	Casterton Beds and Otway Group Non–marine clastics and volcanogenic sediments	
	Contorted fill in first stage rift	Lower rift–fill	Alluvial fan and/or volcanics	3000 +					
U13						105			
S(12–13)	Bedded fill in first stage rift Now incorporated into tilted blocks beneath lower continental slope	Upper rift–fill, probably preceding marine transgression ? Development of shelf edge on U12	Fluvial–lacustrine possibly grading to marginal marine	0–?1000	"late" Early Cretaceous (? Albian)			Probably time equivalent to Eumeralla Formation (Otway Gp) Continental environments with volcanism	This sequence appears confined to the first stage rift
U12						95	34		
S(11–12)	Well stratified with onlap onto U12 U12/13 block–faulted beneath continental shelf	U12 (possibly U13) is main rift–onset unconformity in Otway Basin S(11–12) marine transgression	Marginal marine–marine (foram evidence from Ribis and Apthorpe, 1969)	0–?1000	Late Cretaceous (approx Cenomanian)		Slow spreading episode (Cande and Mutter, 1982)	Approximate Waarre Formation (Sherbrook Group) equivalent Shoreline facies	Wrenching and uplift of the tilted blocks beneath lower slope commenced (Willcox and Symonds, in preparation)
U11									
S(10–11)	Stratified sediment wedge with onlap onto U11 Basal channelling land ward of old shelf edge	U11 eustatic lowstand in ? Coniacian (Vail et al., 1977) S(10–11) basin transgr restricted by blocks below lower continental slope	Shallow marine (restricted basin)	0–1000 +	Late Cretaceous			Belfast Mudstone and Flaxman Formation (Sherbrook Group) Marginal marine–marine	1570 m Belfast Mudstone in Voluta 1
U10									
S(9–10)	Stratified sediment wedging out below lower slope Downlap onto U10	U9 and U10 relative falls in sea level U9–slowing or termination of movement of tilted blocks beneath lower slope	Shallow marine (regressive)	0–500 +	Late Cretaceous (approx Maastrichtian)			Curdies/Paaratte Formations (Sherbrook Group) Shoreline–continental	Slow spreading episode in southeast Indian Ocean has less influence on outer Otway Basin
U9						65	29		
S(8–9)	S(5–6) to S(8–9) are distinctive, high frequency, downlapping sequences beneath lower continental slope Lower frequency, continuous, high amplitude beneath upper continental slope	A period of minimal subsidence in the outer Otway Basin due to contact between Australian and Antarctic plates in Tasmanian region Sedimentation influenced by elevated blocks beneath lower continental slope Outbuilding of fine clastics with minimal aggradation Unconformities largely reflect eustatic changes in sea level	Shelf clastics, grading into fine grained progradational wedges at palaeoshelf–edge (largely terrigenous)	200–1500	Paleocene— Middle Eocene		?	Age equivalent of the Wangerrip Group Shallow marine→shoreface→ continental (regressive)	Sequences S(5–6) to S(8–9) are believed equivalent to depositional cycles TP1, TP2, TE1 and ? TE2 of Vail et al., (1977)
U8									
S(7–8)									
U7									
S(6–7)									
U6									
S(5–6)									
U5						42	18	? ?	
S(4–5)	Stratified, onlapping S(3–4) extends across outer tilted blocks	Accelerated movement along Australian–Antarctic plate boundary Major wrenching and development of flower structures in southeast Otway Basin and western margin of Tasmania	Shallow marine (largely terrigenous)	0–800	Late Eocene— earliest Oligocene			Nirranda Group (transgressive) — shallow marine	? Minor volcanism at U5 time
U4									
S(3–4)									
U3						35	13		
S(2–3)	Stratified, channelled, shelf–edge progradation	U3 is widespread Early Oligocene unconformity marking clearance of Australian and Antarctic plates and establishment of open marine conditions	Shelf–open marine (largely carbonate)	0–600	Late Oligocene and Neogene		Southeast Indian Ocean spreading	Heytesbury Group (transgressive) marine carbonates	Main episode of seafloor spreading
U2									
S(1–2)									
U1									

23/K55/15

*For stratigraphy refer to BMR line 22/23 (Figure)

Figure 33: Correlation of seismic-stratigraphic sequences with unconformities and tectonic events in the southeast Otway Basin and the western Tasmanian margin (after Hinz & others, 1987).

defined on the monitor records.

The question of how far the Polda Trough extends to the west and the nature of its termermination may be resolved once the processed sections become available. The monitor records allow only a blurred view of the sedimentary sequences within the trough, and even Gawler Block basement is commonly difficult to identify and follow. Previous attempts to map sequences, such as the Jurassic, deep within the trough have not met with much success, and it is hoped that our processed data will provide new insight into the early tectonic and sedimentary evolution of the Polda Trough.

Gravity

On lines 65/101 - 65/104 the Polda Trough is expressed in the gravity profiles (Fig. 34) as a 20 mGal deep, E-W trending depression. The continental shelf in this area varies smoothly in depth from 80-100 m; consequently, terrain effects should be minimal, and the gravity field should reflect geological structures. In contrast, in the SW part of Figure 34, water depths increase rapidly and irregularly on the canyon-dominated upper slope. Because of the appreciable terrain effects, the known structural complexity, and increased water-depth, delineation of the westward extent of the Polda Trough is probably not feasible with the gravity data.

Comparison of gravity anomalies seen in the profiles (making due allowance for effects of seafloor topography) with seismic basement depths as mapped by earlier work, reveals general correlation.

The southern extremity of the D'Entrecasteaux regional gravity ridge - a structure within Gawler Block basement to the north-west of the Polda Trough (Willcox,1978), appears in the gravity profiles as a 60 mGal high.

Magnetics

The metamorphic and igneous rocks of the Gawler Block basement appear to include a high proportion of highly magnetised units; this greatly simplifies the delineation of sediment accummulations such as the Polda Trough.

As can be seen in the magnetic anomaly profile map (Fig. 35), the Polda Trough is characterized by a pronounced smooth magnetic low. The basin thus delineated is about 20 km wide and coincides closely with the location of the trough as defined by previous seismic surveys and aeromagnetic mapping.

At crossings of the inferred basin margins from the basin side, an abrupt transition from smooth variation to relatively short wave-length anomalies is commonly seen in the profiles. This suggests rapid shallowing of basement - consistent with large-throw, high-angle faulting of magnetic basement.

Long-wavelength anomalies WSW of the mapped Polda Trough reflect greater source depth (?magnetic basement) due to deeper water (to 800m) off the edge of the shelf and a thicker sedimentary section, which may include down-faulted blocks of the Polda Trough sequence.

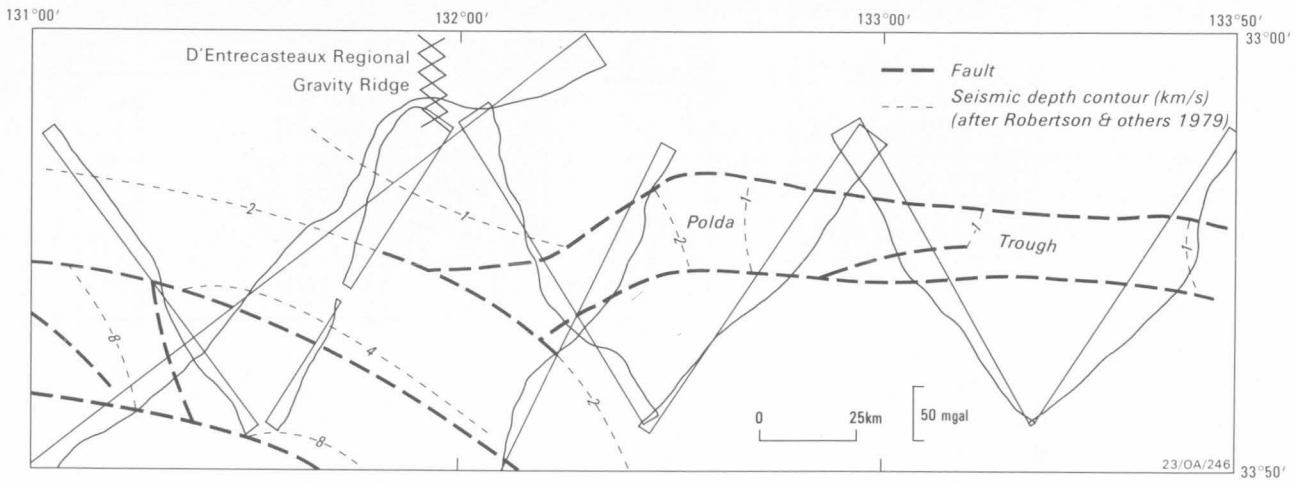

Figure 34: Free-air gravity profiles across the Polda Trough acquired during Leg 1. Major tectonic features are also shown.

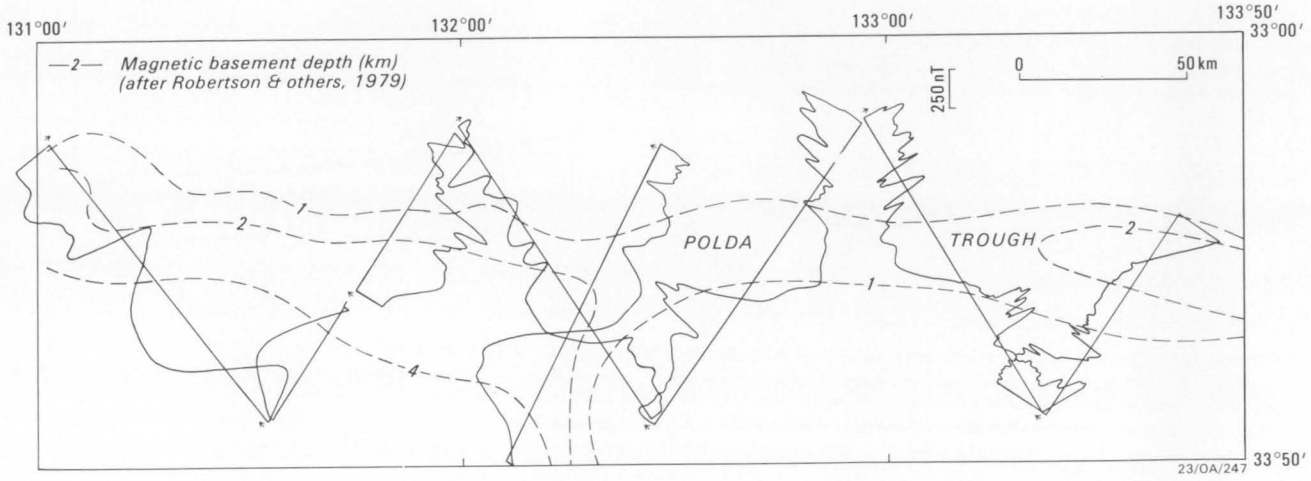

Figure 35: Magnetic anomaly profiles across the Polda Trough acquired during Leg 1. Major tectonic features are also shown.

MAGNETIC SPREADING ANOMALIES - TECTONIC IMPLICATIONS (JJV)

Magnetic profiles along Lines 65/13, 65/14, and 65/15 across the COB off the southwestern Ceduna Terrace (Figs 36 & 37) contain the following features, previously identified by Veevers (1986, 1987):

1. Seafloor spreading anomaly A34, at the edge of the Cretaceous long normal-polarity interval (KLNPI) or Cretaceous Quiet Zone (86 Ma);

2. The KLNPI from 86 Ma to the COB (96 Ma), including part of

3. the COB magnetic anomaly, defined by a crest (A22 of Weissel & Hayes, 1972) on either side of flanking slopes, with the COB interpreted as about mid-way down the landward flank, corresponding in the seismic profile to the landward edge of an envelope of diffraction events, and

4. the magnetic trough (MT) (Table 2), as defined by Talwani & others (1979), which bisects the study area on an easterly trend and bends southward at either end (Figs 38 & 39), in sympathy with the trend of the COB, as does the equivalent feature in conjugate Antarctica.

Off Australia and the conjugate part of Antarctica, the apparent lineation of A34 and younger anomalies out to A20, as indicated on N-S lines >100 km apart, is E-W. The detailed survey seaward of the Ceduna Terrace between 130 30' and 131 E suggests a refinement of the lineation trend. A34 is identified at the oceanward foot of the COB anomaly (bb') (see the block model in Fig. 40) and its trend is 075 , roughly parallel to other equivalent parts (a,c,d) of the magnetic profiles, and to a ridge (e) in the oceanic basement (Fig. 41). The implied spreading direction of 075 + 90 = 165 agrees with the synthetic spreading direction derived from the motion of Antarctica relative to Australia during the stage of slow drifting from the position at breakup (96 Ma) to A20 (44 Ma) by a rotation of -6.82 about a pole at 35.74 S, 73.85 E (Veevers, 1987; Veevers & Eittreim, in prep.; Fig. 42). J.B. Willcox (pers. comm.) has noted a 075 trend in some LDGO profiles further west. The strike of the older magnetic anomalies, that is A31-A34, was determined during Leg 2 by detailed magnetic surveying at about longitude 127 E. It was confirmed that these anomalies trend 090 (Fig. 43).

The trend of the crest of the COB anomaly bends at 16/136 from westerly (towards 65/14) to southeasterly (towards 65/15), in sympathy with the trend of the COB. The westerly trend continues to 127 E and the east-southeasterly trend to about 131 30'E (see Fig. 38A), beyond which an easterly trend is resumed to 133 E. Together with the east-southeasterly parallel offset of the conjugate Antarctic margin (cf A and B in Fig. 38), this offset is the chief constraint on the E-W fit of the Australian and Antarctic COBs.

The ESE trend is parallel to the trend of the deep faults of the Ceduna Terrace and the Duntroon, Otway, Bass and Gippsland Basins, and at a right-angle to the trend of the transfer faults of the Bass Basin (Etheridge & others, 1985), which is taken as indicating the direction of continental extension in the mid-Jurassic to mid-Cretaceous pre-breakup stage in the suture zone of Australia/Antarctica. The two trends are particularly clear in the COB of the southern margin between 127 and 138 E

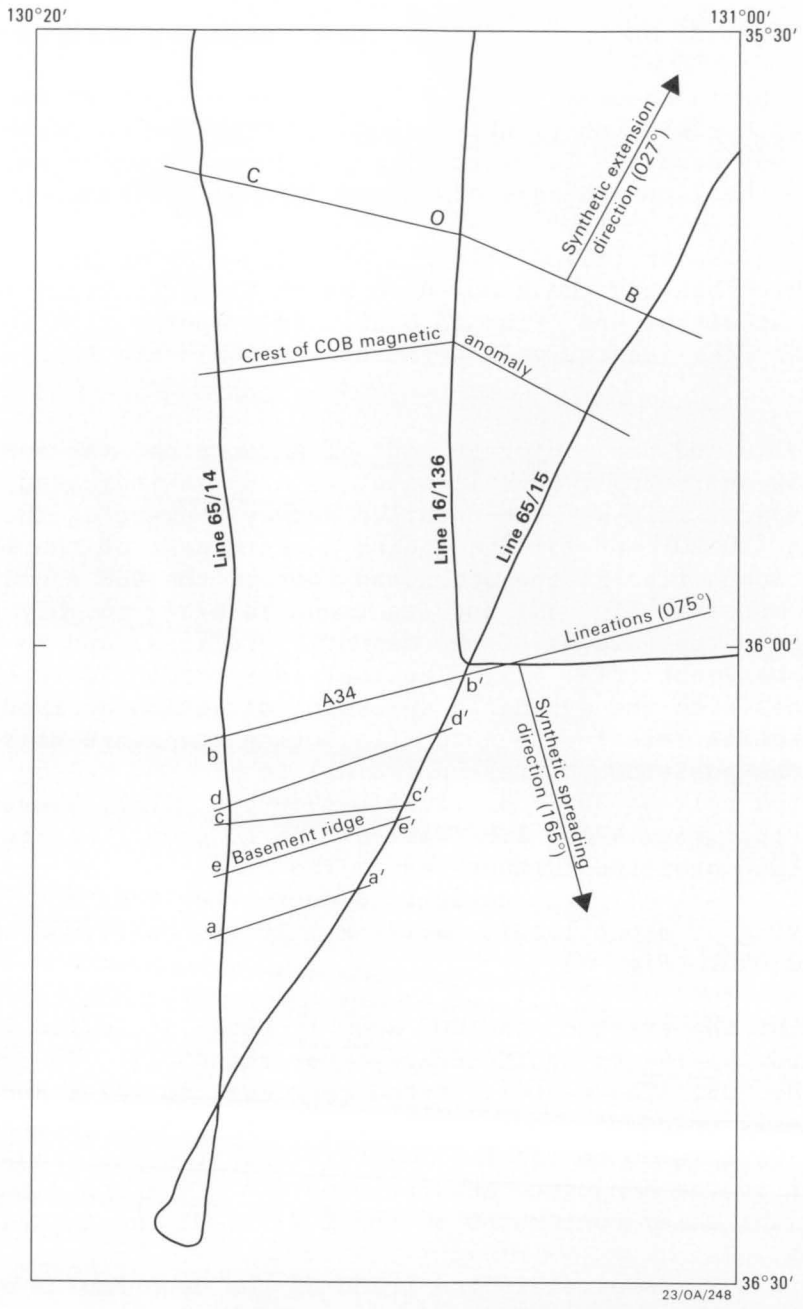

Figure 36: Tracks of Surveys 65 (lines 65/14, 15) and 16 (line 16/136), showing the principal magnetic features referred to in the text.

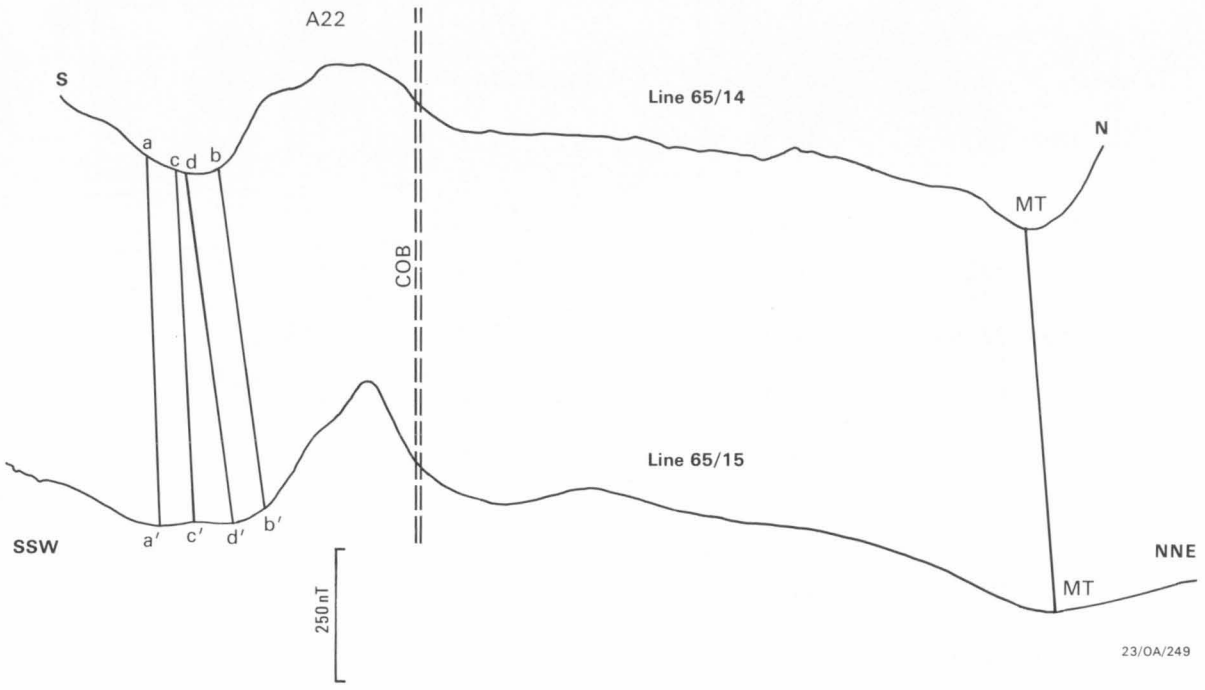

Figure 37: magnetic anomaly profiles along lines 65/14 and 65/15, showing the principal magnetic features referred to in the text.

Table 2: Location, arranged from east to west, and value of axis of magnetic trough.

Line	GMT	Latitude S	Longitude E	Value (nT)
1	293.1627	34 16.5'	127 04.2	-8
4	303.1830	34 12.5'	127 29.8'	-20
6	305.0218	34 14.4'	128 07.0'	-119
10	307.2240	34 17.5'	128 52.9'	-84
3	302.1630	34 14.5'	128 55.7'	-96
7	305.2235	34 19.4'	129 26.3'	-36
2	296.1430	34 21'	130 02'	-92
13	310.0224	34 22.0'	130 11.3'	-105
8	306.1754	34 22.7'	130 30.0'	-101
15	312.1600	34 29.2'	131 41.6'	-166

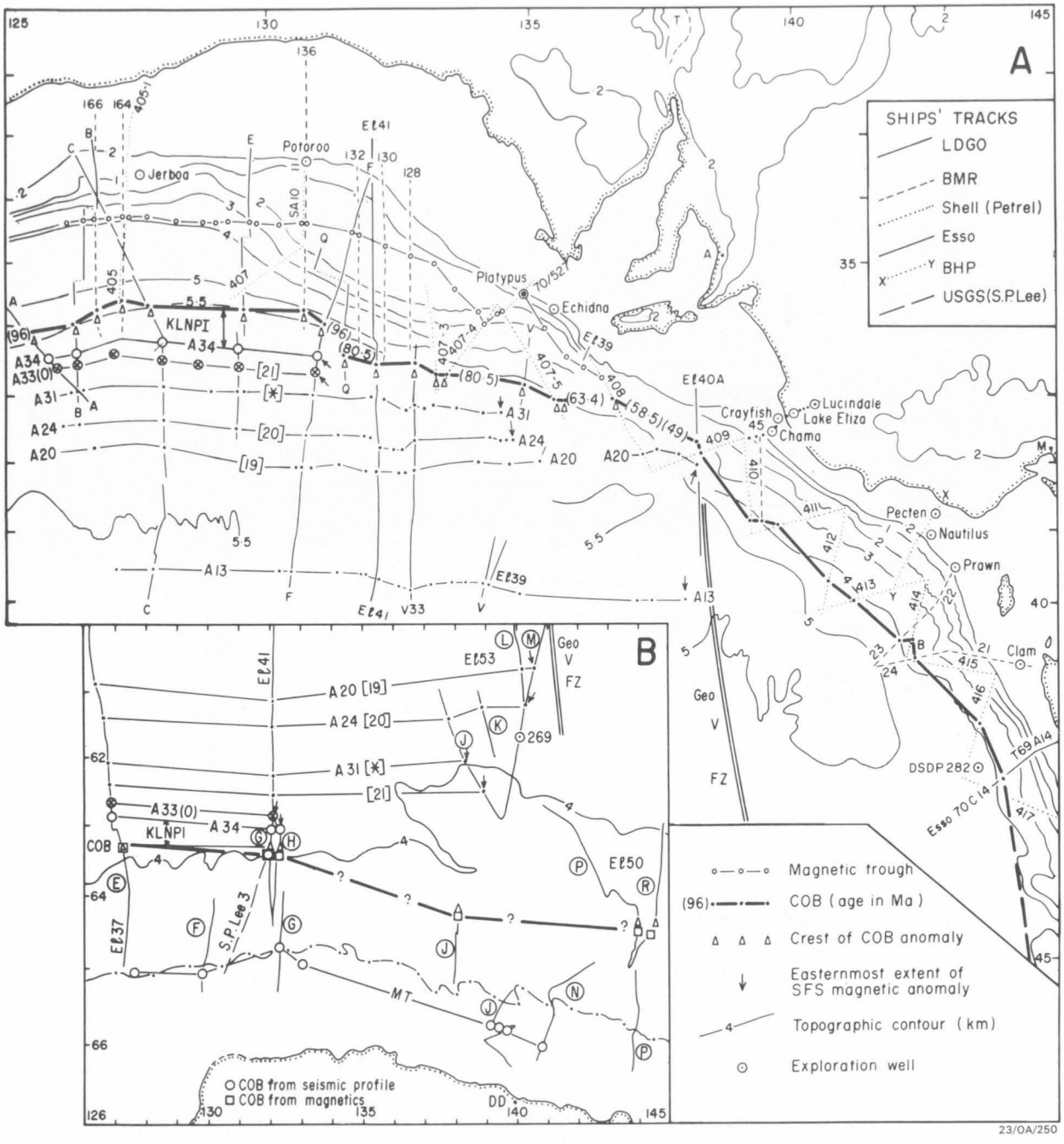

Figure 38: A. Southern Australian margin between 125 E and 145 E showing selected ships tracks of BMR, L-DGO, Shell, Esso, and BHP, seafloor spreading magnetic anomalies, continent-ocean boundary, exploration wells, and bathymetry. B. Wilkes Land, Antarctica, at similar scale to A, and conjugate with Australian sector west of line 408, showing location of ships tracks, seafloor spreading magnetic anomalies, continent-ocean boundary, COB anomaly crest, and magnetic trough (MT) (after Veevers, 1986).

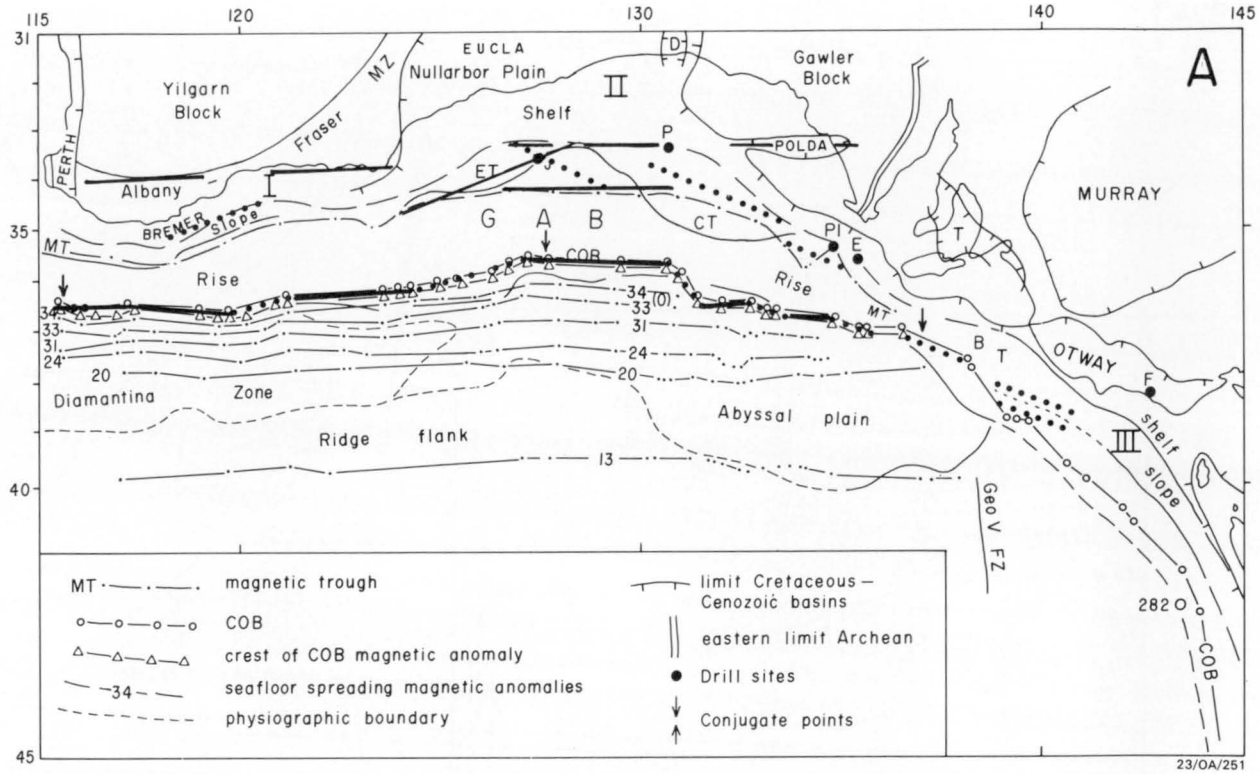

Figure 39: Southern margin of Australia, showing the magnetic trough, COB, COB magnetic anomaly, seafloor spreading magnetic anomalies, and the principal physiographic boundaries (modified from Veevers, 1987; reprinted by permission of Circum-Pacific Council for Energy and Mineral Resources).

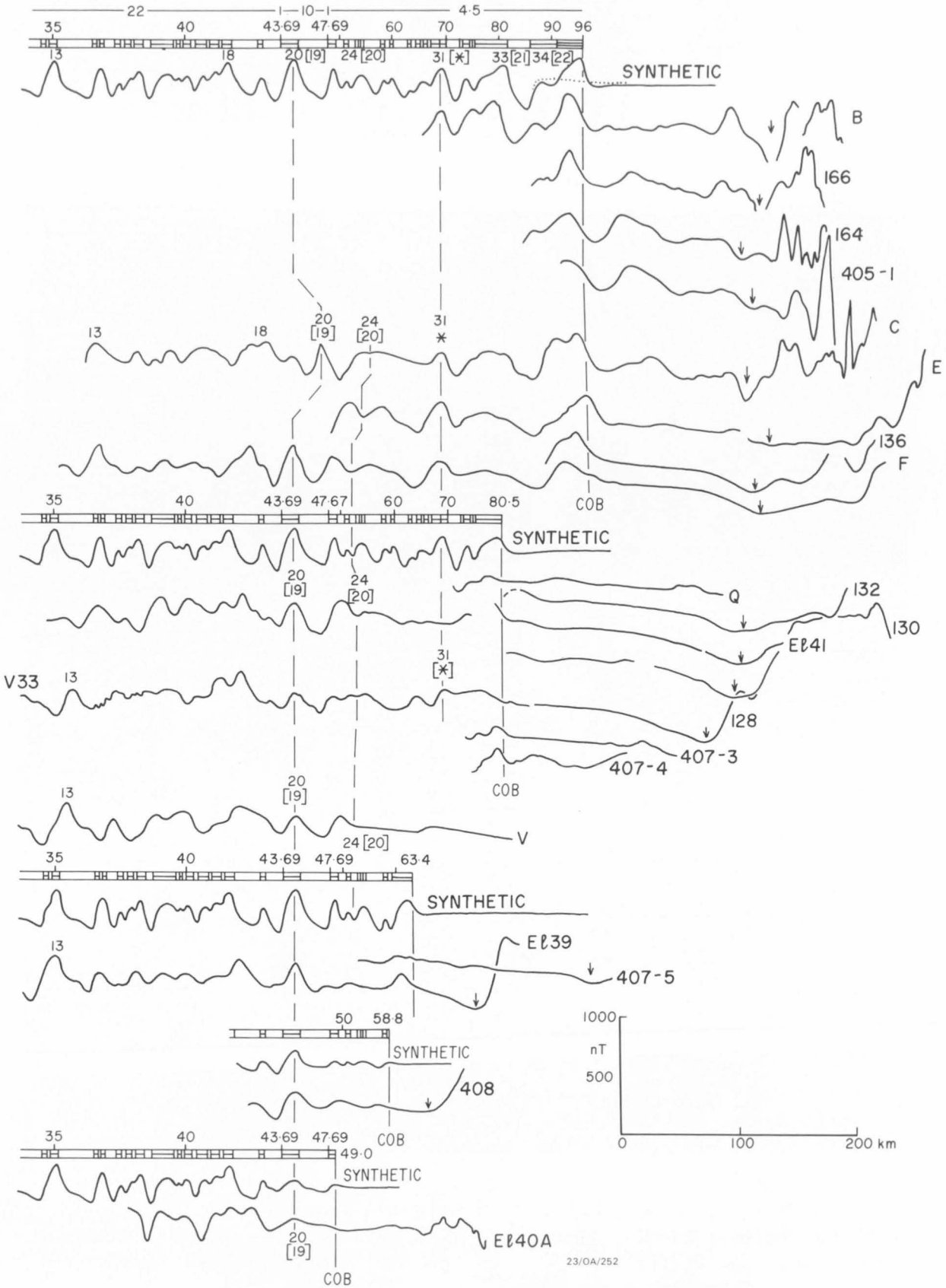

Figure 40: magnetic anomaly profiles along the southern Australian margin, alligned along the COB, projected on an azimuth of 180 degrees, and compared with synthetic profiles (after Veevers, 1986).

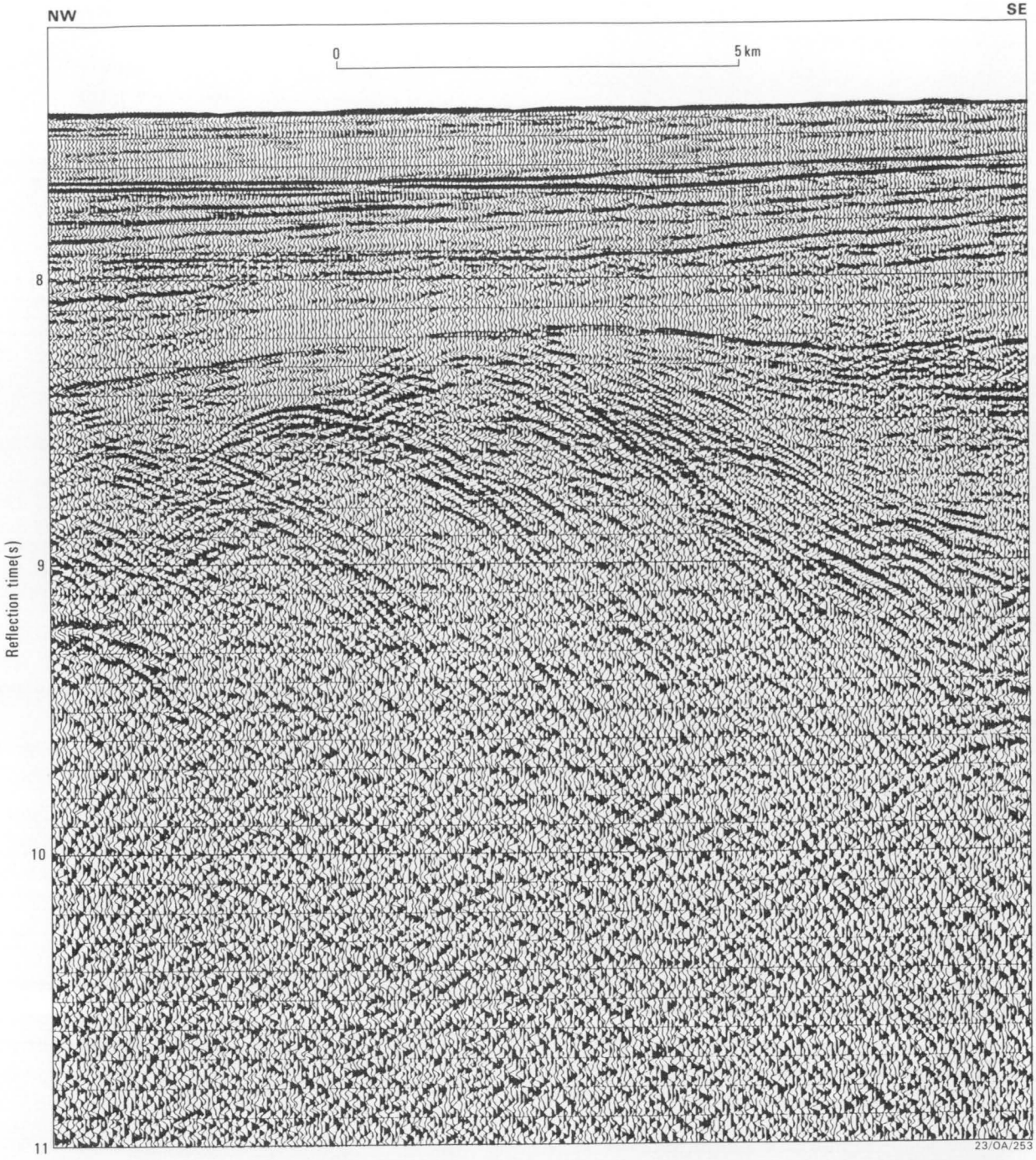

Figure 41: Seismic profile along line 65/15, showing the ridge in oceanic basement adjacent to the COB.

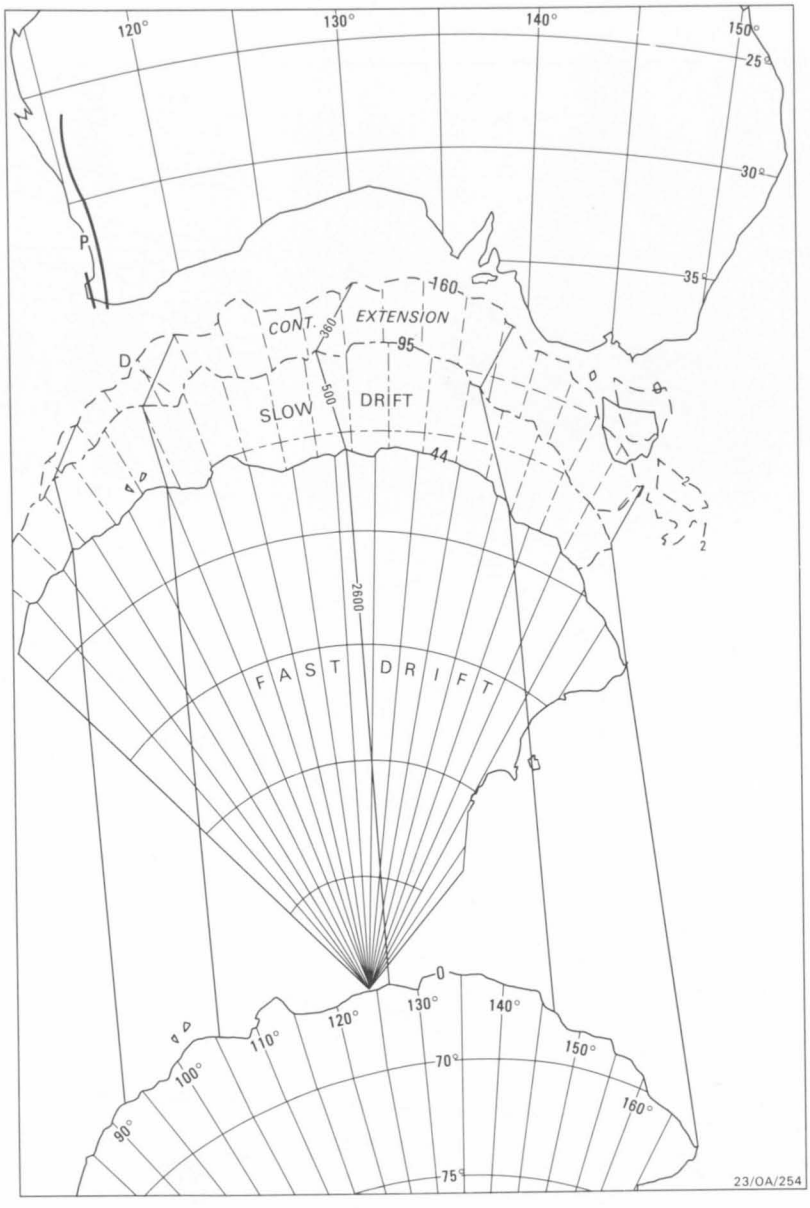

Figure 42: Three-stage separation of Antarctica from mainland Australia, from the initial pole position at 160 Ma, through the stage of continental extension to 96 Ma, then through the stage of slow drift to 44 Ma, and finally through the stage of fast drift to the present; arrows indicate the direction of separation (after Veevers & Eittreim, in press).

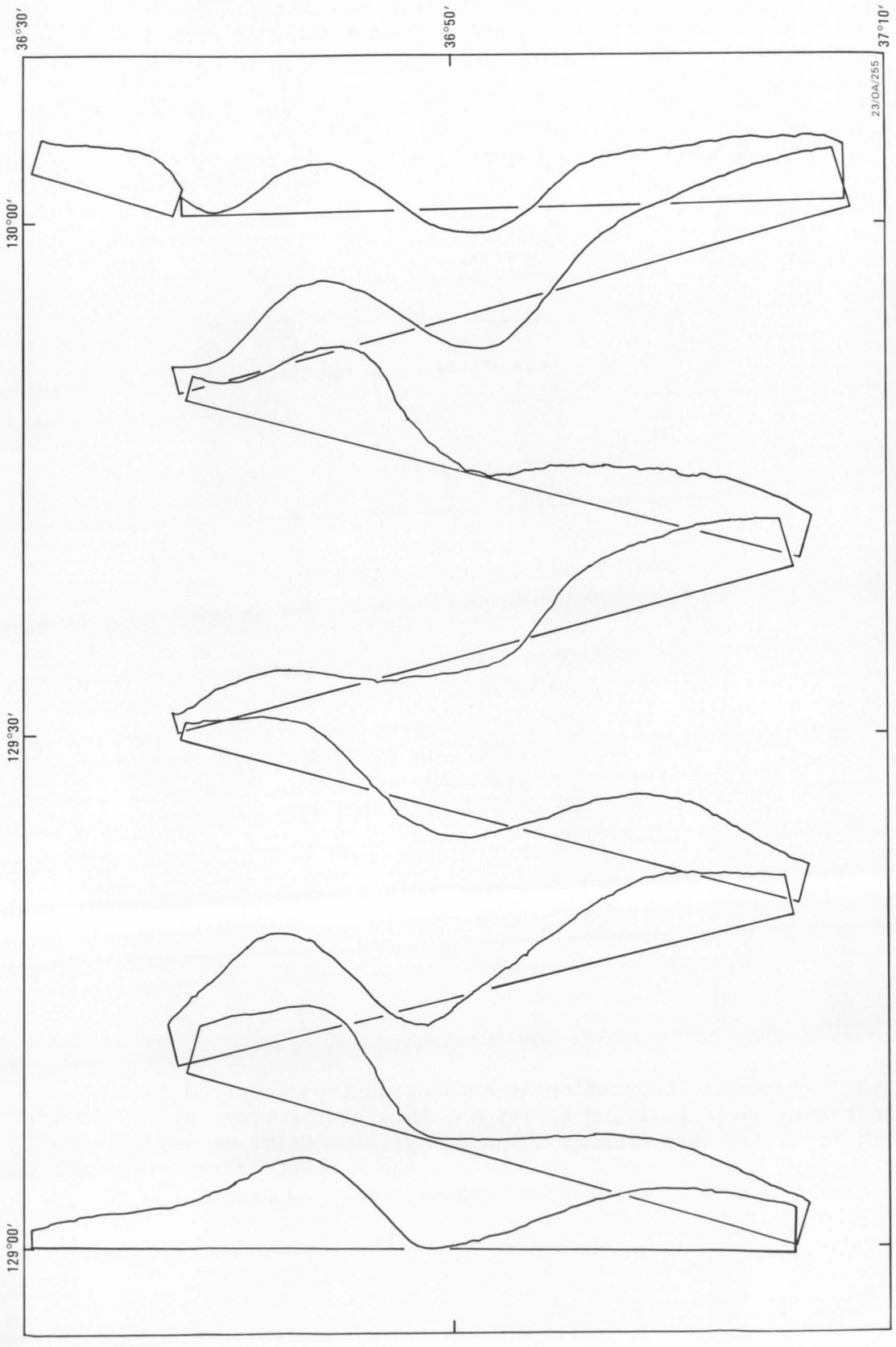

Figure 43: Magnetic profiles recorded across anomaly A-31 during Leg 2.

(Fig. 39), and dominates the rest of the margin up to its eastern end; the easterly trend continues westward to the western margin, with the ESE trend replaced by a WSW trend, and an overlap of all three trends in the Jerboa area (Bein & Taylor, 1981). Structures aligned on the easterly trend are the western part of the Albany-Fraser Mobile Zone, the Polda Trough, Kangaroo Island, the Robe-Penola Trough, and the northern edge of the Otway-Gippsland Basin; more than half of the COB to 138 E and much of the magnetic trough are aligned with the easterly trend, as is the morphological trend of Bass Strait. The oldest sediment associated with the easterly trend is mid-Jurassic, which, in the eastern half of Australia, marks the inception of this structural trend over the older (Palaeozoic) structural grain. In the west, only the western part of the curvi-linear Albany-Fraser Mobile Zone is alligned with the easterly trend; its middle part, at 120 E, is alligned with the WSW trend, as is the trend of the foot of the upper slope.

Two of the three principal trends of the southern margin can be tentatively identified with a mechanism: 1) the ESE trend with continental extension during the mid-Jurassic to mid-Cretaceous (160-96 Ma), and 2) the WSW trend with the gross trend of breakup at 96 Ma and subsequent spreading in the west and at 130 30' E, as seen in the Leg 2 magnetic data, and the orthogonal SSE trend of the western margin of Tasmania. The origin of the easterly trend is less obvious.

A possibility suggested by the easterly trend of the western part of the Albany-Fraser Mobile Zone (~1300 Ma old) and of the Kanmantoo Group of Kangaroo Island (generated during the Delamerian event, ~500 Ma ago) is that the intervening part of the southern margin is underlain by an E-W trending Proterozoic to Early Palaeozoic mobile zone that wraps around the Archaean Yilgarn and Gawler Blocks. This mobile zone may have become the line of weakness along which Australia west of 138 E (or further east if the Gambier-Beaconsfield fault zone be taken into account) and conjugate Antarctica separated in the same way as South America and conjugate Africa separated along the Proterozoic cement between Archaean nuclei. This does not explain the easterly trend of the Gippsland Basin, which was superimposed upon the pervasive meridional trend of the Tasman Fold Zone, unless the inherited easterly trend in the west propagated eastward during extension.

DREDGED ROCKS (HLD, JDAC)

OPERATIONS

The prime objective of the dredging program was to sample Mesozoic and Early Cainozoic sediments, the strata of most interest in terms of break-up history and petroleum prospectivity. The program was to concentrate on the shelf and slope at the junction of the Eyre and Ceduna Terraces, in the area gridded by Leg 1 seismic reflection lines (127 -130 30'E). However, this proved to be an area of gentle, sediment-covered slopes with few dredgeable targets. We found only one major canyon, here called 'Eucla' Canyon, on line 65/10, sampled in dredge hauls 1 and 3 (Figs 23 & 44); other smaller canyons were dredged unsuccessfully, probably because the uppermost 200-300 m of sediment is too poorly lithified to be retained in the dredge chain bag. Because of the lack of targets, we moved operations eastward to between 130 30'E and Kangaroo Island, where terrace and slope

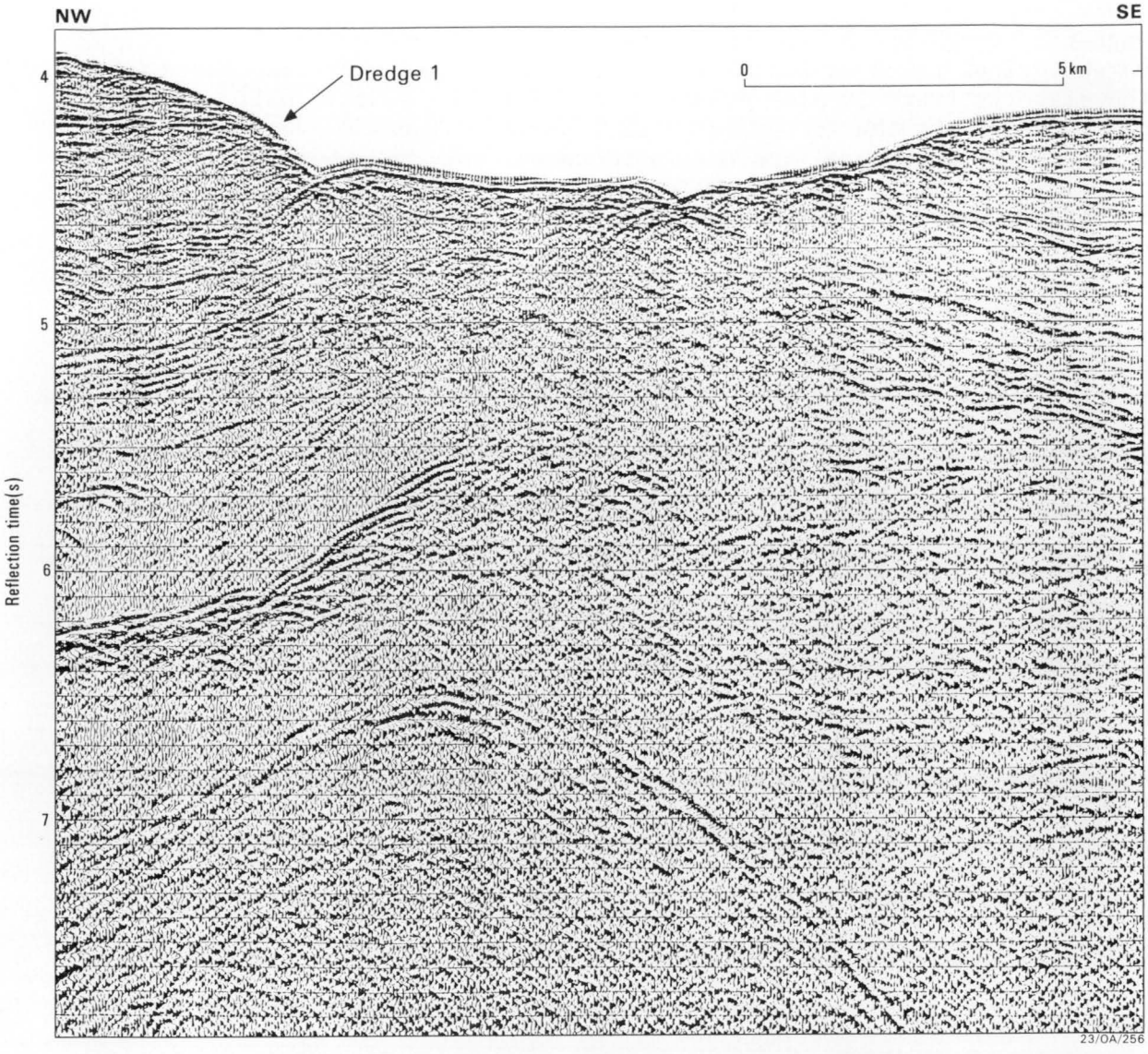

Figure 44: Stacked multichannel seismic reflection profile across 'Eucla' Canyon at about 33 55'S, 128 38'E, shows partly eroded anticline in Mesozoic strata. Dredge 1 recovered Maastrichtian, Palaeocene, and Early to Middle Eocene siliciclastic and carbonate/phosphate-siliciclastic sediments with some Tertiary? alkali basalt lava, and Late Eocene and younger foraminiferal spicular wackestone (fine pelagic limestone) from the NW slope. Strong reflector (level with arrow-head) may represent unconformity at base of Late Eocene and younger fine limestone. Dredge 3 encountered a similar rock suite down-canyon to the SW.

are dissected by major canyons.

Targets were defined by recording bathymetric and some seismic profiles parallel to the slope in water depths of 2.5-3.5 km. The depth of dredging was limited because an accident prior to the cruise had reduced the length of dredge wire from 10 to 4.2 km. The program was further inhibited by several failures of the winch hydraulic system. Probable Mesozoic targets at the base of the continental slope, which had been identified in pre-cruise planning, were beyond the depth limit.

A total of 16 sites were occupied (Fig. 23; Appendix D). Two of these were unsuccessful with no indication that the dredge had touched bottom, probably because of excessive ship speed; in one of these cases the ship was maneouvred with some difficulty in cross winds which averaged 40 knots. The largest dredge haul was about 750 kg of mixed sediment with some volcanics (dredge 1) and other hauls ranging from 2 to 250 kg (Appendix A in Davies & others, 1988).

After the cruise, selected samples were examined for age-diagnostic foraminifera, nannoplanckton, and spores and pollen by B. McGowran, S. Shafik, and N. F. Alley, respectively. Petrographic descriptions and initial reports were prepared by Clarke and Davies, and minerals and volcanic glass were analysed by electron probe microanalyser by Davies. Additional palynological work by E.M. Truswell is in progress. Preliminary results of all except Truswell's work are integrated into the following review and are discussed more fully in Davies & others (1988).

The dredge, designed and constructed at the University of Sydney, had a rectangular mouth of soft steel plate, about 70 x 40 cm, with a scalloped leading edge, a chain bag 2 m deep, and a harness of two 2-m lengths of chain. A pipe dredge was suspended above the main dredge, and 100 kg of ballast was secured to the dredge wire a few metres up from the harness.

RESULTS

In most dredge hauls we recovered

a) brown, weakly lithified, terrigenous mudstone, siltstone, muddy and gravelly sandstone, and minor peat of generally Late Cretaceous to Middle Eocene age, and

b) white lithified and semi-lithified pelagic limestone (packstone and wackestone) of Early Eocene to Pliocene or Quaternary age.

Other notable dredged samples included Precambrian, moderately sheared, pink granodiorite (dredge 2), Paleocene phosphatic sediment (dredge 1), fragments of ?Tertiary alkali basalt lava (dredges 1 and 3), a fragment of solitary scleractinian coral limestone in dredge 7, a branching, tubular piece of hematite-cemented, gravelly quartz sandstone in dredge 8, and sharks' teeth in Late Cretaceous gravelly quartz sandstone and in Late Oligocene soft pelagic limestone in dredges 3 and 11, respectively (Pledge & Clarke, in prep.). Unconsolidated Quaternary sediment collected in the pipe dredge commonly was carbonate ooze and mud and, less commonly, sand.

Brief descriptions of each dredge haul are given in Appendix A in Davies & others (1988) and the main rock types are discussed below.

Granodiorite

Moderately altered, finely jointed and locally cataclastic, coarse grained, pink hornblende-biotite granodiorite was collected in dredge 2 from a south-facing escarpment immediately south of Eyre Terrace. Plagioclase is dominant over perthite and microcline which latter are altered to clay and sericite; hornblende is partly altered to epidote. Minor talus-like sediment of fine angular granodiorite clasts, attached to the large blocks of granodiorite, has a hard limonite-cemented outer shell and is friable internally. The age of the granodiorite is not known but is presumed to be Precambrian.

Basaltic Lava

Fragments of amygdaloidal pillow lava were collected in dredges 1 and 3. In the largest sample in dredge 1 fine hyaloclastite breccia is attached to a curved pillow surface of chilled lava; the proportion and size of amygdules within the lava increase inward, away from the chilled surface. There are small euhedra of forsteritic olivine, Fo84, in the chilled rim. Glass from the rim is sodic phonotephrite (nomenclature of le Maitre, 1984), or undersaturated alkali basalt, with 8.35% total alkalis and 50.5% silica (Table 3). The abundance of large amygdules indicates eruption at relatively shallow depth.

Terrigenous siliciclastic sediments

Siliciclastic, terrigenous, marginal marine and less commonly non-marine sediments are prominent in four dredge hauls (1,3,7 and 9; Figs 23 and 44) and present in five others (8, 11, 12, 14 and 15). Ages range from Late Cretaceous (Maastrichtian) to Early and Middle Eocene.

Most common are weakly indurated brown siltstones and mudstones, typically organic rich with small organic fragments and occasional coal or wood fragments, less common sponge spicules and foraminifera, and traces of glauconite in the form of small peloids. Measured total organic carbon contents are between about 0.2 and 2.0 percent (Table 4). The sediments commonly show wispy to parallel lamination with occasional burrows and cross lamination.

Coarser clastic sediments include fine to gravelly sandstones with angular to sub-rounded grains of intrusive and metamorphic provenance, some polycrystalline quartz and glauconite, and small amounts of chert, feldspar, volcanogenic quartz, reworked quartz-cemented sand grains, chamosite grains, intraclasts and fossils (predominantly foraminifera). The most common cement is poikiotropic ferroan calcite. Other common cements are clastic and carbonate muds. Minor cement types are phosphate, pyrite and meniscus iron oxides.

The presence of glauconite in nearly all the terrigenous rocks, and of marine fossils in some, indicates a predominantly marine environment. The low fossil content, abundant organic matter and occasional wood and coal fragments suggest a nearshore to marginal marine setting. Sand grains were derived from a predominantly intrusive and metamorphic source, most likely the uplifted margins of the Albany-Fraser and Gawler cratons, with a minor input of reworked sand grains from older sediments

Table 3: Chemical composition of sodic phonotephrite glass 66DR1J

	Wt %	
SiO	50.6	Analysis of glassy selvage using
TiO	2.25	Cameca electron probe microanalyser
Al O	16.2	at Research School of Earth Sciences,
FeO*	8.55	Australian National University,
MnO	.13	19 August 1987. Beam current 18 nA,
MgO	5.01	rastering an area of 26 micron .
CaO	8.07	Average of 7 analyses. If Fe O /FeO
Na O	5.07	ratio is assumed to be 1:4, then
K O	3.30	SiO recalculates to 50.5% and other
P O	.78	values are slightly reduced.
	99.96	Average recalculated to sum to ~100, volatile free.

Table 4: Total organic carbon in selected samples

Sample	Organic carbon as C, %	
66DR01G	.17	Maastrichtian calcareous silty organic mudstone.
66DR07E	2.00	Late Paleocene to Early Eocene organic-rich muddy siltstone.
66DR08F	1.70	Late Paleocene organic-rich, sandy, silty mudstone with plant fragments.
66DR09A	.70	Pliocene dark brown poorly lithified silty mudstone.
66DR11D	1.88	Organic-rich muddy siltstone, Maastrichtian with Miocene contamination.
66DR12D	1.60	Early to Middle Paleocene dark greyish brown mudstone with possible carbonaceous fragments.
66DR14F	1.50	Early Eocene dark greyish brown mudstone and muddy sandstone, soft and friable.

Data from AMDEL Report AC 2813/87 of 29 January 1987 (M. R. Hanckel).
Method: Z/Combustion

of the GAB Basin. The overall setting is of estuarine, lagoonal, deltaic and nearshore sedimentation, transitional to fluvial or, more commonly, offshore conditions. Some of the clean sands contain abundant glauconite and even chamosite suggesting low rates of deposition. The chamositic clasts in DR1E resemble replaced limestones, suggesting seafloor alteration of exposed carbonates.

Diagenesis of the clastic sediments took place during burial, presumably by compaction and by cementation through carbonate and clay recrystallisation. The poikiotropic ferroan calcite cements were precipitated during deep burial from reducing pore waters (Choquette & James, 1987). An exception is sample DR12F, a mixed terrigenous clastic and carbonate sediment, which contains small fenestral cavities filled by drusy calcite, indicating a tidal flat environment with rapid cementation followed by meteoric phreatic diagenesis. In a few samples the matrix and cement have been replaced by other material. Examples of this are DR1I and DR11F where a calcareous matrix has been partly replaced by phosphate and DR7B where the matrix has been replaced by pyrite. In one sample (DR8G) there is a cement of meniscus haematite suggesting cementation in a soil horizon. In this sample the hematitic gravelly sandstone is in the form of a branching tubular concretion, perhaps indicating precipitation around a tree root.

Carbonates

Carbonate sediments are of four types: chalk, siliceous carbonate, limestone and dolomite. Chalks are most common and dolomites least common.

Chalks (lithified and semi-lithified pelagic limestones) are composed of white, soft, fine-grained carbonate and range from lime mudstones to packstones. The grains are predominantly foraminifera and sponge spicules. The foraminifera are most commonly planktic but include arenaceous agglutinating forms. The sponge spicules represent calcisponges, hexactinallids and demosponges. Other fossils include echinoderm plates, ostracods and thin-walled molluscs, probably pteropods. Also present in some samples are small glauconitic, and less commonly calcareous, peloids. The matrix is white, microcrystalline carbonate, probably of coccoliths. Sedimentary structures include wispy laminae, thin winnowed beds, filled and unfilled burrows, and borings. Burrow fillings are chalky carbonate and, less commonly, glauconitic sediment. Some borings, in common with other exposed surfaces, are lined and coated with a crust of iron and manganese oxides. The crust ranges in thickness from a thin film to several mm.

Lithification is variable, ranging from unconsolidated ooze to relatively well indurated chalk. Lithification is generally due to compaction, the well compacted samples having presumably undergone some cementation by microcrystalline carbonate (Schlanger & Douglas, 1974). Some samples which show extensive evidence of seafloor exposure (borings, iron and manganese crusts) are more strongly lithified; this is interpreted to indicate sea floor case hardening. Such samples (DR6C, DR11G, DR12A & C, DR14C) show dissolution of molluscs and partial cavity fill by glauconite. In DR6C, spicules have been dissolved and replaced by manganese oxides. In most the fabric has become denser due to precipitation of microcrystalline carbonate; in these rocks the

fabric may take on a clotted appearance.

Siliceous carbonates appear to have originated as chalks and limestones which contained abundant siliceous sponge spicules and radiolara. In one example volcanic glass shards may also have been present (DR3E). Silica is present as a cement, fossil fill, and replacing fossils; most is microcrystalline, and true cherty silica was seen in only one sample (DR15C). The pattern of silicification is commonly nodular with the boundary between nodule and surrounding sediment marked by limited dissolution of carbonate. Many of the siliceous carbonates are quite soft and are thus superfically similar to the more prevalent normal chalks and limestones. Glauconite is slightly more abundant in siliceous than in non-siliceous carbonates. Petrographically the siliceous carbonates resemble those of the Tortachilla, Blanche Point and Port Willunga Formations of the St Vincent Basin in South Australia (Cooper, 1979; Jones & Fitzgerald, 1986).

Limestones other than chalks are rare. The most notable example is DR7G, an echinoderm coral floatstone, possibly boundstone, with solitary scleractinian coral. This contains bivalves, brachiopods and planktic foraminifera, and has a matrix of lime mudstone. Aragonitic and high magnesium calcite components have been dissolved away and the cavities lined by small drusy calcite crystals. Other limestones resemble impure chalks, and are commonly silty and glauconitic.

Dolomitic rocks include DR1C and DR3D, both of which are burrowed intraclastic silty wackestone with a weathering rind of iron oxide; probably they are from the one source. DR16A is a skeltal dolomitic packstone.

The carbonates were deposited in a range of environments. The chalks accumulated in a pelagic-dominated environment with very little input from shelf or continent. In this they resemble the Quaternary oozes recovered in our soft sediment cores (see later). They were therefore deposited in an environment similar to that prevailing today, on slope, terrace or possibly pelagic shelf. The limestones are thought to have been deposited in shallower shelf environments with varing degrees of pelagic influence. The coralline limestone presumably was formed in a shallow marine, low energy environment, possibly biohermal. The siliceous carbonates closely resemble the chalks and limestones and presumably were deposited in similar environment. The silicification appears to be due to later diagnesis rather than any depositional control, apart from the greater abundance of siliceous fossils and the possible presence in some of volcanic glass shards. The depositional environment of the dolomites in DR1 and DR3 is less clear. The fine grain size indicates a low energy environment, while the scarcity of fossils suggests restriction. The dolomite is very fine grained and therefore probably formed early. The most likely environment is a tidal flat.

Most of the carbonates have undergone very limited diagenesis. The chalks have been variably compacted and cemented, with greatest effects seen in those which have been exposed on the sea floor or have been silicified. The former are encrusted with rinds of iron and manganese oxides, have undergone dissolution of some fossils, and have cavities

filled by glauconite or iron and manganese oxides. There has also been extensive case hardening through precipitation of microcrystalline carbonate resulting in a reduction of porosity and an increase in rock density. The coralline limestone has had a complex history. The preservation of moulds indicates rapid cementation either on the seafloor or soon after burial but before the formation of the moulds; dissolution is probably due to exposure to meteoric water; and the presence of thin cavity linings of drusy calcite indicates precipitation in a meteoric phreatic environment (James & Choquette, 1984). Other limestones have had a diagnetic history similar to that of the chalks. In the siliceous carbonates the pattern of silicification is petrographically similar to that which affects the Tertiary carbonates of the St Vincent Basin (Cooper, 1979), as described for the Blanche Point Formation by Jones & Fitzgerald (1984, 1986, 1987). Jones & Fitzgerald concluded that silica was mobilised from volcaniclastic material. However the scarcity of volcanogenic detritus in both the St Vincents sediments and those from our sampling program argues against this. Our petrographic data suggest that a more likely source of silica is from the abundant siliceous fossils. A biogenic origin for silica in marine sediments has been argued by Wise & Weaver (1974) and Calvert (1974). The dolomites, if the tidal flat interpretation is correct, would have been cemented very early with synsedimentary dolomitisation. They appear to have undergone little subsequent diagensis apart from the formation of an iron-rich weathering rind during exposure on the sea floor.

Phosphates

The well-lithified Paleocene phosphatic sediment DR1I was examined and described by R. C. Garrison (pers. comm., 1987). The rock is a laminated micrite and fine sandstone that includes a phosphorite interbed 25 mm thick . The sandstone laminae are mostly angular quartz grains with scattered glauconite, phosphate peloids, fish bone, carbonate skeletal fragments including ?bryozoa, carbonate peloids, pyrite, and disseminated organic matter. The micrite was formerly a lime mud or an accumulation of carbonate pellets. The phosphorite interbed is mostly a peloidal phosphorite with variable amounts (5-15%) of silt to fine sand size siliciclastic grains (mainly quartz) and minor glauconite. Later generations of phosphate, which bond the peloids, glauconite, and siliciclastic grains, are difficult to differentiate from first generation phosphate. In places, adjacent to the phosphate horizon, later phosphate appears to have replaced micritic carbonate. The laminated micrite and sandstone developed by passive accumulation of carbonate mud with periodic current-transported influx of silt to sand-size siliciclastic grains, perhaps by storms. The phosphorite horizon probably represents an interval of reduced rate of sediment accumulation, perhaps due to fluctuation in sea level, which permitted phosphatisation of peloids, reworking and winnowing, influx of some siliciclastic grains, and cementation, or replacement of micrite matrix, by phosphate.

DR11F is another mixed carbonate-siliciclastic sediment in which matrix has been partly replaced by phosphate and pyrite.

DISCUSSION

The dredged rocks document a transition from generally terrigenous marine, and rarely non-marine, sedimentation in the Maastrichtian, Paleocene and Early to Mid Eocene, to accumulation of pelagic carbonate from the Middle Eocene through to the Quaternary. The only exceptions to this pattern are the possibly Lower Miocene mudstones with quartz detritus in dredges 7 and 9 (Appendix A in Davies & others, 1988). The older samples provide the first record of truly marine Maastrichtian sediments with abundant calcareous nannoplankton in southern Australia. (A horizon in the Gippsland Basin with dinoflagellates also has been dated as Maastrichtian.) This is the first clear demonstration of a Maastrichtian marine connection from southern Australia to the Indian Ocean (B. McGowran in Davies & others, 1988), although the concept of Late Cretaceous sea floor spreading between Australia and Antarctica is well established. The assemblages are remarkably well preserved and diverse, and are of value as a high palaeolatitude datum for Maastrichtian biogeography (McGowran in Davies & others, 1988). Similarly, much of the microfaunal content of the Eocene samples is new and of biostratigraphic significance. Early Eocene sediments in dredges 8 and 14 are older than the oldest Eocene sediments intersected by DSDP drilling on the Naturaliste Plateau (Davies, Luyendyk, & others, 1974; Hayes, Frakes, & others, 1975).

The Cretaceous to Middle Eocene clastics, both fine and coarse grained, probably correlate with the Potoroo Formation and possibly the Wigunda and Platypus Formations. All of these are marginal marine (Robertson & others, 1979). The Cretaceous dolomites may correlate with those from the Wigunda Formation from the Ceduna Terrace (Robertson & others, 1979). The siliceous carbonates correlate with other Palaeogene siliceous carbonates common elsewhere on the Cainozoic rifted margins of Australia (Jones & Fitzgerald, 1986). The Eocene sandstones and carbonates correlate with the Nullarbor, Wilsons Bluff and Abrakurrie Formations of the Eucla Basin, and the coralline limestone may be a correlative of coralline limestones in the Nullabor Formation near Watson (Ludbrook, 1958). The Tertiary pelagic limestones which we encountered in almost all dredge hauls were not sampled in the various petroleum exploration wells and so have not been formally defined. They are time equivalents of the younger strata of the Eucla Basin.

SEDIMENT CORES AND PIPE DREDGE (JDAC, HLD)

A total of 41.16 m of soft Quaternary sediment was collected in 19 gravity cores and one piston core (Fig. 23; Table 5). Average core length was 2.08 m and longest core was 3.46 m. In addition, soft sediment was collected in the pipe dredge at each of the dredge stations. Three coring attempts encountered hard bottom and were unsuccessful. Seismic profiles over two of these sites (GC 1 on the Ceduna Terrace and GC 9 on the Eyre Terrace; Fig. 23) suggest that soft sea floor sediments may have been removed by bottom currents, and diffraction of seismic waves at the third site (GC 6) suggests an irregular, rough sea floor with little sediment cover.

Table 5: Core locations and descriptions.

CORE NO.	WATER DEPTH(m)	LAT	LONG	LENGTH (cm)	BRIEF DESCRIPTION
Eyre Terrace					
8	1151	33 39.901	127 42.206	186	Pelagic calcareous ooze with one turbidite horizon
Ceduna Terrace, Line 65/2					
5	1134	34 02.305	130 41.483	247	Pelagic calcareous ooze with several sandy horizons
Slope below Ceduna Terrace, Line 65/2					
7	3662	34 35.438	129 31.716	90	Several beds of reworked pelagic sand, some ooze
Slope below Ceduna Terrace, Line 65/15					
1(PC)	2646	35 16.599	131 11.545	234	Pelagic calcareous ooze, minor foram sands
10	2643	35 16.668	131 10.897	176	Pelagic calcareous ooze with alternating colour bands
11	2326	35 12.156	131 13.597	100	Pelagic calcareous ooze
Ceduna Terrace, Line 65/15					
2	591	33 50.398	132 04.700	321	Pelagic calcareous ooze
3	600	33 51.069	132 05.308	346	Pelagic calcareous ooze
4	701	33 55.820	132 02.441	215	Pelagic calcareous ooze with two shelly horizons
12	2010	35 09.216	131 16.225	167	Pelagic calcareous ooze
13	1734	34 59.643	131 21.541	160	Pelagic calcareous ooze
14	1498	34 50.137	131 25.983	215	Pelagic calcareous ooze with colour banding, one horizon larger planktic forams
15	1376	34 41.721	131 33.056	207	Pelagic calcareous ooze
16	1253	34 32.528	131 39.272	91	Pelagic calcareous ooze
17	1186	34 24.251	131 44.095	213	Pelagic calcareous ooze
18	1247	34 16.234	131 49.083	124	Pelagic calcareous ooze
Ceduna Canyon					
19	2396	35 28.320	132 55.042	246	Sequence of terrigenous siltstone/mudstone and gravel overlain by pelagic calcareous ooze
'Thevenard' Canyon, floor					
20	2810	35 41.743	133 18.761	186	Shell hash, quartz sand, and rock fragments overlain by pelagic calcareous ooze
'Thevenard' Canyon, eastern slope					
21	2717	35 41.283	133 19.867	295	Pelagic calcareous ooze with one horizon X-bedded quartz and foram sand
22	2316	35 41.981	133 21.227	262	Pelagic calcareous ooze with one turbidite horizon of echinoid detritus

Cores from terraces and upper slope were taken in conjunction with the heat flow program. These cores were predominantly pelagic calcareous ooze, but reworked pelagic sands were encountered in two cores from the upper slope off Ceduna Terrace (PC 1 and GC 7; Fig. 45). Cores from the floor of Ceduna and 'Thevenard' Canyons (GC 19 and 20) included terrigenous turbidite and debris-flow deposits beneath a blanket of pelagic calcareous ooze, and a pipe dredge sample from an unnamed canyon south of the Eyre Peninsula (DR 14; Fig. 23) contained shelf-derived carbonate debris. Two attempts to core Neogene or older sediments which form benches on the eastern slope of the 'Thevenard' Canyon (GC 20 and 21) encountered only a cover of Quaternary pelagic calcareous ooze.

RESULTS

Pelagic calcareous ooze

Pelagic calcareous ooze is the dominant cored sediment (Fig. 45) and was also recovered in most pipe dredge hauls. The ooze is more than 60 percent very fine grained sediment, probably nannofossils such as coccoliths. A few samples, such as GC 10, 186-188 cm (Fig. 46), have a higher proportion of coarse grains, most of which are of pelagic or deep water origin: foraminifera with minor shell hash, siliceous and calcareous sponge spicules, and small aggregates; the only shelf-derived component is a small amount of terrigenous silt and perhaps some of the shell hash and sponge spicules. Typical ooze contains 15-20 percent of non-carbonate material as siliceous spicules and terrigenous silt (Table 6). In many of the cores a pale yellow or cream-coloured upper oxidised zone passes down core into a grey or green reduced zone. This is best seen in core GC 10, where the colour banding is repeated at intervals of 25-50 cm. In this core there is no correlation between sample colour and sorting or carbonate content, and the colour banding is therefore attributed to variations in bottom water oxidation during deposition rather than to physical sedimentary controls or gross carbonate chemistry. Some other Ceduna Terrace cores show less distinct colour bands. In other cores the colour change appears to be related to burial processes.

Ooze recovered in the pipe dredge is similar to that recovered in the cores and is essentially an unlithified foraminiferal wackestone with nannoplankton as the mud fraction. Other common components are siliceous spicules from demosponges and well-rounded quartz silt grains. Less common are molluscan hash, calcareous spicules, and possible radiolaria and ostracods.

Reworked pelagic sands

Reworked pelagic sand horizons in cores PC 1 and GC 7 (Fig. 45) have sharp top and bottom contacts, little or no grading, and are either massive or poorly cross bedded. The grains are mostly large foraminifera such as *Orbiculoides* with minor shell hash and spicules. Some of the foraminifera are yellow-brown in colour and probably have been reworked from older sediments. The sands are moderately to well sorted and contain only small amounts of mud. They are essentially winnowed and sorted pelagic material, without any obvious component of shelf origin.

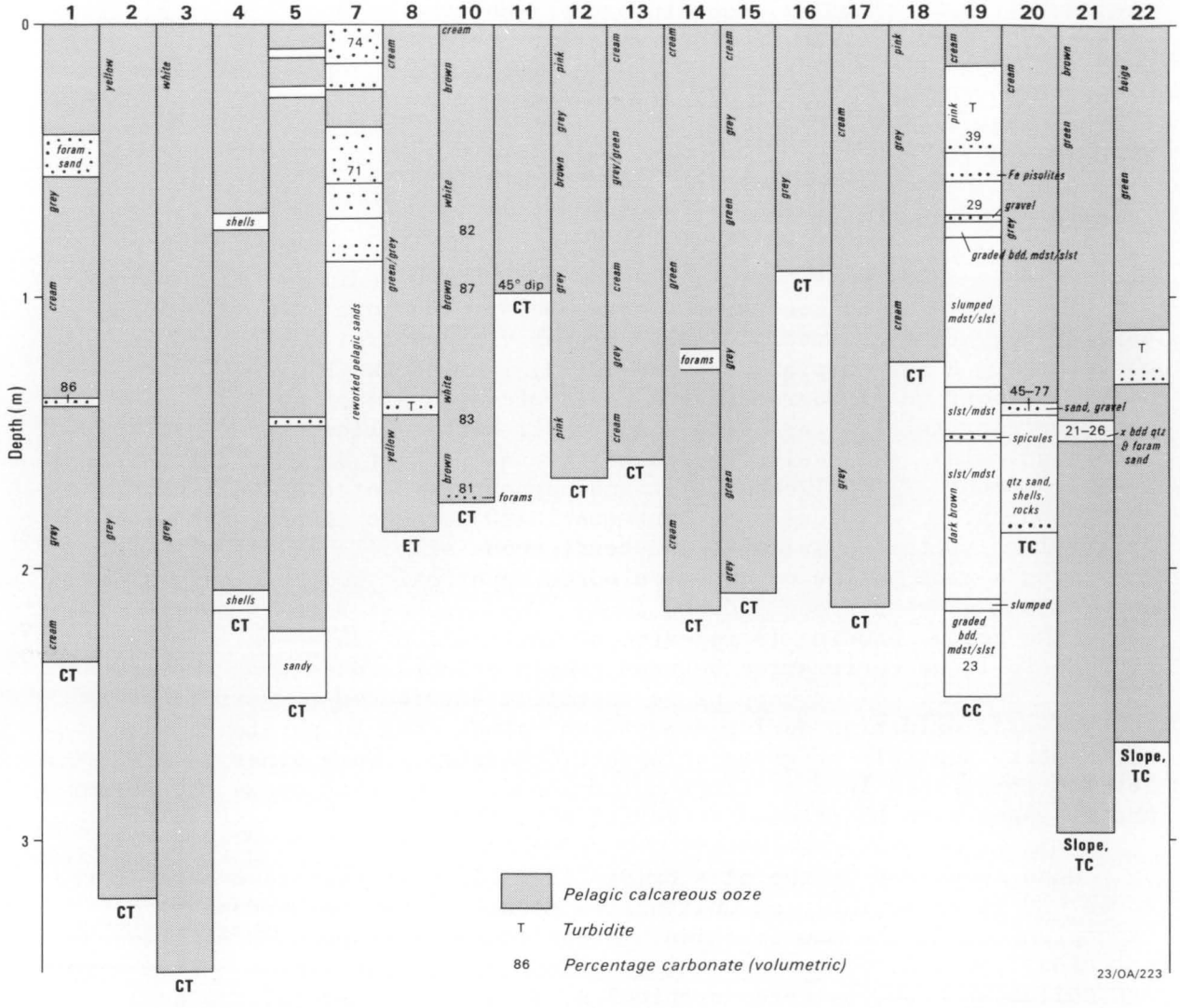

Figure 45: Summary graphic logs of all cores illustrate predominance of calcareous pelagic ooze on terrace and upper slope. Cores from canyons (GC 19-22) show that turbidite and debris flow deposits in canyons are buried beneath a cover of pelagic ooze. ET Eyre terrace; CT Ceduna Terrace; CC Ceduna Canyon; TC 'Thevenard' Canyon. Summary of core locations: 8 Eyre Terrace; 5 and 7 Ceduna Terrace on seismic line 65/2; PC 1, GC 2-4, and 10-18 Ceduna Terrace line 65/15; 19 Ceduna Canyon; 20-22 'Thevenard' Canyon on floor, bench on east slope, and east slope, respectively.

Table 6: Carbonate content of selected soft sediment.

Sample	% Carbonate
PC 1.148-150 cm (sand)	86.1
DR 14 pipe dredge sand	85.2
GC 7 4-6 cm (sand)	73.9
GC 7 60-62 cm (sand)	70.8
GC 10 4-6 cm	82.5
GC 10 80-82 cm	81.5
GC 10 100-102 cm	87.3
GC 10 150-152 cm	83.1
GC 10 186-188 cm	81.0
GC 19C (sand)	38.7
GC 19B (sand)	29.3
GC 19A (silt at bottom)	23.2
GC 20 22-24 cm	82.1
GC 20 sand	44.8
GC 20 sand	76.9
GC 21 sand	20.8
GC 21 sand	26.1

Note: All analyses by volumetric techniques except GC 19B which used Acid Insoluble Residue. GC 20 & 21 show considerable variation between runs due to coarse grained nature of sample.

Detrital sediments in canyons

Detrital sediments recovered from beneath the floor of Ceduna Canyon and 'Thevenard' Canyon, and dredged from an unnamed canyon further to the east (DR 14; Fig. 23), are mixed terrigenous and carbonate sand, silt and mud. Detrital sediment from the eastern canyon had the highest carbonate content (85%), while that from Ceduna Canyon had the lowest (Fig. 45; Table 6). The carbonate detritus includes shelf-derived fragmented molluscs, bryozoans, brachiopods, corals and worms, and reworked pelagic fossils and lithoclasts of chalk. Terrigenous components included well-rounded quartz sand and gravel and abundant heavy minerals, including zircon, garnet and ilmenite. Core GC 19 from Ceduna Canyon also includes abundant ferruginous pisolites, possibly derived from erosion of lateritic soil profiles or pisolitic limestones such as the Tortachila Limestone of the St Vincent Basin. The heavy minerals probably were derived from the igneous and metamorphic rocks of the Gawler Craton and of the Kanmantoo trough.

Typically the detrital sediments are medium to coarse grained sands, but finer silt and mud dominate the lower part of core GC 19. The silt and mud are terrigenous and form fine graded sequences with sharp basal contacts; probably they are fine turbidites. Parts are reworked by slumping. The coarser deposits are generally unstratified or poorly stratified with either massive or cross bedding. In GC 19 the sands are very poorly sorted (Fig. 46) and may represent either turbidites or debris flow products. In GC 20 the detrital horizons have sharp boundaries and are probably grainflows rather than turbidites. In GC 21, from a bench on the eastern slope of 'Thevenard' Canyon, there is a single, cross-bedded sand horizon which probably represents the migration of a single sand wave within an otherwise pelagic depositional setting.

Terrigenous dark brown and dark grey muds recovered in the pipe dredge from other canyons are unconsolidated to stiff and are composed of fine, well-rounded quartz grains in a clay matrix. Small black flecks of authigenic pyrite and organic matter are present in some, and rare fossils include mollusc fragments, sponge spicules and foraminifera.

In the cores from Ceduna and 'Thevenard' Canyons the detrital sequence is overlain by up to 1.2 m of pelagic calcareous ooze.

DISCUSSION

The coring program demonstrated that the Eyre and Ceduna Terraces are regions of pelagic calcareous sedimentation, with little input from the landmass to north and east. Hard bottom in some areas, and evidence of scour on seismic profiles, indicate some erosion by bottom currents.

Reworked pelagic sands cored on the upper slope off the Ceduna Terrace are probably contourites or locally sourced grainflows. They lack the grading, poor sorting, and abundant matrix characteristic of turbidites. Similar deposits on other continental slopes (MacIlreath & James, 1984) are attributed to grainflow (possibly storm generated), reworking of turbidites, storm deposits, and contour-hugging currents.

Figure 46 (next page): Grain-size distribution in selected samples; ten histograms compare sandy horizons in cores PC 1 and GC 7, 19-21, and sand from pipe dredge of Dredge 14; five others compare the differently-coloured layers in core GC 10. See also Table 6 (Carbonate content of selected samples).

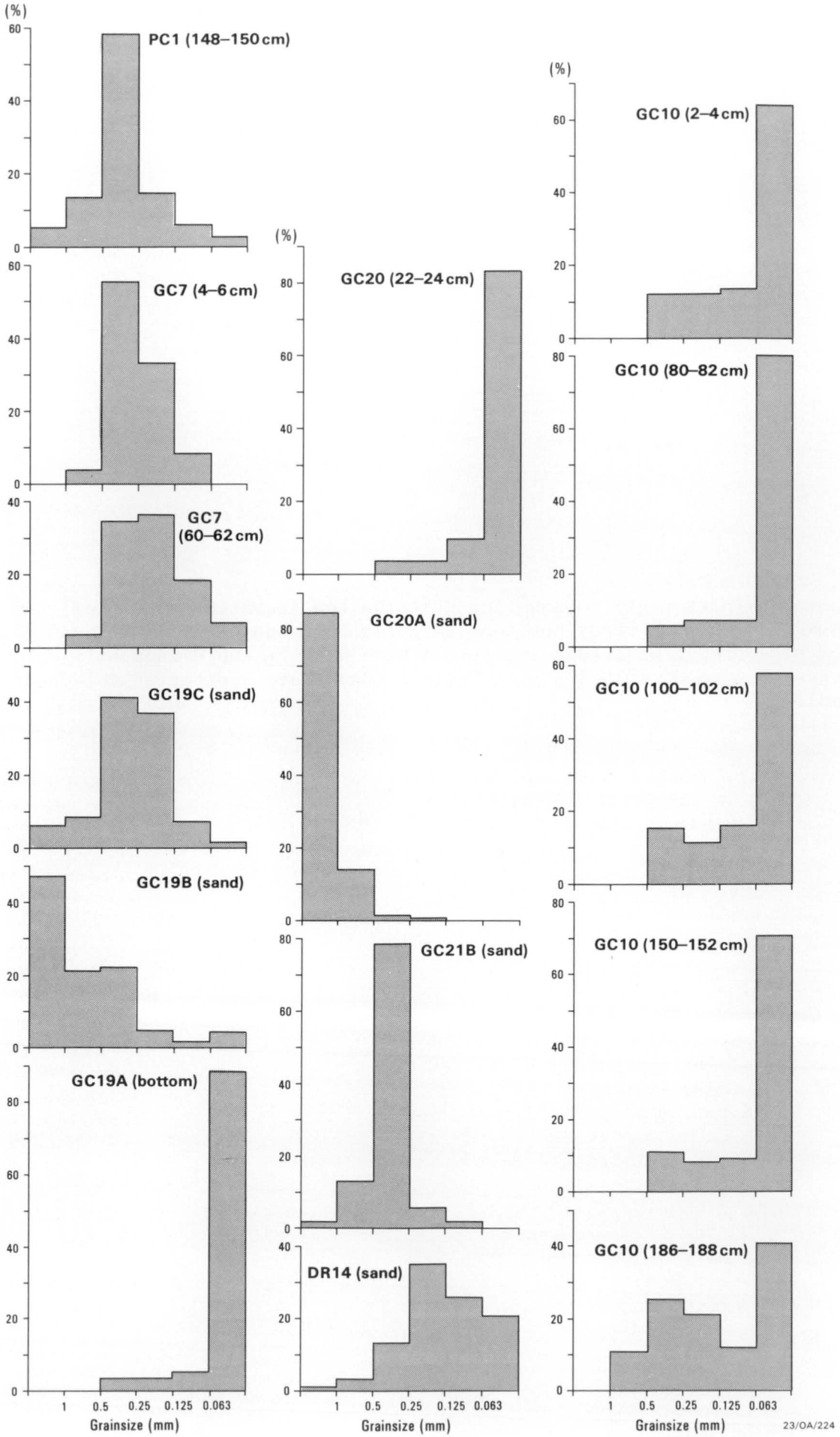
(%)
PC1 (148–150 cm)
GC7 (4–6 cm)
GC7 (60–62 cm)
GC19C (sand)
GC19B (sand)
GC19A (bottom)
(%)
GC20 (22–24 cm)
GC20A (sand)
GC21B (sand)
DR14 (sand)
(%)
GC10 (2–4 cm)
GC10 (80–82 cm)
GC10 (100–102 cm)
GC10 (150–152 cm)
GC10 (186–188 cm)
1 0.5 0.25 0.125 0.063
Grainsize (mm)
23/OA/224

The water depth of the sands in PC 1 and GC 7 precludes an origin as storm deposits, and the lack of shelf fauna argues against origin by grainflow from the shelf or upper slope. Contour currents are known to flow along the southern Australian margin, for example, the Leeuwin current, which follows the shelf break (Rochford, 1986). Such a shelf- following current would inhibit the movement of sediment down the slope, and thus would explain the apparent lack of shelf-source sediment on the southern margin slope. This contrasts with the slope off the Otway margin where there is much movement of shelf sediment down slope (Exon, Lee & others, 1987), possibly related to storm-driven on and off-shelf currents (Fandry, 1983).

The blanket of pelagic ooze encountered in the floor of the Ceduna and 'Thevenard' Canyons indicates that these are currently not active sediment channel ways. The eastern, unnamed canyon (DR 14), on the other hand, may well be active. Presumably all were active during intervals of lower sea level in the Neogene and Quaternary. Abyssal plain sediments off southern Australia are composed of fine grained shelf sands, aggregates and calcretised lithoclasts (Conolly & von der Borch, 1967). Canyons were probably the conduits for this sediment, given the absence of any evidence of down slope sediment transport in our cores and in the cores from the continental slope collected by Conolly and von der Borch.

HEATFLOW STUDIES

The heatflow program originally proposed for the southern margin by Willcox & others (1986, their Appendix C) envisaged three heatflow transects: N-S across the Ceduna Terrace, NW-SE across the Eyre Terrace and continental rise, and NE-SW across the southwest margin of the Ceduna Terrace, linking the first two transects (Fig. 21). These profiles had dual objectives - to examine the variation of heatflow across a classical (though complex) rifted margin, and to carry out hydrocarbon maturation studies in the GAB Basin and the Eyre Sub-basin. These plans were effectively thwarted when more than half the main coring winch wire was lost prior to the first southern margin cruise. This loss restricted the heatflow program to water depths of less than 3500 m - *ie* to the Eyre and Ceduna Terraces only. The inability to complete a heatflow transect to the deep ocean basin also meant that the prime scientific objective became the study of sediment maturation for hydrocarbons.

In addition to the Nichiyu Giken NTS-11 thermal gradient equipment owned by BMR, the study also had access to a Lamont-Doherty DHF-5 thermal gradient meter, the property of the Geological Survey of Japan (GSJ), who participated in the cruise under the Australia-Japan Science Agreement. As well as the equipment, GSJ also supplied a heatflow technical expert (M. Joshima) for the sampling cruise. The objectives of this cooperative study were three-fold - to carry out comparisons between two sets of thermal gradient equipment of differing types and vintages; to assist our development of an underwater telemetry system for the NTS-11 which would allow real-time monitoring of equipment performance; and to gain technical experience in the acquisition, reduction, and interpretation of heatflow data. Unfortunately, the DHF-5 was seriously damaged at the first heatflow station when the pressure casing leaked, and was thereafter unusable; this effectively nullified the first two stated aims. All succeeding heatflow stations were completed using the NTS-11 equipment. For completeness, a comparison of the specifications of the NTS-11 and DHF-5 is included as

Table 7.

THERMAL GRADIENT MEASUREMENTS

Thermal gradient measurements were made with a gravity corer-type system (Fig. 47). The electronics package was housed inside the corer head, while the thermistors were mounted on outriggers in a spiral arrangement along the core barrel; this spiral arrangement ensures that each thermistor enters relatively undisturbed sediments. Previous BMR heatflow studies (*eg* Choi, Stagg, & others, 1987) utilised a 'needle' probe or 'lance' rather than a corer; however, that system was chronically subject to probe bending. It was felt that the use of a corer would reduce these problems, due to the greater rigidity of the core barrel compared to a lance, and that greater penetration would be achieved with the extra weight of the core head.

For the first stations, a 5 m core barrel was used. However, bottom conditions (?very soft thin sediments overlying a hard sub-strate) again caused severe bending problems due to incomplete corer penetration. The optimum barrel length was finally settled at about 2.5 m, with thermistors at a separation of 0.5 m along the barrel. With this arrangement, near full penetration was achieved at most of the later stations and reasonably reliable thermal gradient measurements were obtained. The corer-type gradient measuring system also has the advantage that as a core is taken at every heatflow station, thermal conductivity measurements can be made coincidentally with the thermal gradient, thereby producing more reliable heatflow values.

The restricted penetration of the heatflow probe in water depths less than about 2000 m may give rise to problems caused by the seasonal fluctuation of bottom water temperatures setting up thermal transients in the shallow sediments. However, until we have a substantial shallow water data set over a long period of time, it is not possible to quantify such errors, if they exist.

The flow of data processing for the NTS-11 is shown in Table 8. The processing fnow for the NTS-11 has been modified from previous cruises with the addition of two new programs (JCAL and STAT1) that simplify and speed the processing and improve the accuracy of the thermal gradient.

THERMAL CONDUCTIVITY

Thermal conductivity measurements on the sediment cores were made with a BMR-constructed needle probe using the thermal transient technique pioneered by Von Herzen (1959; Appendix H). The equipment used for the measurements was described in some detail by Choi, Stagg, & others (1987).

After retrieval, cores were allowed to come to thermal equilibrium at room temperature for at least 6 hours. Several tests indicated that

Table 7 : Comparison of specifications of DHF-5 and NTS-11 thermal gradient measuring equipment.

	DHF-5	NTS-11
Weight	40 kg	30 kg
Dimensions	82 x 14.5 cm	81.5 x 17.0 cm
Memory	80 kbytes on cassette	64 kbytes RAM
Battery depletion time	30 hours	127 hours
Number of thermistors	1 to 8	2 to 8 (max 32)
Dynamic range	0 to 16 C	-2 to 32 C
Usable resistance at 0 C	2 kohm to 10 kohm	15.2 kohm only
Resolution	0.0005 C	0.001 C
Cycle rate	6 to 30 sec (1-8 thermistors)	30 to 120 sec (8 thermistors)
Thermistor self-heating	0.025 to 0.012 mW	0.01 mW
Tilt recording	3 stages (0, 15, 30 degrees)	X and Y directions up to 45 degrees
Pressure recording	0 to 6000 m	no
Acoustic telemetry	pair pulse by pinger; 0.5 sec sweep	no

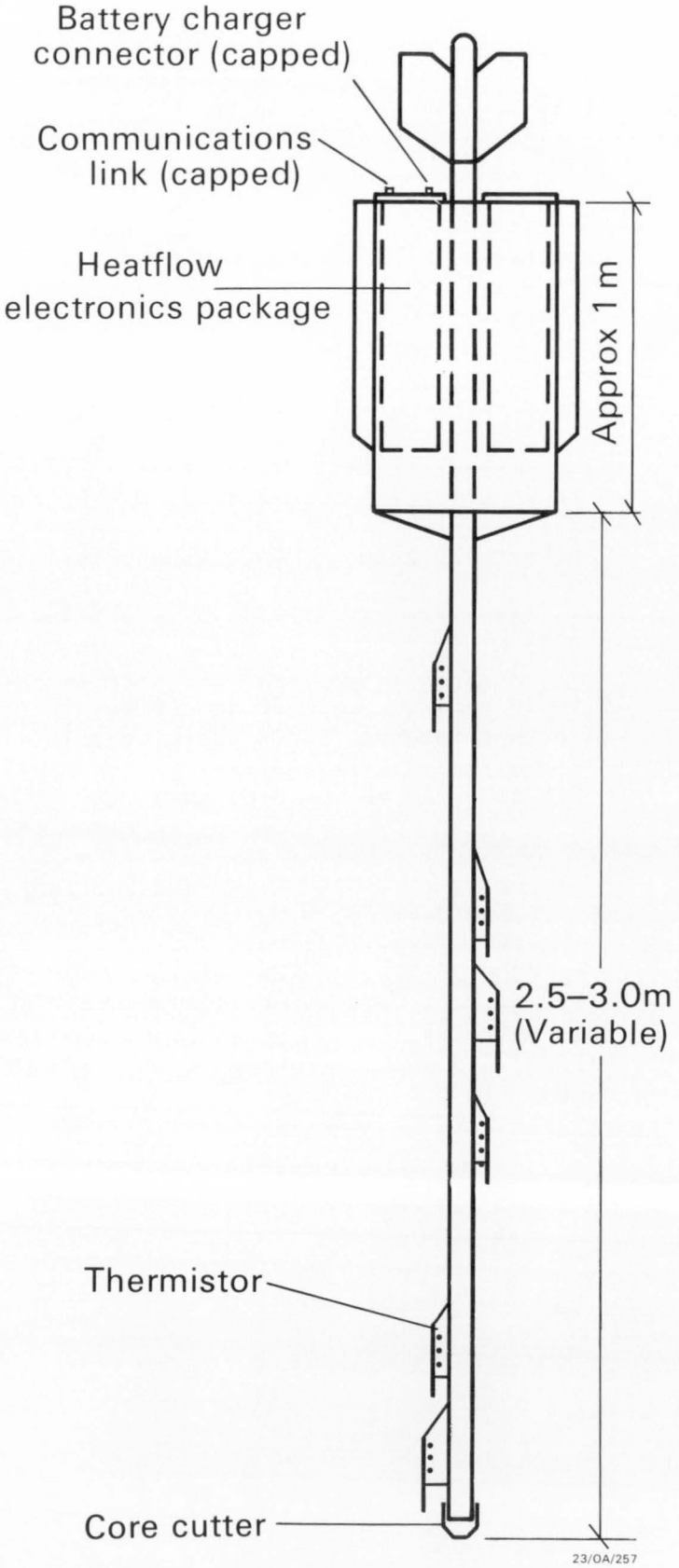

Figure 47: Thermal gradient meter (gravity corer-type).

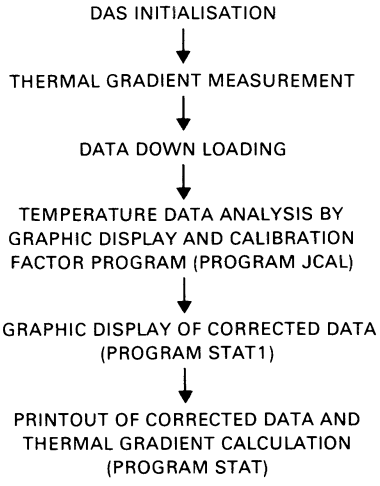

Table 8: NTS-11 data processing flow

23/OA/267

the core centres reached room temperature in 3.5-4 hours.

Conductivities were measured on both split and unsplit cores to check for any differences. For unsplit cores, measurements were taken every 30 cm along each core by drilling through the core liner. After it was found that values obtained from split cores were consistently 10% higher than for unsplit cores, new measurements were taken from all split cores, with the needle probe being inserted in every representative lithology. The conductivity values in Figure 48 are those made on split cores, while the results of all measurements are included in Table 9.

RESULTS

A total of 21 heatflow stations were occupied during the survey in water depths ranging from 600 to 2700 m (Appendix D). Despite the thin sediment cover and severe problems with bent probes, a total of 10 heatflow values of fair to good reliability were obtained (Table 10).

Thermal Gradients

Because of the generally poor penetration achieved, thermal gradients are in most cases based on the temperatures from only two or three thermistors. However, rigorous examination of the performance of each thermistor (Appendix I) indicates that the calculated gradients should be reliable. Plots of thermistor temperatures at all successful heatflow stations are included in Appendix J.

Thermal gradients on the Ceduna Terrace were generally high with several superimposed anomalous highs. After the exclusion of a single extreme gradient of 448 C/km, the average of the remaining ten gradients is 84 C/km.

Thermal Conductivities

As was found on an earlier cruise (Choi, Stagg, & others, 1987), thermal conductivities showed relatively little variation within the range 0.7-1.0 W/(m.K). Some low values of less than 0.6 W/(m.K) were obtained from coarse sediments saturated with sea water. In general, calcareous sands showed lower values than quartz-rich sands. For the cores obtained at successful thermal gradient stations, the average conductivity was 0.90 W/(m.K), with extremes of 0.80 and 0.96 W/(m.K).

Heatflow

Heatflow values obtained by multiplying the thermal gradient with the thermal conductivity are shown in Table 10. Heatflow values are generally high on the central Ceduna Terrace and low on the southwestern flank of the terrace. The average heatflow value at 10 stations is 75 mW/m2; the single station referred to above with a very high thermal gradient gave a similarly high heatflow value of 358 mW/m2. These values are somewhat higher than the world-wide average (Jessop & others, 1976). Values that are anomalously high along the profile may be related to volcanics that are apparent in the seismic data.

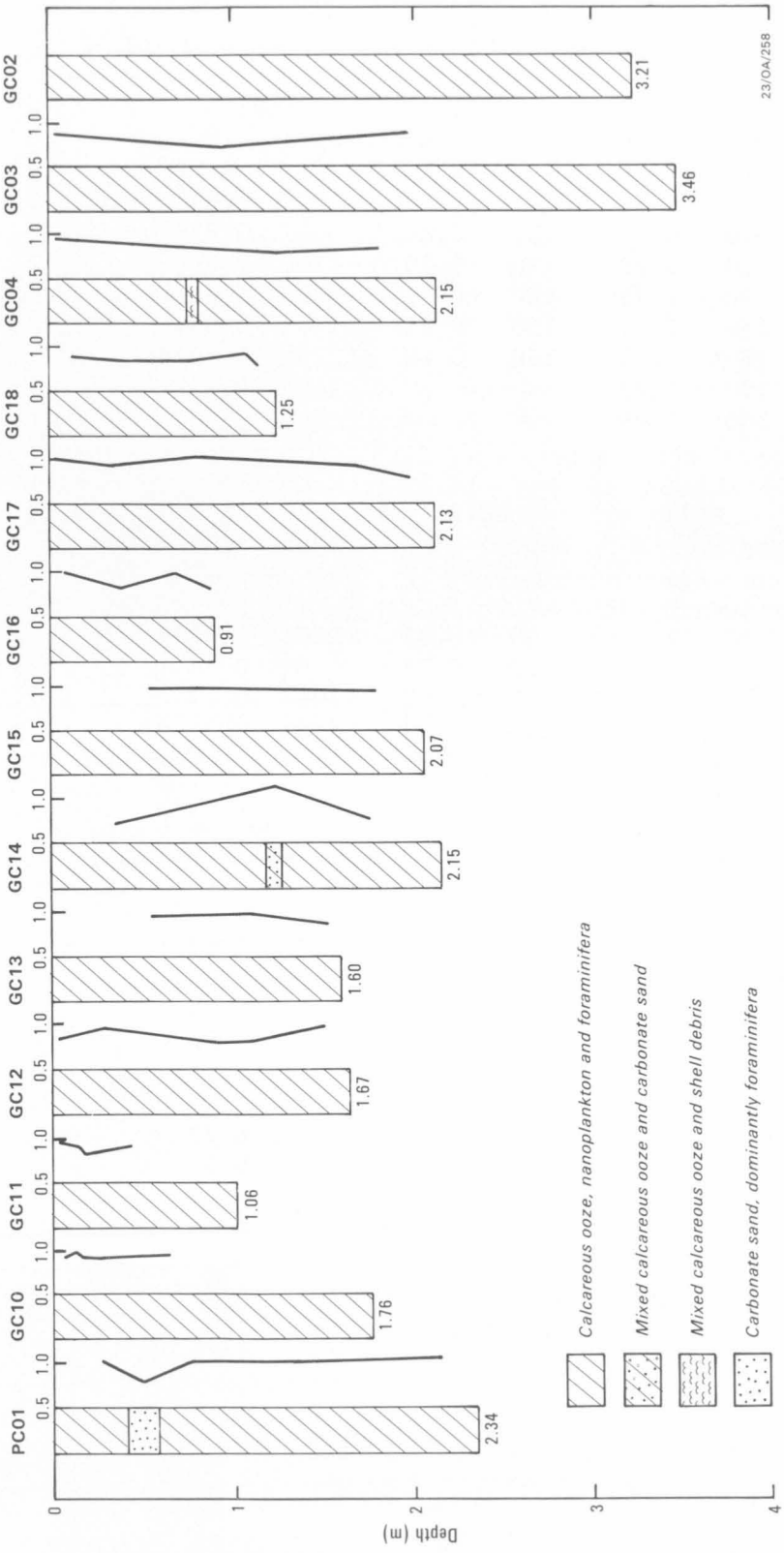

Figure 48: Thermal conductivity plots for cores collected during Leg 2.

Table 9 : Sediment core thermal conductivity.

A. Unsplit cores - conductivity (K) in W/m/K; depth in cm.

GC02		GC03		GC04		GC05	
depth	K	depth	K	depth	K	depth	K
		10	0.79			10	0.84
40	0.70	40	0.77	33	0.80	40	0.85
70	0.82	70	0.78	70	0.79	70	0.89
100	0.81	100	0.79	100	0.81	100	0.88
130	0.75	130	0.77	130	0.81	130	0.85
160	0.81	160	0.70	160	0.80	220	0.89
190	0.77	190	0.77			240	0.82
		340	0.79				

GC10		GC11		GC12		GC13	
depth	K	depth	K	depth	K	depth	K
		10	0.87				
35	0.86	40	0.89	40	0.82	40	0.80
69	1.03	60	0.69	70	0.79	70	0.76
		98	0.79	100	0.67	100	0.79
126	0.83			130	0.87	130	0.75
155	0.76			160	0.81		

GC14		GC15		GC16		GC17	
depth	K	depth	K	depth	K	depth	K
		10	0.85	4	0.80	10	0.81
40	0.79	40	0.77	22	0.81	40	0.89
70	0.83	70	0.84	53	0.81	70	0.82
100	0.80	100	0.80	83	0.79	100	0.84
130	0.86	130	0.80			130	0.84
160	0.82	160	0.77			160	0.92
190	0.81	190	0.79			190	0.75
210	0.85					210	0.83

GC18	
depth	K
5	0.79
31	0.86
62	0.77
92	0.76
122	0.68

Table 9 (continued)

B. Split cores - conductivity (k) W/m/K; depth in cm.

GC03		GC04		GC05		GC07	
depth	K	depth	K	depth	K	depth	K
2	0.86	1	0.96	1	0.78	11	0.52
100	0.72	130	0.78	60	0.96	14	0.77
200	0.86	190	0.83	133	0.91	17	0.55
				147	0.63	19	0.43
				200	0.96	22	0.80
				250	0.76	36	0.77
						50	0.72
						55	0.78
						65	0.76
						68	0.59
						71	0.73
						76	0.86
						89	0.96

GC08		GC10		GC11		PC01	
depth	K	depth	K	depth	K	depth	K
16	0.62	6	0.94	6	0.94	27	1.01
57	0.69	11.5	0.97	12	0.89	27	0.78
98	0.57	14	0.94	13.5	0.82	77	0.99
142	0.69	25	0.91	38	0.91	100	1.00
		60	0.91			216	1.04

GC12		GC13		GC14		GC15	
depth	K	depth	K	depth	K	depth	K
2	0.82	55	0.95	36	0.73	55	0.96
27	0.95	110	0.97	55	0.96	80	0.91
90	0.78	130	0.75	123	1.11	175	0.94
112	0.81	154	0.92	175	0.77		
150	0.98						

GC16		GC17		GC18		GC19	
depth	K	depth	K	depth	K	depth	K
?	0.99	2	1.00	15	0.90	10	1.00
?	0.81	33	1.01	48	0.85	40	1.22
?	0.99	170	0.93	80	0.84	59	1.27
?	0.80	200	0.80	110	0.91	70	0.63
				116	0.78	100	0.70
						130	0.68
						160	0.71
						190	0.69
						220	0.62
						229	0.63
						236	0.78

Table 10 : Heatflow data.

Stn	Lat	Long	WD	N	Temp	Core	Rec.	K	G	Q
HF01	33 51.069	132 05.308	600	3		GC2/3	3.21 3.46			
HF02	33 55.820	132 02.441	701	3	6.87	GC04	2.15	0.80	448	358
HF03	34 01.774	131 58.218	879	3	4.83	(GC04)		0.80	152	122
HF04	34 07.345	131 54.699	1092	0	3.47					
HF05	34 12.998	131 51.533	1195	1	3.15	(GC18)				
HF06	34 22.711	131 45.743	1178	1	3.27					
HF07	34 32.843	131 39.159	1250	2	2.95					
HF08	34 02.212	130 40.060	1151	3	3.23	GC05	2.47			
HF09	34 07.822	130 27.228	1302	2	3.3	(GC05)				
HF10	34 15.932	130 12.405	1676	3	2.56	(GC05)		0.83	55	46
HF11	34 24.056	129 57.746	2175	1	2.19	(GC07)				
HF12	33 39.901	127 42.206	1063	3	3.8	GC08	1.86			
HF13	35 16.668	131 10.897	2643	2	1.93	PC01	2.34	0.96	65	62
HF14	35 12.156	131 13.597	2326	3	2.12	GC11	1.0	0.89	68	61
HF15	35 09.216	131 16.225	2010	4	2.33	GC12	1.67	0.87	68	59
HF16	34 59.643	131 21.541	1734	3	2.54	GC13	1.6	0.95	101	96
HF17	34 50.137	131 25.983	1498	4	2.67	GC14	2.18	0.87	75	65
Hf18	34 41.721	131 33.056	1376	4	2.86	GC15	2.07	0.94	47	44
HF19	34 32.528	131 39.272	1253	3	2.97	GC16	0.91	0.90	126	113
HF20	34 24.251	131 44.095	1186	3	3.13	GC17	2.13	0.93	84	78
HF21	34 16.234	131 49.083	1247	1	2.99	GC18	1.25			

Column headings as follows:-

Stn	- Heatflow station number
Lat, Long	- Station position in degrees and minutes
WD	- Water depth in metres
N	- Number of thermistors that penetrated
Temp	- Bottom water temperature in degrees C.
Core	- Core number used for thermal conductivity
Rec.	- Core recovery in metres
K	- Thermal conductivity in W/m/K
G	- Thermal gradient in degrees C/km
Q	- Heatflow in mW/m2

SEISMIC SYSTEM

Airguns

The major change instituted in the seismic system during the first Southern Margin cruise was the replacement of the original two BOLT airguns with an airgun array supplied and installed by Geophysical Service International (GSI). The first 10 days of the cruise were largely involved with rectifying teething troubles, both in the towing arrangements for the gun string and in the software used to control gun synchronisation. During this initial period, mechanical breakdowns were frequent, and Line 65/001, in particular, was broken a number of times. For the remainder of the cruise, the gun array performed quite reliably.

The array consists of 12 identical guns arranged in four clusters of two guns and two clusters of two guns (Fig. 49A). Normal practice is that only 10 guns be fired at any one time, with clusters of 1, 2, 3, and 4 guns being used. The clustering gives effective volumes of 2.62, 5.25, 7.87, and 10.49 litres (160, 320, 480, and 640 cu in), and a total volume of 26.219 litres (1600 cu in). The remaining two guns in the string can be switched in at any time that an operational gun goes off-line. In this way, it is possible to keep the full array firing after a single gun fails, and there is a 36% or 72% chance of keeping the array going in the event of a second failure. With a third failure, the gun string would normally be retrieved, unless the end of a line was imminent.

The BMR-designed and built gun array firing system enables the control and firing of individual array gun outputs to be synchronised to a single fire pulse command. The gun firing system consists of two units (Fig. 49A) -

1. 12-gun firing box: The firing box consists of 12 single gun firing modules, with each module providing the necessary signal level conversion and pulse timing requirements to drive an airgun firing solenoid.

   Input to the fire module can be via a manual switch for gun testing purposes, or externally from the gun controller (see below). Each fire module provides input pulses and gun solenoid status information. An overall safety interlock feature has been incorporated to disable gun firing during charged shipboard deployment and retrieval.

2. 12 gun controller: The microprocessor-based controller provides the facility to generate individual down-line loaded airgun delays, and interpret gun shuttle returns. Timing information, gun fire delays, and received shuttle times are communicated via an RS-232C link between the controller and the seismic acquisition system. On receiving a single fire pulse command, the controller generates the individual programmed gun delays to be sent to the respective gun firing modules (Fig. 49B). The actual gun firing time is a function of the mechanical response characteristics of each gun, and is sensed by the gun shuttle sensor with subsequent signal level conversion

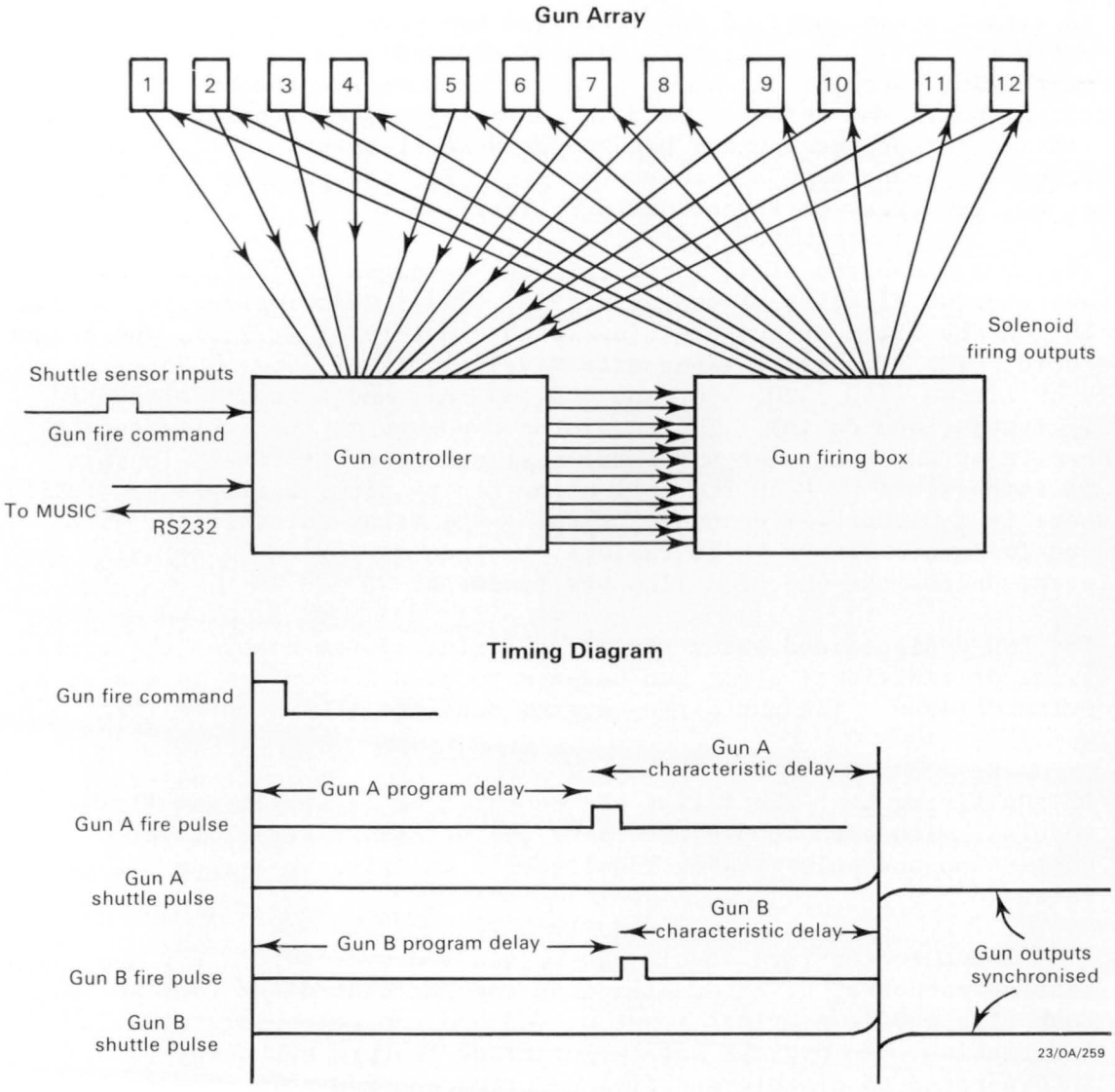

Figure 49: A. Schematic diagram for airgun array controller, firing box, and airgun array. B. Timing diagram for airgun array controller, firing box, and airgun array.

Separate gun shuttle delay times are determined within the controller and are sent to the seismic acquisition system for calculation of updated gun firing times. Trigger and shuttle pulses are available with a resolution of 0.1 msec.

Once production work began, the gun controller operated reliably, with little operator intervention required. In regular operation, the guns rarely drifted more than 1 msec from their required firing times.

Hydrophone Streamer

The 2400 m Teledyne streamer was completely re-ballasted and re-built on the winch prior to the cruise. All sections were filled with sufficient fluid to keep the jacket off the spacers, and then ballasted with lead as shown in Figure 50. The cable was configured with forty-eight 50 m active groups, 5 water-break sections, and 13 depth transducers. A lack of appropriate cards in the seismic amplifiers meant that only seven of the depth transducers were available to the recording system during the cruise. Cable depth was controlled using 13 Syntron RCL-2 individually addressable 'birds' spaced at 200 m intervals along the cable. The full cable configuration is also shown in Figure 50.

Streamer performance was generally satisfactory, with the exception of the following problems -

1. Channels 29 and 30 'died' progressively due to fish bites causing the cable fluid to be flushed out by seawater. This also caused major problems with cable ballasting during the first part of the cruise. Section was replaced.

2. 'Bird' controller wire in one stretch section went open circuit; section was replaced.

3. Channel 30 went dead again; section not replaced until end of cruise.

4. Channel 14 showing strong oscillator noise; source of problem not identified.

5. Channel 6 progressively died towards the end of the cruise; section not replaced until end of cruise.

The 600 m, 12-channel Teledyne streamer used for the majority of the work in the Polda Trough during the gun array test period performed without any trouble. The configuration of this cable was identical to the first 600 m of the 2400 m cable.

Seismic Acquisition System (MUSIC)

The principal change made to MUSIC prior to and during the first cruise, was the incorporation of software required to drive the gun array controller. This was done successfully and gun control was generally satisfactory for the cruise. The technique adopted was

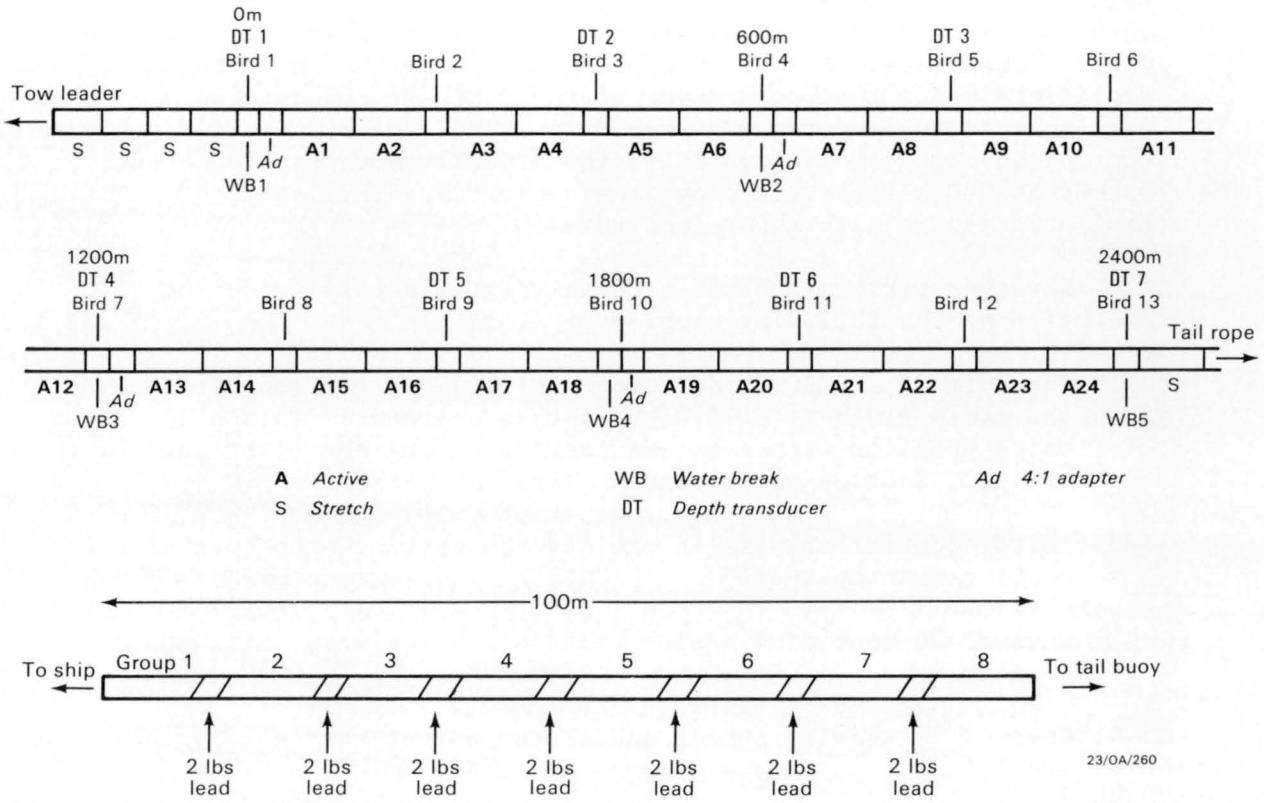

Figure 50: Hydrophone streamer configuration for Leg 1.

to save the previous ten firing delays from each gun and to use those delays to compute an average trigger delay for each gun at each shot. The averaging approach was used to minmise the effects of gun 'jitter'. In practice, a slightly more sophisticated system will be required, such that the occasional misfire (firing errors of more than a few milliseconds) will be ignored in the calculation of the trigger delays. All gun control was done automatically, and individual guns were turned on or off by the seismic system operator from the main MUSIC console.

Unfortunately, the seismic system was plagued by software/hardware crashes throughout the cruise. These crashes were on a highly irregular basis and at the end of the cruise, it was still not clear whether the problem was hardware or software related. Most crashes appeared to be related to writing to magnetic tape; however, insufficient spare equipment or time was available to allow thorough testing of the problem. The crashes were a major irritant to operations, although ultimately the processing and interpretation will probably suffer little.

NON-SEISMIC SYSTEM

The non-seismic data aquisition system (DAS) ran for both cruises without any failures. Major software changes made prior to Leg 1 proved successful, making the system easier to maintain and to extend. All processing programs can now be removed, altered and replaced on-line without loss of data. Additions to the hardware prior to the cruise have also proved beneficial. The DAS computer can now access up to 145 Mbyte of disc space which gives ample space for the saving of on-line data and for post processing of daily magnetic data tapes. Development work was carried out during the cruise which will lead to the eventual saving of updated positions on-line, allowing for the production of track maps with updated positions as opposed to the present non-updated position.

Navigation

Positioning of the ship is derived from two largely independent systems. Considerable skill is required to choose the best system as each exhibits limitations from time to time.

Global Positioning System: A Magnavox T-Set gives continuous absolute positioning within about 20 metres r.m.s. under optimum conditions. However the system is in the experimental stage with only 7 of the proposed 24 satellites in orbit. Positioning is possible for some 8 hours a day but this can be extended to 12 hours in the two-satellite mode by using an atomic frequency standard. Success depends entirely upon an acceptable frequency bias between the satellite transmissions and the standard being determined during the previous period of three to four satellite visibility. Effective use of periods of only two satellites was found to have considerable uncertainty. Experimentation with the system in Perth prior to the start of the cruise showed that the two-satellite system was unreliable, giving considerable position errors which compounded the longer the system operated on two satellites. It is still not clear whether this is due to the Magnavox software, which is a new version (Release 2.7), or due

to an inaccuracy in the rubidium standard used on board. However, during periods of three and four satellites no appreciable change in frequency bias was detected which tends to indicate that the atomic standard is relatively stable in output even if it is inaccurate. Because of this imperfection, it was found undesirable to begin navigating on two satellites after 'dead' periods; thus the use of the instrument was limited to about 8 hours a day.

In an unfortunate accident on Day 303, the T-Set was damaged during heavy weather, rendering it inoperational for the remainder of Leg 1.

Dead-reckoning (DR) System: Two independent DR systems incorporating gyro compass, dual-axis sonar-doppler log, and TRANSIT satnav receiver provide basic dead reckoning for periods where the GPS system was non-operational.

The primary dead reckoning system of Arma-Brown gyro-compass, Magnavox MX610D sonar-doppler, and Magnavox MX1107RS satnav receiver provides the best available positioning of this type. A lower grade system of Robertson gyro, Raytheon DSN450 sonar-doppler, and Magnavox MX1142 satnav receiver is the backup.

Both systems have problems in rough weather or when heading into the sea, due to air being trapped under the hull and blanking the transmission of all sonar systems. A small paddle wheel log has proven to be useful in bad weather as it is not affected by the under-bottom turbulence to the same extent as the sonar-dopplers, mainly because it can be pushed further under the hull than the sonar-dopplers. In general, the sonar-dopplers operated very well and the majority of the dead reckoned positions were within acceptable distances from the satellite fixes.

Bathymetry: Both the 3.5 kHz and the 12 KHz echo sounders operated very well for most of the cruise, only missing data for several hours during some particularly bad weather. Digital depth data was obtained for most of the cruise and this should clean up very quickly during the post processing phase.

Magnetics: Good single channel magnetic data was obtained for most of the cruise. A problem with noisy data at the start of the cruise was quickly traced and for the greater part of the cruise the data were very clean.

Gravity: No problems were experienced with the Bodenseewerke KSS-31 marine gravity meter, data being collected for the entire cruise. Gravity ties were performed at Fremantle, Port Lincoln, and Adelaide.

REFERENCES

BEIN, J., & TAYLOR, M.L., 1981 - The Eyre Sub-basin: recent exploration results. *APEA J.*, 21 (1), 91-8.

BOEUF, M.G., & DOUST, H., 1975 - Structure and development of the southern margin of Australia. *APEA J.*, 15, 33-43.

CALVERT, S.E., 1974 - Deposition and diagenesis of silica in marine sediments. *Special Publication of the International Association of Sedimentoligists,* 1, 273-99.

CANDE, S.C., & MUTTER, J.C., 1982 - A revised identification of the oldest sea-floor spreading anomalies between Australia and Antarctica. *Earth & Planetary Science Letters,*, 58, 151-60.

CHOI, D.R., STAGG, H.M.J., & others, 1987 - Rig Seismic Research Cruise 6: northern Australia heatflow - post-cruise report. *Bureau Mineral Resources, Australia Report*, 274.

CHOQUETTE, P.W., & JAMES, N.P., 1987 - Diagenesis in limestones 3. The deep burial environment. *Geoscience Canada,* 14, 3-35.

CONOLLY, J.R., FLAVELLE, A., & DIETZ, R.S., 1970 - Continental margin of the Great Australian Bight. *marine Geology*, 8, 31-58.

CONOLLY, J.R., & Von Der BORCH, C.C., 1967 - Sedimentation and physiography of the sea-floor south of Australia. *Sedimentary Geology*, 1, 181-220.

COONEY, P.M., EVANS, P.R., & EYLES, D., 1974 - Southern Ocean and its margins. In Veevers, J.J. (ed), Deep sea drilling in Australasian waters. *Challenger Symposium,* Sydney, 26-7.

COOPER, B.J., 1979 - Eocene to Miocene stratigraphy of the Willunga embayment. *South Australian Department of Mines Report of Investigation,* 50.

DAVIES, H.L., CLARKE, J.D.A., STAGG, H.M.J., MCGOWRAN, B., SHAFIK, S., ALLEY, N.F., & WILLCOX, J.B., 1988 - Geological results of *Rig Seismic* cruise 11, Great Australian Bight Basin 1986. *Bureau Mineral Resources, Australia Record*, 88/16.

DAVIES, T.A., LUYENDYK, B.P., & others, 1974 - Initial Reports of the Deep Sea Drilling Project, Vol. XXVI, Washington, (U.S. Govt. Printing Office).

DEIGHTON, I., FALVEY, D.A., & TAYLOR, D.J., 1976 - Depositional environments and geotectonic framework - southern Australian continental margin. *APEA J.*, 16 (1), 25-36.

ETHERIDGE, M.A., BRANSON, J.C., FALVEY, D.A., LOCKWOOD, K.L., STUART-SMITH, P.G., & SCHERL, A.S., 1985 - Basin-forming structures and their relevance to hydrocarbon exploration in Bass Basin, southeastern Australia. *BMR Journal of Australian Geology &*

Geophysics, 9, 197-206.

EXON, N.F., LEE, C-S, & others, 1987 - Preliminary post-cruise report, *Rig Seismic* research cruise 1987: Otway Basin and western Tasmania sampling. *Bureau Mineral Resources, Australia Record*, 87/11.

FALVEY, D.A., 1974 - The development of continental margins in plate tectonic theory. *APEA J.*, 14 (1), 96-106.

FALVEY, D.A., & MUTTER, J.C., 1981 - Regional plate tectonics and evolution of Australia's passive continental margins. *BMR Journal of Australian Geology & Geophysics*, 6, 1-29.

FANDRY, C.B., 1983 - Model for the three-dimensional structure of wind and tidal driven circulation in Bass Strait. In Imberger, J., (ed), Physical Oceanography in Australia. *CSIRO, Melbourne*, 121-42.

FRASER, A.R., & TILBURY, L.A., 1979 - Structure and stratigraphy of the Ceduna Terrace region, Great Australian Bight. *APEA J.*, 19 (1), 53-65.

HAMMONS, R.H., 1966 - Aeromagnetic survey offshore South Australia, OEL 33 and 58. *Bureau Mineral Resources, Australia Petroleum Search Subsidy Report*, Ref. 66/4620.

HAYES, D.E., FRAKES, L.A., & others, 1975 - Initial Reports of the Deep Sea Drilling Project, Vol. XXVIII, Washington, (U.S. Govt. Printing Office).

HINZ, K., WILLCOX, J.B., WHITICAR, M., KUDRASS, H.-R., EXON, N.F., & FEARY, D.A., 1987 - The west Tasmanian margin: an underrated petroleum province. In Glenie, R.C. (ed), *Second South-eastern Australia Oil Exploration Symposium*, Petroleum Exploration Society of Australia Symposium, Melbourne, 1985, 395-410.

von HERZEN, R.P., 1959 - The measurement of thermal conductivity of deep sea sediments by the needle probe method. *Journal of Geophysical Research*, 64, 1557-63.

JAMES, N.P., & CHOQUETTE, P.W., 1984 - Diagenesis 9. Limestones - the meteoritic environment. *Geoscience Canada*, 11 161-94.

JESSOP, A.M., HOBART, M.A., & SCLATER, J.G., 1976 - The world heat flow data collection - 1975. *Geothermal Series*, 5, Ottawa, Canada.

JONES, J.B., & FITZGERALD, M.J., 1984 - Extensive volcanism associated with the separation of Australia and Antarctica. *Science*, 226, 246-8.

JONES, J.B., & FITZGERALD, M.J., 1986 - Silica-rich layering at Blanche Point, South Australia. *Australian Journal of Earth Sciences*, 33, 529-51.

JONES, J.B., & FITZGERALD, M.J., 1987 - An unusual and characteristic sedimentary mineral suite associated with the evolution of passive margins. *Sedimentary Geology*, 52, 45-63.

KONIG, M., 1980 - Geophysical investigations of the southern continental margin of Australia and the conjugate sector of East Antarctica. *PhD Thesis,* Columbia University, New York.

KONIG, M., & TALWANI, M., 1977 - A geophysical study of the southern continental margin of Australia - Great Australian Bight and western sections. *Geological Society of America Bulletin*, 88, 1000-14.

LE MAITRE, R.W., 1984 - A proposal by the IUGS Subcommission on the systemmatics of igneous rocks for a chemical classification of volcanic rocks based on the total alkali silica (TAS) diagram. *Australian Journal of Earth Sciences,* 31, 243-55.

LUDBROOK, N.H., 1958 - The Eucla Basin in South Australia. In Glaessner, M.F., & Parkin, L.W., (eds), The Geology of South Australia. *Geological Society of Australia,* 127-135.

MACILREATH, I.A., & JAMES, N.P., 1984 - Carbonate slopes. In Walker, R.J., (ed), Facies Models. *Geoscience Canada Reprint Series, Second Edition,* 1, 245-58.

MUTTER, J.C., 1978 - An analysis of the Mesozoic-Early Cenozoic rifting history of Australia and Antarctica - implications for generalised geodynamic models of rifting. *M.Sc. Thesis,* Univ. of Sydney.

NELSON, R.G., CRABB, T.N., & GERDES, R.A., 1986 - A review of geophysical exploration in the Polda Basin, South Australia. *APEA J.*, 26, 319-33.

PLEDGE, N., & CLARKE, J.D.A., in prep. - Fossil sharks' teeth dredged from the Great Australian Bight.

ROBERTSON, C.S., CRONK, D.K., NICHOLAS, E., MAYNE, S.J., & TOWNSEND, D.G., 1979 - A review of petroleum exploration and prospects in the Great Australian Bight region. *Bureau Mineral Resources, Australia Record*, 79/20.

ROCHFORD, D.J., 1986 - Seasonal changes in the distribution of Leeuwin Current waters off Southern Australia. *Australian Journal of Marine and Freshwater Research*, 37, 1-10.

SCHLANGER, S.O., & DOUGLAS, R.G., 1975 - The pelagic ooze-chalk-limestone transition and its implications for marine stratigraphy. *Special Publication of the International Association of Sedimentoligists,* 1, 117-48.

SMITH, R., & KAMERLING, P., 1969 - Geological framework of the Great Australian Bight. *APEA J.*, 9 (2), 60-5.

SPROLL, W.P., & DIETZ, R.S., 1969 - Morphological continental-drift fit of Australia and Antarctica. *Nature,* 222, 345-8.

STOW, D.A.V., & LOVELL, J.P.B., 1979 - Contourites: their recognition in modern and ancient sediments. *Earth Science Reviews,* 15, 251-91.

TALWANI, M., MUTTER, J., HOUTZ, R., & KONIG, M., 1979 - The crustal structure and evolution of the area underlying the magnetic quiet zone on the margin south of Australia. In J.S. Watkins, L. Montadert, & P.W. Dickerson (eds), *American Association of Petroleum Geologists Memoir*, 29, 151-75.

TILBURY, L.A., & FRASER, A.R., 1981 - Submarine valleys on the Ceduna Terrace. *BMR Journal of Australian Geology & Geophysics*, 6 (3), 259-64.

VAIL, P.R., MITCHUM, Jr, R.M., & THOMPSON, III, S., 1977 - Global cycles of relative changes of sea level. In E.C. Payton (ed), Seismic stratigraphy - applications to hydrocarbon exploration, *American Association of Petroleum Geologists Memoir*, 26, 83-98.

VEEVERS, J.J., 1986 - Breakup of Australia and Antarctica estimated as mid-Cretaceous (95+/-5 Ma) from magnetic and seismic data at the continental margin. *Earth & Planetary Science Letters*, 77, 91-9.

VEEVERS, J.J., 1987 - The conjugate margins of Antarctica and Australia. In Eittreim, S.L., & Hampton, M.A., (eds) - The Antarctic continental margin: geology and geophysics of offshore Wilkes Land. *CPCEMR Earth Science Ser.*, 5A, Houston, Texas, Circum-Pacific Council for Energy and Mineral Resources, 45-73.

VEEVERS, J.J., & EITTREIM, S.L., in press - Reconstruction of Antarctica and Australia at breakup (95 +/-5 Ma) and before rifting (160 Ma). *Australian Journal of Earth Sciences*.

VEEVERS, J.J., & EVANS, P.R., 1975 - Late Palaeozoic and Mesozoic history of Australia. In Campbell, V.S.W., (ed), *Gondwana Geology: 3rd Gondwana Symposium*, Canberra, 1973, 579-607.

VON DER BORCH, C.C., CONOLLY, J.R., & DIETZ, R.S., 1970 - Sedimentation and structure of the continental margin in the vicinity of the Otway Basin, southern Australia. *Marine Geology*, 8, 59-83.

VOGT, P.R., CHERKIS, N.Z., & MORGAN, G.A., 1983 - Project Investigator-I: Evolution of the Australia-Antarctic Discordance deduced from a detailed aeromagnetic study. In R.L. Oliver, P.R. James, & J.B. Jago (eds), *Antarctic Earth Science*, Australian Academy of Science, Canberra, 608-13.

WEISSEL, J.K., & HAYES, D.E., 1972 - Magnetic anomalies in the southeast Indian Ocean. In D.E. Hayes (ed), Antarctic oceanology II; Australian-New Zealand sector: *Antarctica Research Series*, 19, 234-49.

WEISSEL, J.K., & HAYES, D.E., 1974 - The Australian-Antarctic Discordance: new results and implications. *Journal of Geophysical Research*, 179, 2579-87.

WHYTE, R., 1978 - Shell's offshore venture in South Australia. *APEA J.*, 18 (1), 44-51.

WILLCOX, J.B., 1978 - The Great Australian Bight - a regional interpretation of gravity, magnetic, and seismic data from the

Continental Margin Survey. *Bureau Mineral Resources, Australia Report*, 201.

WILLCOX, J.B., 1981 - Petroleum prospectivity of Australian marginal plateaus. In Halbouty, M.T. (ed) Energy Resources of the Pacific Region, *American Association of Petroleum Geologists Studies in Geology*, 12, 245-72.

WILLCOX, J.B., STAGG, H.M.J., & DAVIES, H.L., 1986 - Research cruise proposal: Structure, stratigraphy, and tectonic development of the Great Australian Bight Basin. *Bureau Mineral Resources, Australia Research Cruise Proposal*.

WILLCOX, J.B., STAGG, H.M.J., & DAVIES, H.L., 1988 - *Rig Seismic* research cruises 10 & 11: structure, stratigraphy, and tectonic development of the Great Australian Bight region - preliminary report. *Bureau Mineral Resources, Australia Record*, 88/13.

WISE, S.W., & WEAVER, F.M., 1974 - Chertification of oceanic sediments. *Special Publication of the International Association of Sedimentoligists*, 1, 301-26.

APPENDIX A: Crew List

Leg 1 - Scientific Crew

J.B. Willcox
H.M.J. Stagg
H.L. Davies
P.J. Hill
N.A. Johnston
M. Walton (Resource Assessment Division, BMR)
G. Saunders
J. Kossatz
J. Bedford
I. Roach
C. Lawson
B. Jones
R. Curtis-Nuthall
B. Maplestone
P. Walker
P. Harris
J.J. Veevers (Macquarie University)
Liu Zhong-chen (Peoples Republic of China)

Ship Crew

D. Harvey (Master)
W. Boot
P. Mosely
C. de Souza
T. Ireland
W. Hansen
L. Clarke
W. Fowler
G. Lemaire
J. Caminiti
M. Cumner
P. Birch
B. Marsh
G. Pretzel

Leg 2 Scientific Crew

H.L. Davies
H.M.J. Stagg
D. Choi
T. Graham
M. Walton
J. Clarke (Flinders University)
M. Joshima (Geological Survey of Japan)
C. Conor (University of Adelaide)
P. Haines (University of Adelaide)
J. Stuart
M. O'Connor
K. Revill
J. Kossatz
N. Clark
D. Pryce
L. Miller
D. Holdway
R. McMahon
R. Schuler

Ship Crew

D. Harvey (Master)
R. Hardinge
P. Mosely
S. Johnson
P. Pittiglio
P. Jiear
J. Thornton
H. Dekker
G. Conley
S. O'Rourke
M. Cumner
P. Birch
D. Kane
N. Luscombe

APPENDIX B : Summary from cruise proposal.

In October-December 1986, it is proposed to use the BMR research vessel *Rig Seismic* for two 1-month cruises in the Great Australian Bight on the southern margin of Australia. During the first cruise, it is intended that up to 4000 km of 96-channel, tuned airgun array seismic data, together with gravity, magnetic, and bathymetric data will be acquired along NW-SE and SW-NE lines across the western Ceduna Terrace, Eyre Terrace, and the adjacent continental rise. Interpreted along with earlier oil company data in the region, the seismic studies will provide a coherent regional framework for analysis of the structure and stratigraphy of the Great Australian Bight Basin and the Eyre Sub-basin. These basins are presently tested by only two wells. The study will be oriented towards delineation of the structural style and analysis of the distribution of seismic facies, particularly in relation to the various marine incursions of Cretaceous age; these aspects have direct relevance to the hydrocarbon prospectivity of the region.

The second leg will be devoted to a program of rock and sediment sampling and heat-flow measurements both in the area covered by Leg 1 and along the southern margin of the Ceduna Terrace. The geological sampling is intended to provide a geological basis for interpretation of the Leg 1 and earlier seismic data and the heat-flow program to provide information on tectonic history and sediment hydrocarbon maturity.

APPENDIX C : Seismic line way points - Leg 1

Line	Start		Stop		SP's	Fold	Source	Length (km)
001A	33 12	126 23	33 24	126 31	447	24	array	25
001B	33 13	126 23	33 46	126 44	1379	24	array	69
001C	33 44	126 43	33 57	126 52	588	24	array	30
001D	33 56	126 51	34 22	127 08	1158	24	array	57
001E	34 18	127 06	35 11	127 40	2369	24	array	115
001E	35 11	127 40	35 26	127 49	566	24	BOLT	35
002A	35 24	127 46	35 02	128 35	1618	24	BOLT	89
002B	34 57	128 48	34 00	130 47	4123	24	array	233
101A	33 06	133 48	33 46	133 21	3328	12	array	87
102A	33 45	133 22	33 42	133 20	213	12	array	7
102B	33 42	133 20	33 09	132 56	2676	12	array	72
103A	33 10	132 57	33 45	132 28	3069	12	array	81
104A	33 45	132 26	33 38	132 23	454	12	array	16
104B	33 38	132 22	33 25	132 12	1062	12	array	30
104C	33 24	132 11	33 09	131 59	1318	12	array	35
105A	33 10	131 59	33 33	131 42	1806	12	array	52
105B	33 28	131 46	33 45	131 33	826	24	array	48
106A	33 45	131 32	33 28	131 17	720	24	array	40
106B	33 27	131 16	33 11	131 01	811	24	array	41
003 (A-H)	33 12	131 05	34 44	127 47	6862	24	array	357
004 (A-E)	34 46	127 50	33 21	126 57	3301	24	array	183
005	33 22	126 55	33 15	127 28	1017	24	array	57
006 (A-B)	33 16	127 26	34 50	128 31	3806	24	array	205
007	34 48	128 30	33 56	130 12	3763	24	array	188
008 (A-C)	33 58	130 10	34 29	130 26	1482	24	array	76
009 (A-B)	34 29	130 36	35 06	129 24	2601	24	array	130
010 (A-B)	35 08	129 28	33 26	128 17	4187	24	array	224
011 (A-C)	33 27	128 18	34 02	128 19	1186	24	array	67
012 (A-C)	34 02	128 20	33 37	129 07	1706	24	array	88
012 (D-E)	33 35	129 12	33 24	129 32	656	24	array	45
013 (A-B)	33 22	129 30	34 50	130 32	3666	24	array	196
014 (A-B)	34 46	130 30	36 25	130 30	3600	24	array	189
015 (A-E)	36 25	130 29	34 43	131 32	3898	24	array	213
015 (F-J)	34 36	131 37	33 10	132 30	3442	24	array	194

TOTALS	24-fold	array	3070 km
	12-fold	array	380 km
	24-fold	BOLT	124 km
			3574 km

BOLT - single BOLT 8.2 l airgun.

APPENDIX D : Listing of Sampling/Heatflow Stations

Station	Time	Lat	Long	Depth (m)
66/SM/DR01	318.0928	33 55.984	128 38.260	3288
66/SM/DR01	318.1259	33 53.589	128 36.740	2945
66/SM/DR02	319.0404	34 2.319	126 44.051	2640
66/SM/DR02	319.0712	34 .381	126 43.521	2176
66/SM/GC01	322.2042	33 44.585	132 9.322	186
66/SM/GC02	322.2338	33 50.398	132 4.700	591
66/SM/GC03	323.0247	33 51.069	132 5.308	600
66/SM/HF01	"	"	"	"
66/SM/GC04	323.0555	33 55.820	132 2.441	701
66/SM/HF02	"	"	"	"
66/SM/HF03	323.1038	34 1.774	131 58.218	879
66/SM/HF04	323.1256	34 7.345	131 54.699	1092
66/SM/HF05	323.1505	34 12.998	131 51.533	1195
66/SM/HF06	323.1751	34 22.711	131 45.743	1178
66/SM/HF07	323.2028	34 32.843	131 39.159	1250
66/SM/GC05	324.0527	34 2.305	130 41.483	1134
66/SM/HF08	324.1141	34 2.212	130 40.060	1151
66/SM/HF09	324.1450	34 7.822	130 27.228	1302
66/SM/HF10	324.1803	34 15.932	130 12.405	1676
66/SM/HF11	324.2122	34 24.056	129 57.746	2175
66/SM/GC06	325.0202	34 31.446	129 40.820	3135
66/SM/GC07	325.0540	34 35.438	129 31.716	3662
66/SM/GC08	325.1901	33 39.901	127 42.206	1063
66/SM/HF12	"	"	"	"
66/SM/GC09	325.2142	33 29.931	127 35.717	757
66/SM/DR03	326.0947	33 58.549	128 36.520	3506
66/SM/DR03	326.1312	33 57.211	128 33.755	3285
66/SM/DR04	326.2142	34 9.512	129 6.379	3302
66/SM/DR04	327.0012	34 9.352	129 7.623	3109
66/SM/PC01	329.1017	35 16.599	131 11.545	2646
66/SM/GC10	329.1345	35 16.668	131 10.897	2643
66/SM/HF13	"	"	"	"
66/SM/GC11	329.1705	35 12.156	131 13.597	2326
66/SM/HF14	"	"	"	"
66/SM/GC12	329.1958	35 9.216	131 16.225	2010
66/SM/HF15	"	"	"	"
66/SM/GC13	329.2333	34 59.643	131 21.541	1734
66/SM/HF16	"	"	"	"
66/SM/GC14	330.0251	34 50.137	131 25.983	1498
66/SM/HF17	"	"	"	"
66/SM/GC15	330.0616	34 41.721	131 33.056	1376
66/SM/HF18	"	"	"	"
66/SM/GC16	330.0921	34 32.528	131 39.272	1253
66/SM/HF19	"	"	"	"
66/SM/GC17	330.1221	34 24.251	131 44.095	1186
66/SM/HF20	"	"	"	"
66/SM/GC18	330.1508	34 16.234	131 49.083	1247
66/SM/HF21	"	"	"	"
66/SM/DR05	Station failed.			
66/SM/DR06	333.0610	35 34.010	132 54.760	2493

66/SM/DR06	333.0818	35	33.293	132	50.660	2018
66/SM/GS01	333.1313	35	28.430	132	54.972	2397
66/SM/GC19	333.1647	35	28.320	132	55.042	2396
66/SM/GC20	334.0220	35	41.743	133	18.761	2810
66/SM/GC21	334.0530	35	41.283	133	19.867	2717
66/SM/GC22	334.0804	35	41.981	133	21.227	2316
66/SM/DR07	334.1105	35	41.974	133	19.537	2792
66/SM/DR07	334.1324	35	42.165	133	17.628	2219
66/SM/DR08	335.0629	35	40.722	134	25.952	2823
66/SM/DR08	335.1054	35	38.102	134	24.602	2238
66/SM/DR09	335.1800	36	.097	134	49.796	3680
66/SM/DR09	335.2039	36	.559	134	53.368	3009
66/SM/DR10	336.0153	35	59.375	134	50.590	3565
66/SM/DR10	336.0609	35	55.526	134	47.563	2920
66/SM/DR11	336.1727	35	49.641	135	9.498	2978
66/SM/DR11	336.2050	35	50.060	135	13.812	2118
66/SM/DR12	337.0145	35	54.805	135	5.427	3622
66/SM/DR12	337.0605	35	55.561	135	8.604	2629
66/SM/DR13	337.1621	35	58.462	135	13.667	3449
66/SM/DR13	337.1820	35	57.458	135	11.450	2535
66/SM/DR14	337.2036	35	58.361	135	13.553	3461
66/SM/DR14	338.0610	35	58.429	135	12.795	3064
66/SM/DR15	338.1831	36	20.061	135	40.140	3393
66/SM/DR15	339.0008	36	19.071	135	36.372	2496

APPENDIX E : Cruise diary, Survey 65.

JD.GMT	Local Date	Remarks
287.1340	14 Oct	Depart Fremantle; transit to GAB.
288.0620	15 Oct	Seismic cable streamed and re-wound
288.1040	15 Oct	Magnetometer streamed.
290.2050	17 Oct	Retrieve magnetometer; stream seismic cable.
292.0337	19 Oct	Commence seismic line 65/001
292.0630	19 Oct	Gun repairs.
292.1550	19 Oct	Resume line 65/001.
292.2335	19 Oct	Gun array repairs.
293.0624	20 Oct	Resume line 65/001.
293.0918	20 Oct	Gun array repairs.
293.1134	20 Oct	Resume line 65/001.
293.1748	20 Oct	Gun array repairs.
293.2155	20 Oct	Resume line 65/001.
294.1041	21 Oct	Gun array down again; switch to single 500 cu in BOLT airgun.
294.1346	21 Oct	Acquisition suspended at end of line 65/001, due to bad weather.
295.1404	22 Oct	Start line 65/002 with BOLT airgun.
295.2247	22 Oct	BOLT gun off-line.
296.0102	23 Oct	Resume line 65/002 with gun array.
296.2314	23 Oct	Acquisition suspended; EOL 65/002; all equipment retrieved.
297.0600	24 Oct	Transit to Thevenard.
297.2230	24 Oct	Pick up GSI gun mechanic at Thevenard.
298.0400	25 Oct	Commence streaming 600 m seismic cable.
298.0622	25 Oct	Start seismic acquisition on line 65/101 in Polda Trough, using gun array.
298.1542	25 Oct	EOL 65/101; gun maintenance.
298.1740	25 Oct	SOL 65/102.
298.1816	25 Oct	Recording suspended when gun array compressor went off-line.
298.1826	25 Oct	Recording resumed on line 65/102.
299.0156	26 Oct	EOL 65/102; gun array maintenance.
299.0402	26 Oct	SOL 65/103.
299.1239	26 Oct	EOL 65/103.
299.1303	26 Oct	SOL 65/104.
299.2112	26 Oct	EOL 65/104; gun array maintenance.
300.0005	27 Oct	SOL 65/105
300.0512	27 Oct	Recording suspended; gun array maintenance; 600 m cable retrieved; 2400 m cable streamed.
300.2317	27 Oct	Resume line 65/105.
301.0356	28 Oct	EOL 65/105; SOL 65/106.
301.1249	28 Oct	EOL 65/106; gun array maintenance.
301.1534	28 Oct	SOL 65/003.
303.0702	30 Oct	EOL 65/003; gun array maintenance.

303.1105	30 Oct	SOL 65/004.
304.0557	31 Oct	EOL 65/004.
304.0646	31 Oct	SOL 65/005.
304.1215	31 Oct	EOL 65/005; gun array maintenance.
304.1315	31 Oct	SOL 65/006.
305.0954	01 Nov	EOL 65/106; gun array maintenance.
305.1155	01 Nov	SOL 65/007.
306.0740	02 Nov	EOL 65/007; gun array maintenance.
306.0926	02 Nov	SOL 65/008.
306.1920	02 Nov	EOL 65/008; SOL 65/009.
307.0940	03 Nov	EOL 65/009; gun array maintenance.
307.1115	03 Nov	SOL 65/010.
308.1000	04 Nov	EOL 65/010; gun array maintenance.
308.1145	04 Nov	SOL 65/011.
308.1858	04 Nov	EOL 65/011
308.1922	04 Nov	SOL 65/012.
309.0939	05 Nov	EOL 65/012; gun array maintenance.
309.1235	05 Nov	SOL 65/013.
310.0851	06 Nov	EOL 65/013; run array maintenance.
310.1043	06 Nov	SOL 65/014.
311.0658	07 Nov	EOL 65/014; gun array maintenance.
311.0843	07 Nov	SOL 65/015; line shot at 4 knots with 10 second records.
312.1204	08 Nov	Recording suspended on line 65/015 for gun array maintenance.
312.1357	08 Nov	Resume line 65/015.
313.1300	09 Nov	Magnetometer retrieved.
313.1342	09 Nov	EOL 65/015; retrieve seismic cable and gun array; steam for Port Lincoln.

APPENDIX F : 1969-76 SHELL SURVEYS

Year	Ship	Km	Source (capacity)	Streamer	Fold
1969	Polaris	3862	TAA* (14.75 l)	2400 m	24
1970		2417	Aquapulse	2400 m	24
1970		2437	TAA (14.1 l)	2400 m	24
1971	Dunlap	4200	TAA (21.3 l)	2400 m	24
1973					
1974	McDermott	1718	TAA (19.68 l)	3200 m	24
1974	McDermott	49	TAA (19.68 l)	3200 m	48
1974	McDermott	981	TAA (19.66 l)	3200 m	24
1976	Prospekta	833	TAA (23.45 l)	2400 m	24

* Tuned Airgun Array

APPENDIX G: Locations of wells in the Great Australian Bight region

Well Basin	Company Year	Lat	Long	wd	td	Status
Echidna Duntroon	Shell 1972	35 36.250	135 37.200	13	3832	PA in Neocomian clay; no traces of hydrocarbons
Platypus Duntroon	Shell 1972	35 25.167	134 49.467	158	3893	PA in Aptian sandstone; no traces of hydrocarbons
Apollo Eucla	Outback 1975	32 32.266	130 51.217	75	877	PA in granite; no traces of hydrocarbons
Gemini Polda	Outback 1975	33 28.733	134 12.066	68	894	PA in granite or syenite; no traces of hydrocarbons
Potoroo GAB	Shell 1975	33 23.233	130 46.117	252	2924	PA in Neocomian sandstone; no significant hydrocarbon shows
Jerboa Eyre	Esso-Hematite 1980	33 30.25	127 36.05	771	2537	PA in ?Precambrian basement; no significant hydrocarbon shows
Mercury Polda	Occid. 1981	33 33.787	134 14.233	77	3251	PA in pre-Jurassic quartzose sandstone; minor hydrocarbon show in rafted lst.
Columbia Polda	Occid. 1982	33 29.648	133 53.075	74	2168	PA in pre-Jurassic red-beds; no hydrocarbon shows

APPENDIX H: Ship-board thermal conductivity measurements of sediments from gravity cores

METHODS

Thermal conductivities were measured using a needle probe inserted into the sediments after the core had been allowed to reach thermal equilibrium at room temperature. Measurements were made by two methods:

1. The probe was inserted through holes drilled through the plastic core casing 10cm below the top of the core and at intervals of 30 cm thereafter. A second hole was drilled at each second test point to allow the entry of a temperature probe.

2. After the core was split and logged, thermal conductivity was determined at selected points to determine the variation of conductivity with sediment composition, grainsize, water-content etc.

OBSERVATIONS

1. Cores were observed to take 3-4 hours to warm up to ambient temperature (usually about 20 C).

2. Damp split cores are generally 2 C cooler than the ambient air temperature, probably due to evaporative cooling at the surface. Temperature also varies along the length of the core due to variations in moisture content and needs to be determined at each point at the time of conductivity measurement.

3. In cores composed of uniform sediment type, the thermal conductivity values are usually quite consistent along the length of the core before splitting, and again after the core has been split. However the average value determined from split core is frequently of the order of 0.1 W/(m.K) higher than the average value determined before splitting. The most likely explanation for this inconsistancy is that the low value before splitting results from incomplete penetration of the probe into the sediment. This is because the plastic casing is 2 mm thick and there is often a small air gap of up to a few millimetres between the top of the sediment and the casing. If the drill hole penetrates the sediment there may be incomplete coupling of sediment and probe surface along the upper part of the probe.

   An attempt to quantify the incomplete penetration effect was made by inserting the probe to varying depths into a beaker of uniform calcareous ooze. The results below suggest that low values can be expected if there is an air gap of more than 10 mm at the top of the probe. This is greater than the typical air gap expected following insertion through plastic casing. More tests are required.

0 }	three	0.72
0 }	different	0.73
0 }	points	0.73
5		0.75
10		0.73
15		0.49
20		0.27
30		0.40
not inserted		0.39

4. Significant variations of thermal conductivity can be correlated with sediment composition, grain-size and water content. Below is a list of maximum, minimum and average thermal conductivity measurements determined from a variety of common sediment types available in the cores. All measurements are from split cores.

a) Pale grey calcareous ooze
-probably composed dominantly of calcareous nanoplankton with scattered foraminifera, clay and detrital components.
number of readings = 23
max. K = 1.01 W/(m.K)
min. K = 0.72
av. K = 0.85

b) Pale brown calcareous ooze
-composition similar to (a).
number of readings = 23
max. K = 1.05 W/(m.K)
min. K = 0.72
av. K = 0.90

c) Yellowish-brown calcareous ooze
-composition similar to (a).
number of readings = 8
max. K = 0.94 W/(m.K)
min. K = 0.72
av. K = 0.83

d) White calcareous ooze
-dominantly nanoplankton ooze.
number of readings = 6
max. K = 1.04 W/(m.K)
min. K = o.78
av. K = 0.90

e) Olive green-brown, non-calcareous mud.
-probably dominantly clay and fine silt components.
number of readings = 4
max. K = 0.71 W/(m.K)
min. K = 0.62
av. K = 0.68

f) Orange-brown, sulphide-rich mud (non-calcareous).
-composition as for (e) but with sulphide.
number of readings = 2
max. K = 0.68 W/(m.K)
min. K = 0.63
Av. K = 0.66

g) Black, sulphide-rich mud (non-calcareous)
-composition as for (e) but with sulphide and organic matter.
number of readings = 2
max. K = 0.63 W/(m.K)
min. K = 0.48
av. K = 0.56

h) Fine calcareous sand (wet)
-dominantly composed of foraminifera (well sorted).
number of readings = 9
max. K = 0.78 W/(m.K)
min. K = 0.43
av. K = 0.55

i) Fine calcareous sand and fine ooze
-composition as for (h) but poorly sorted with calcareous ooze filling pore spaces.
number of readings = 4
max. K = 1.11 W/(m.K)
min. K = 0.55
av. K = 0.81

j) Medium-grained, well sorted quartz sand (wet)
-composed dominantly of quartz with scattered calcareous foraminifera of the same size.
number of readings = 4
max. K = 1.27 W/(m.K)
min. K = 1.06
av. K = 1.20

CONCLUSIONS

The following generalisations can be made:

1. Quartz-rich sediments have higher thermal conductivity values than carbonate-rich sediments of similar grain size and sorting, *ie* average K = 1.20 W/(m.K) for quartz sand, K = 0.55 W/(m.K) for carbonate sand.

2. Clay-rich sediments tend to have lower thermal conductivity than carbonate muds.

3. Thermal conductivity decreases with increasing grain-size for well sorted sediments of the same composition, ie. average 0.87 for all calcareous ooze, K = 0.55 W/(m.K) for well sorted carbonate sand. This inverse relationship is probably related to the increasing volume

of pore water and included air spaces. If the material is not well sorted the thermal conductivity value is similar to that of the fine grained components providing that the overall composition is similar, *ie* average K = 0.81 W/(m.K) for mixed carbonate sand and ooze.

4. The different varieties of calcareous ooze found have similar average conductivities and a similar range of values. The average conductivity for calcareous ooze was 0.87 W/(m.K).

5. The main difficulties encountered with measurement of thermal conductivities on board ship are due to ship motion. Consistent results are obtained if the sediments are stiff and highly cohesive, as is the case with most of the fine oozes. If the sediments are non-cohesive or contain a lot of water, poor results may be obtained due to probe movements and motion of the sediment. Very high conductivity readings may result from wet sediment circulating around the needle probe, while low readings can result from the creation of air spaces around the needle probe. in relatively dry, non-cohesive sediments (*eg* damp sands).

RECOMMENDATIONS

The cause of the inconsistency of thermal conductivity values between split and unsplit core needs further investigation. At this stage it appears that the higher results obtained from split cores may be more accurate and these are the only ones that have been used on the previous pages. The temperature needs to be recorded near each test point when making measurements from split core because of the variability noted along the length of a single core.

The problems with core and probe motion may be partially solved if a stand were made to hold the probe steady at each test point. The core also needs to be kept stationary with a core holding rack. A shorter probe needle would allow complete penetration of the sediment in the split core while the probe is held vertically. Very wet sediments should not be measured on board ship because of the problem of movement within the sediment or movement of pore water in wet sediments.

The desired solution to the above problems is to have the facility to measure thermal conductivities *in situ*, thereby avoiding subjecting the sediments to radical environmental changes before measurement. This advantage would be offset somewhat, however, if only a single conductivity value can be taken at each station.

APPENDIX I: Ship-board thermistor checking and calibration

It is important at all times during a heat-flow study that the thermistors in use are in a 'healthy' condition. This requires continuous monitoring of thermistor performance and the replacement of those considered faulty. To assist this monitoring, two graphics programs (JCAL and STAT1) have been added to the data processing flow.

There are currently three methods of checking thermistors -

(1) by measuring the resistance of the thermistors with a multimeter;
(2) by checking the stability in an ice bath; and
(3) by checking the temperature records from actual stations.

1. Multimeter Testing

The thermistor resistance is measured directly through the connector with a multimeter at room temperature for 20-30 seconds. Although the air temperature will be changing continuously, faulty thermistors will show a more erratic drift than healthy thermistors. The typical reaction of a healthy thermistor to this test is for the resistance to decrease during the first few seconds of the test, then to stabilise. The decrease in resistance (= increase in temperature) is caused by self-heating effects due to the current flowing through the thermistor from the multimeter. The amount of heating (and hence the resistance drop) depends on the voltage output of the multimeter (which varies between multimeters and, for a particular multimeter, with the resistance scale being used) and the actual resistance of the thermistor being tested. Any variation from the typical reaction is indicative of a faulty thermistor.

Although this method is not 100% reliable, it is perhaps 80% reliable for the detection of faulty thermistors and 100% reliable for the detection of 'dead' thermistors, and it is quicker to apply than the following two methods.

2. Ice Test

Faulty thermistors can also be detected by testing in an ice bath. This test requires the thermistors to be connected to the electronics package, as in normal operations, and submerged in a bucket of finely and uniformly crushed ice for a period of at least several minutes. Healthy thermistors should show a temperature between +0.05 C and -0.05 C. Faulty thermistors will usually show a temperature far different to this. It is important that the ice is in a state of partial melting and that there are no air pockets or warm spots around the thermistors. This test unfortunately will give no indication if a thermistor will function at high pressure.

3. Checking Temperature Records

As a final check, the actual temperature records at each station should be examined; processing programs JCAL and STAT1 provide a graphics method of accomplishing this. Figure 51 shows the temperature records during the stabilisation time 100-200 m above the

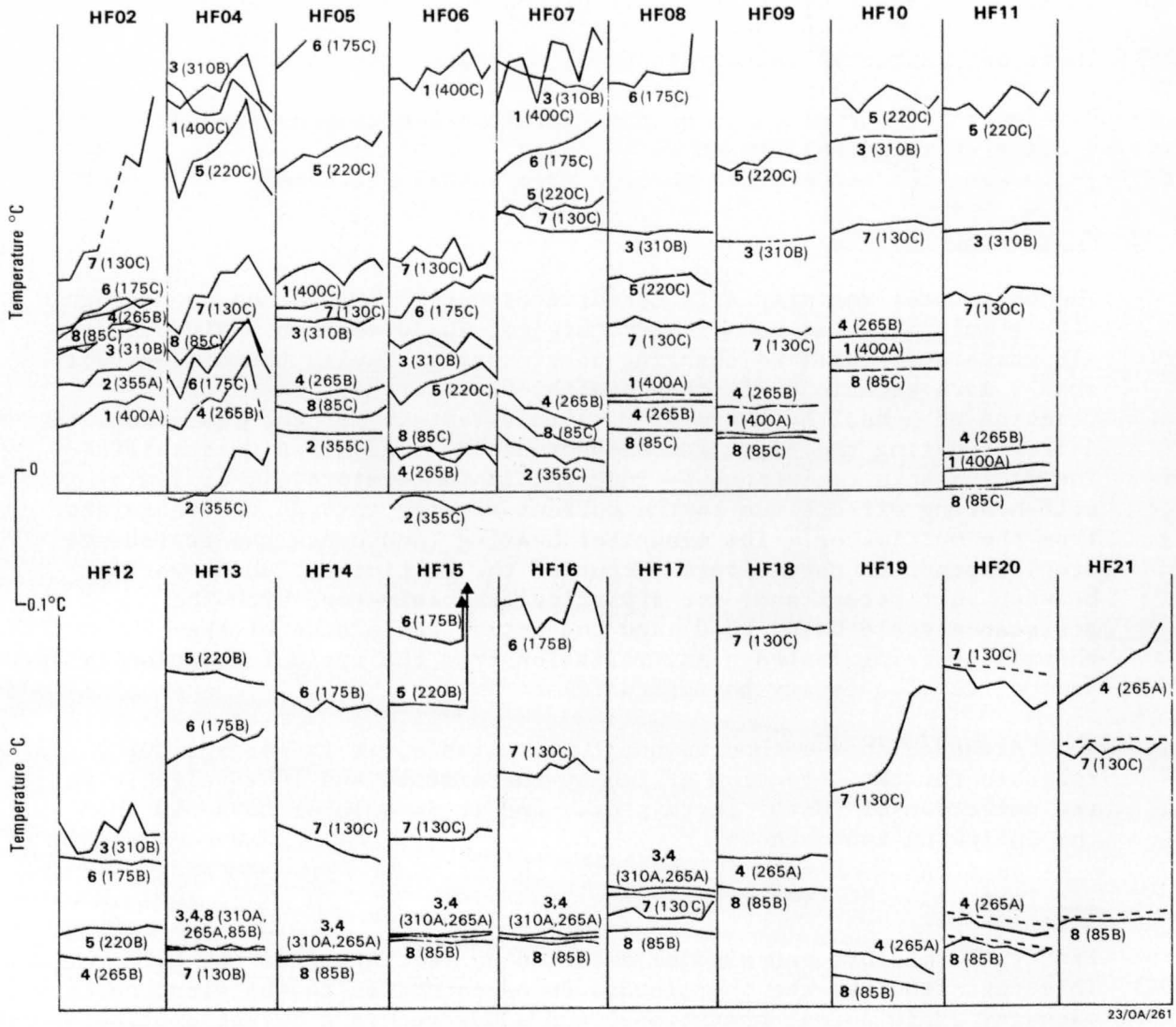

Figure 51: Temperature records during the stabilisation time 100-200 m above seabed for each heatflow station.

seabed for each heat-flow station. Note that the same set of thermistors was used for stations 8-11 and 13-21.

From Figure 51, for example, it can be seen that thermistors 3, 4, 7, and 8 appear healthy at station HF13, but that the indicated temperatures gradually diverge at the succeeding stations and the 'noise' for each thermistor at each station also increases.

Deterioration of Thermistor Sets

Figure 52 shows the change of thermistor calibration factors with increasing station number (*ie* increasing time). Changes in the calibration factors indicate fundamental changes in the thermistors themselves. Three patterns of change can be seen -

- gradual change
- rapid change
- abrupt change

Of these changes, the abrupt change indicates total failure of the thermistor. The period of rapid change (*eg* thermistors 130B, 175B, and 220B) may be related to the water depth, as this change started at the time of the deepest station. Thermistors showing a gradual change in calibration factor may recover after a few days with no use; however, such thermistors appear to quickly deteriorate with further deployments.

At least some thermistor deterioration can be shown to be due to the leakage of seawater. Thermistor 175B, for example, showed a very unstable resistance of about 4.4-5.4 kOhm in a 30 C stabilised water bath. When the cable connector was cut on the lectronics side of the in-line connector, a resistance of 4.40 +/-0.01 kOhm was measured - a little unstable, but close to the original value of 4.475 kOhm. Finally, when the cable was cut on the thermistor side of the in-line connector, the resistance was measured at 4.426 +/-0.003 kOhm, and very stable. Although in this final measurement, thermistor 175B showed more fluctuation than a new thermistor, the difference was very small. Leakage of seawater causes the resistance to decrease - this is translated into an interpreted temperature rise of up to several degrees, which is frequently seen as thermistors deteriorate. We therefore consider it likely that many cases of thermistor deterioration are caused by salt water leakage. If this is correct, then faulty thermistors shoould be repaired by re-cabling and re-termination.

Relation Between Standard Deviation & Water Depth

Figure 53 shows the relationship between the stabilisation water depth and the standard deviations of the temperature data at the time of stabilisation. Only healthy thermistors (those with calibration factors of less than 0.5 C) have been used in this figure. The standard deviation varies from high in shallow water, to very high at around 900-1100 m water depth, and very low in deep water. This may indicate the presence of strong currents in water depths of less than 1100 m, with the strongest currents being at about 900-1100 m depth. This conclusion is supported by the plot of bottom water temperature vs. depth (Fig. 54) which shows greatest scatter at about 1100 m depth.

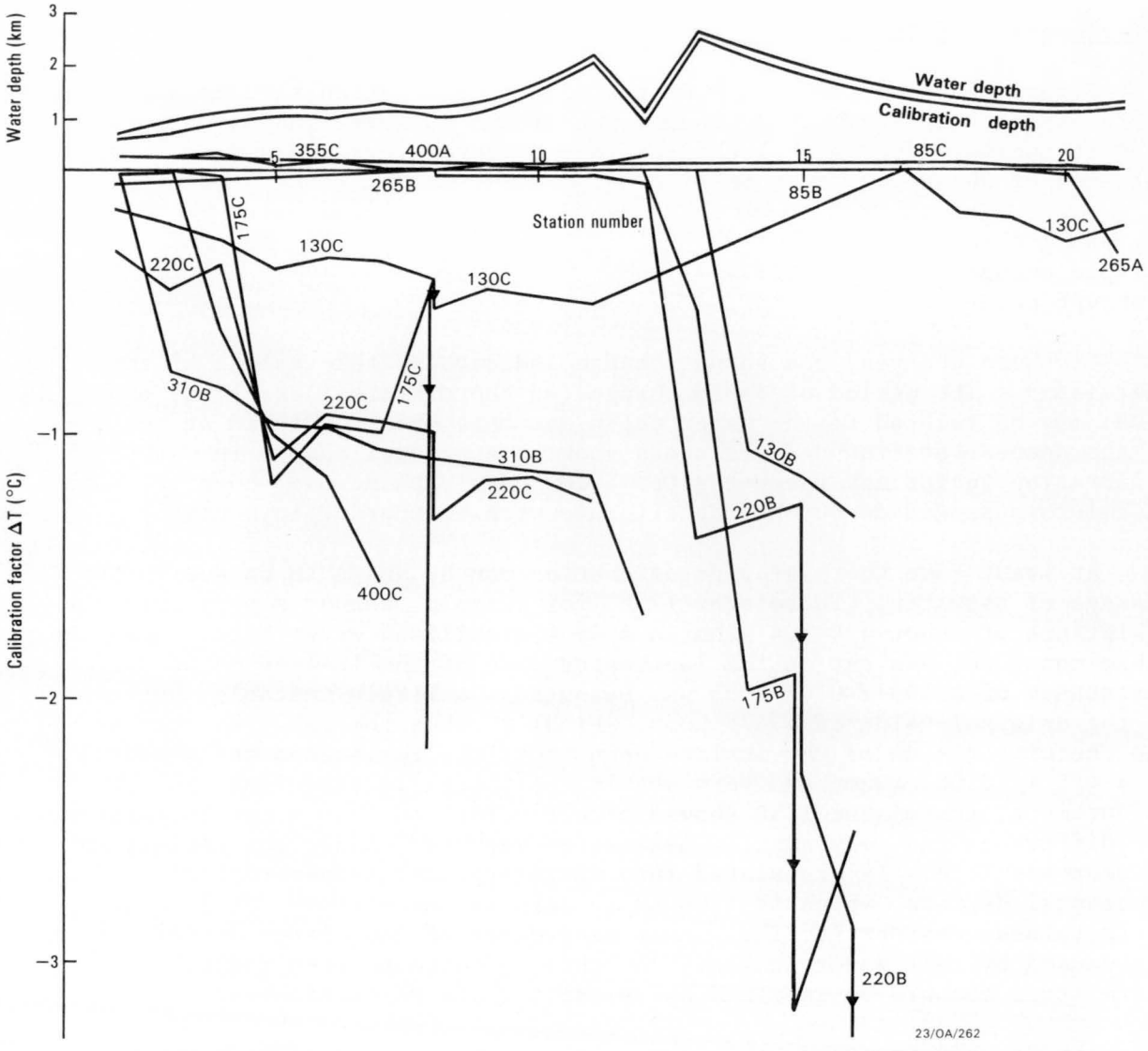

Figure 52: Variation of thermistor calibration factor with increasing station number (*ie* increasing time).

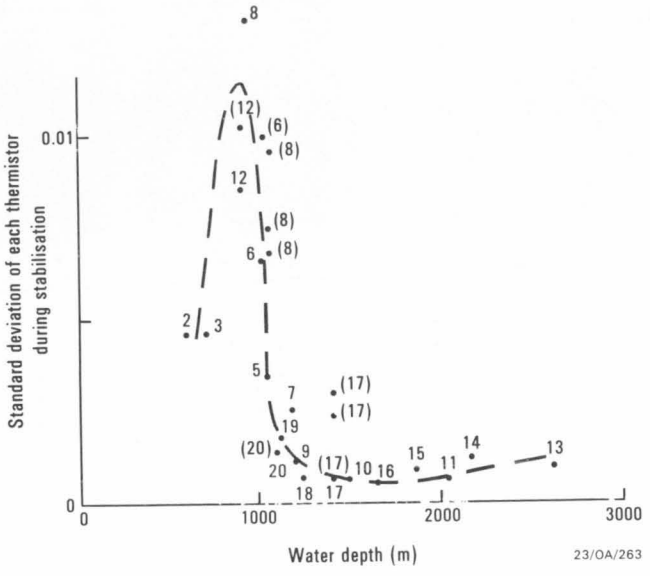

Figure 53: Standard deviation of each thermistor during stabilisation period plotted against water depth.

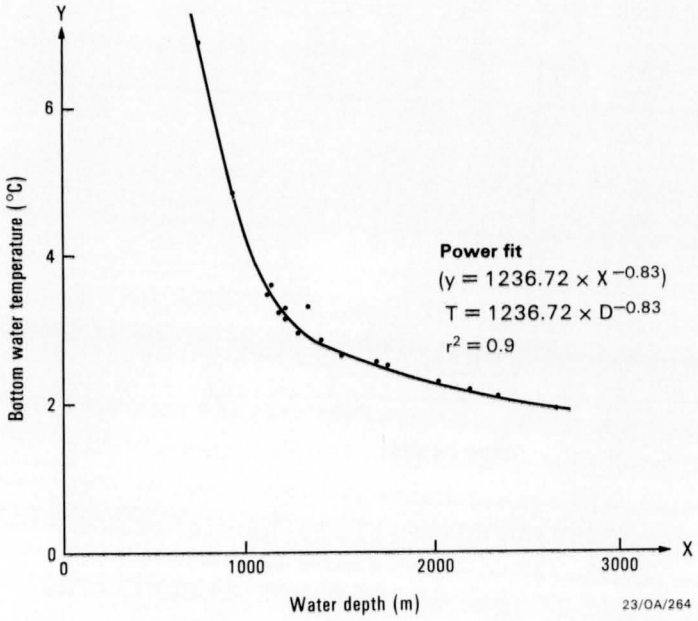

Figure 54: Bottom water temperature plotted against water depth.

APPENDIX J: Heatflow station temperature plots

The following set of figures (Figs 55-65) shows the plots of temperature against time for each thermistor at each successful heatflow station.

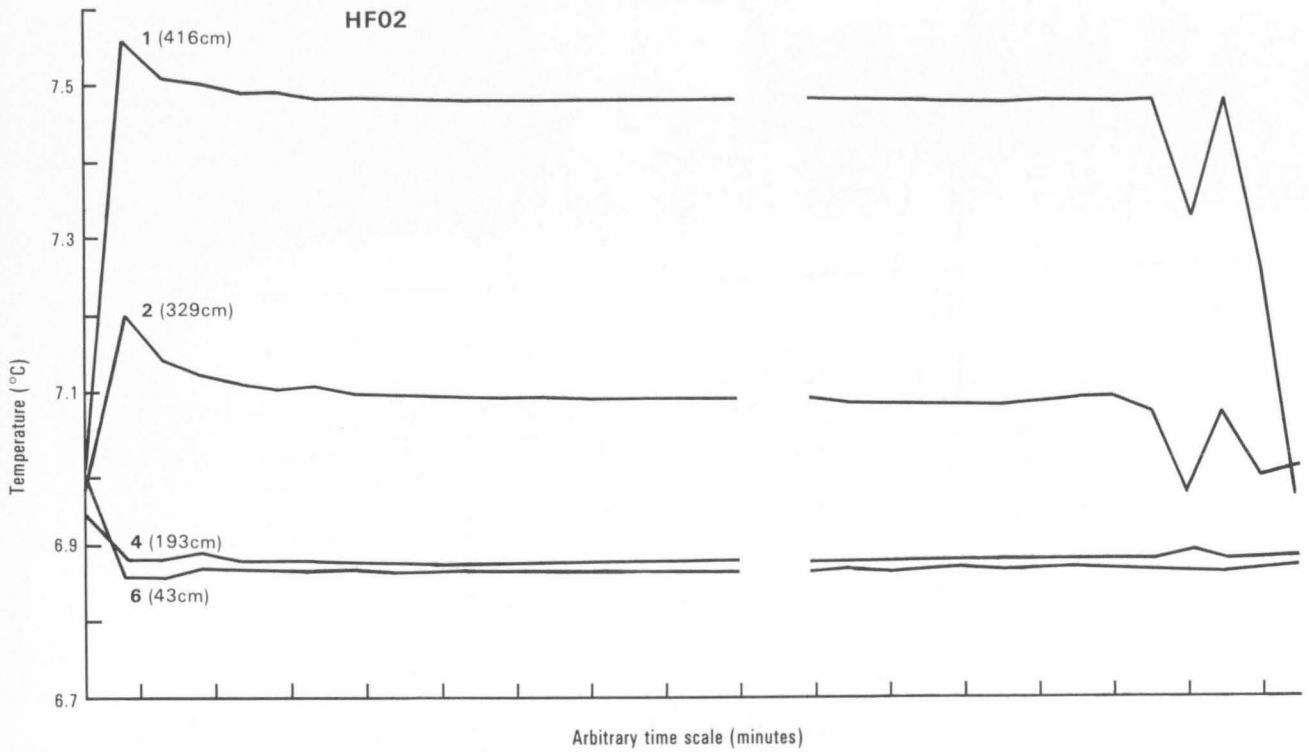

Figure 55: Plot of temperature against time for each thermistor at heatflow station HF02.

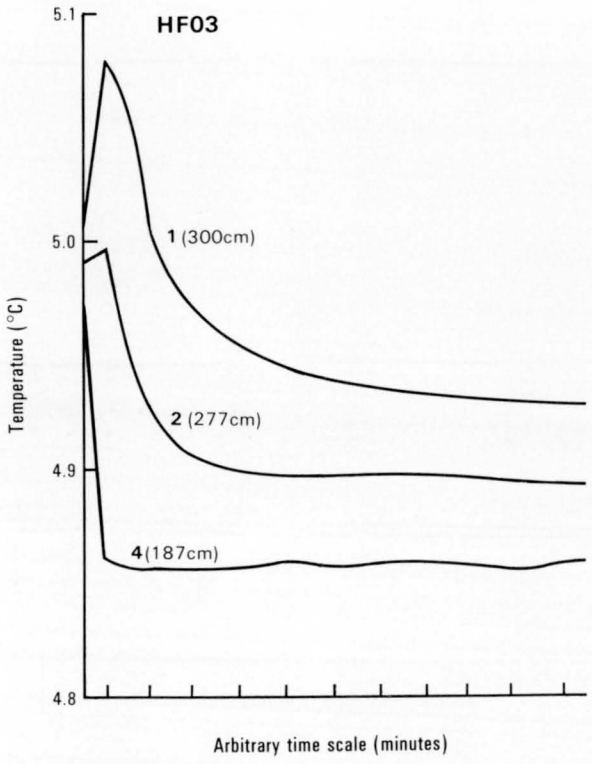

Figure 56: Plot of temperature against time for each thermistor at heatflow station HF03.

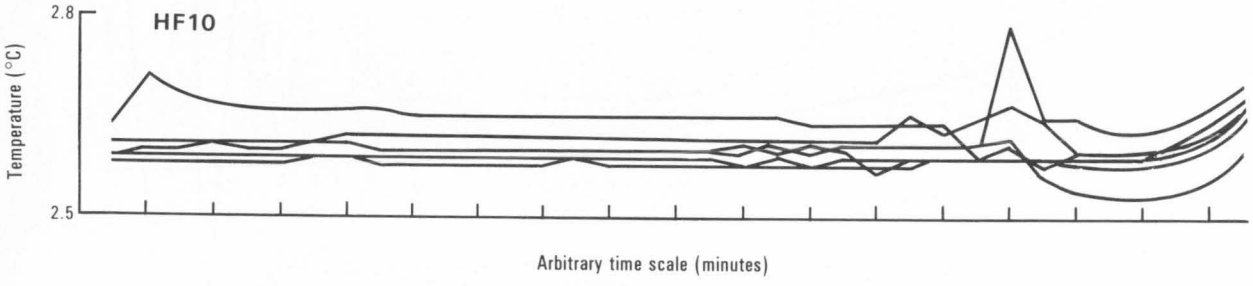

Figure 57: Plot of temperature against time for each thermistor at heatflow station HF10.

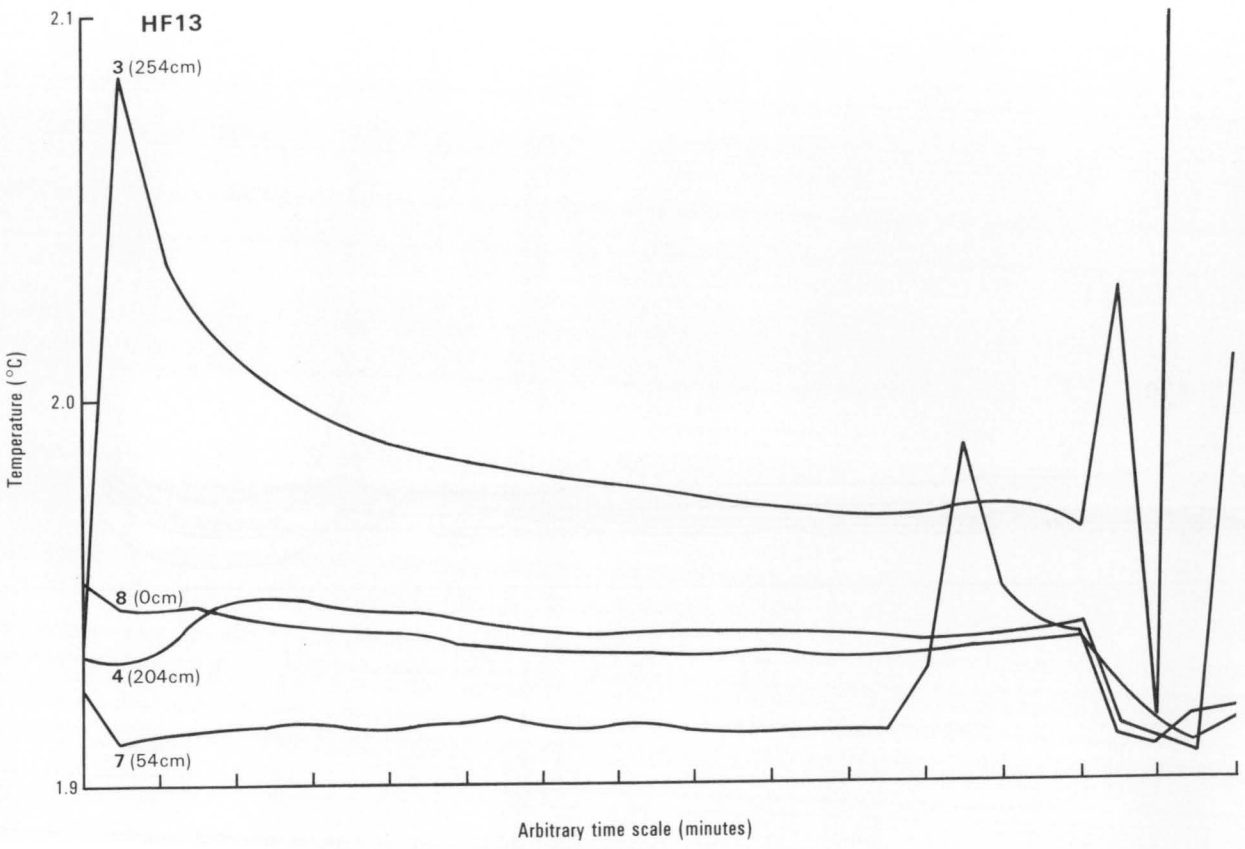

Figure 58: Plot of temperature against time for each thermistor at heatflow station HF13.

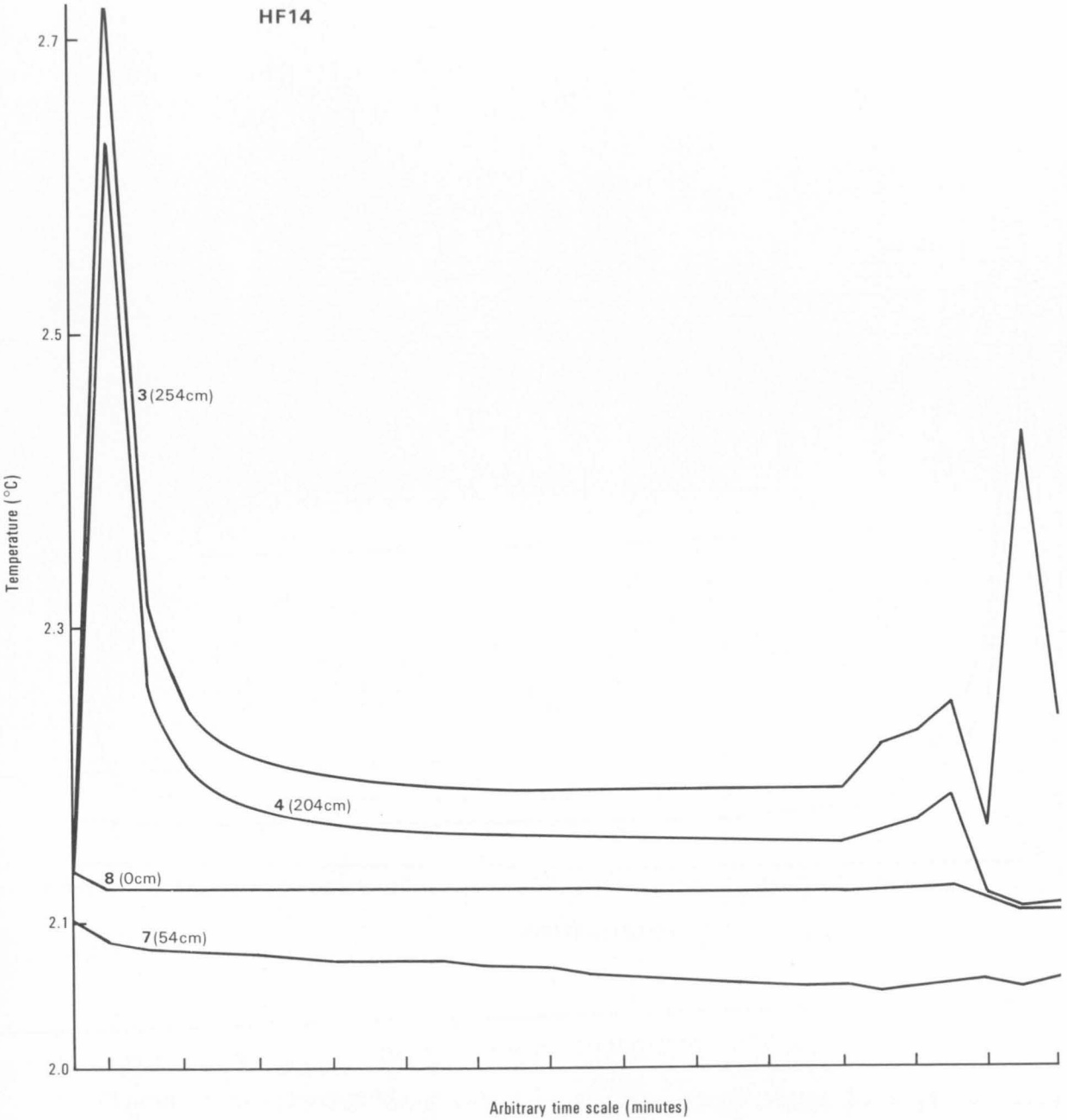

Figure 59: Plot of temperature against time for each thermistor at heatflow station HF14.

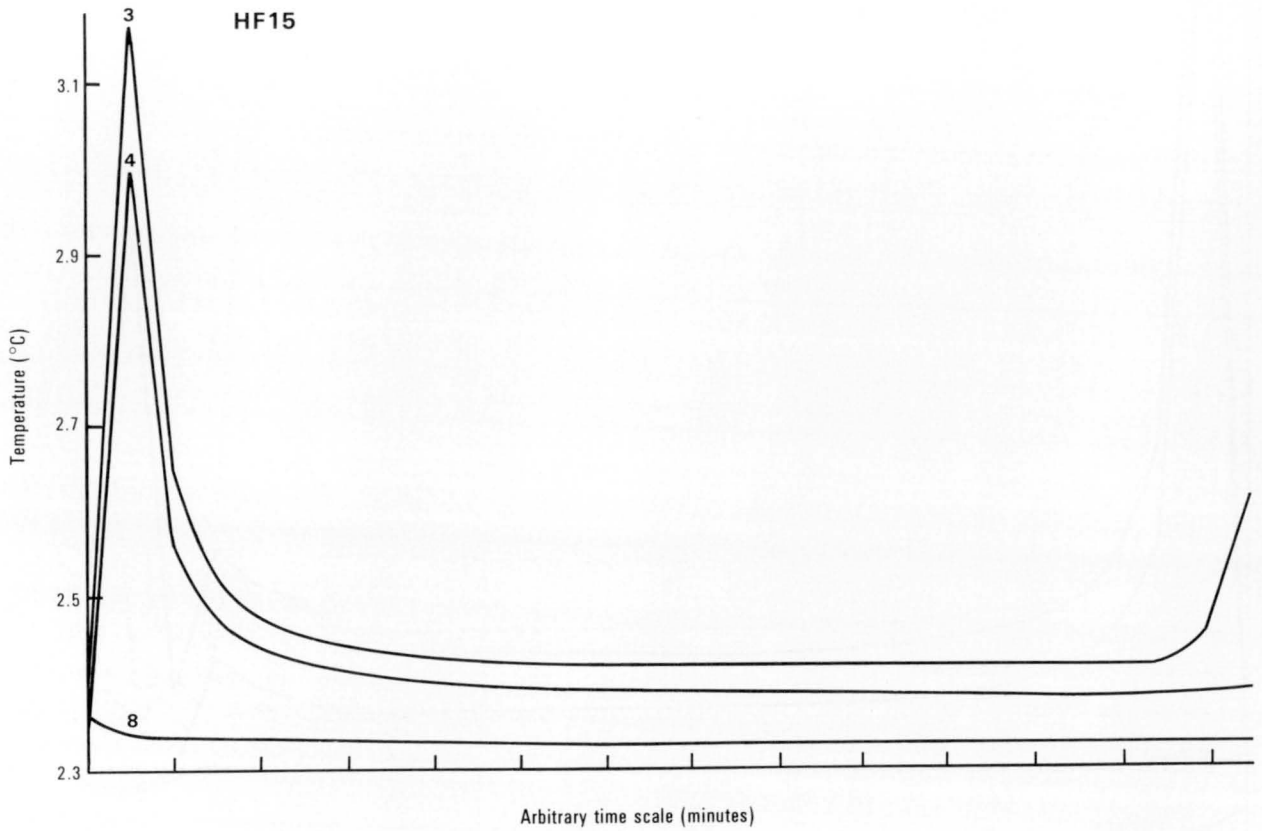

Figure 60: Plot of temperature against time for each thermistor at heatflow station HF15.

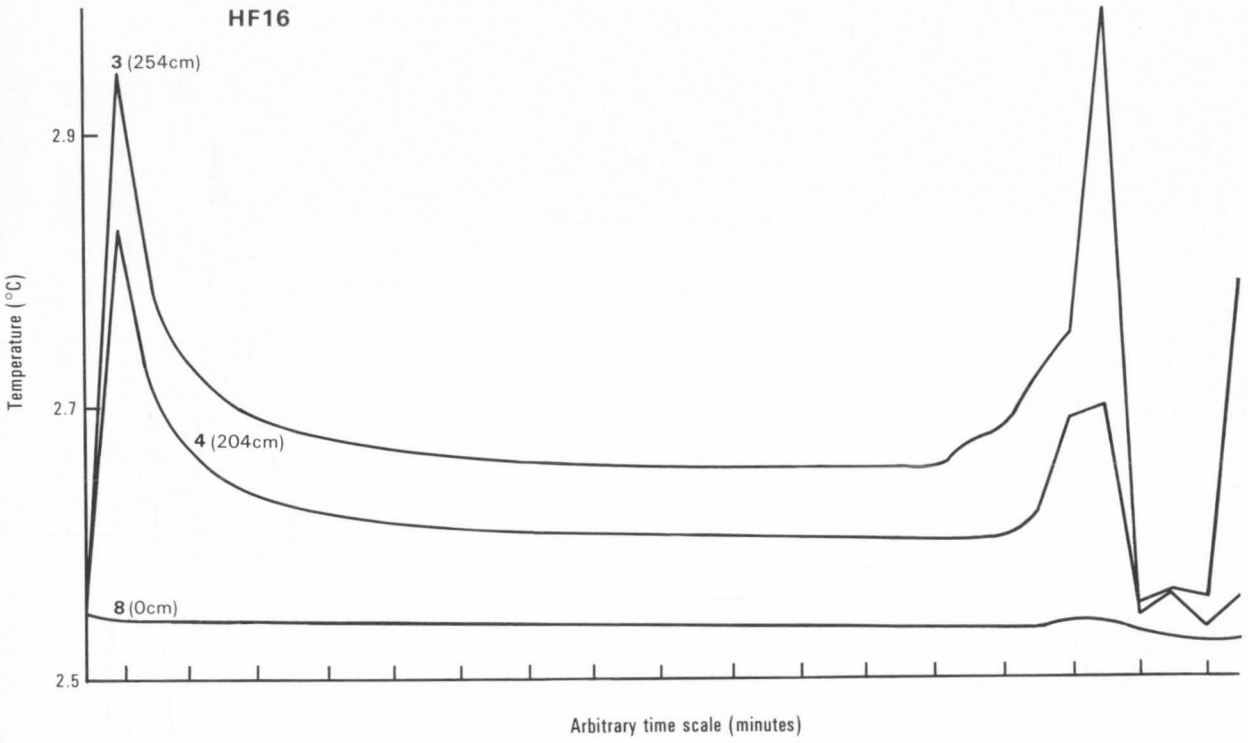

Figure 61: Plot of temperature against time for each thermistor at heatflow station HF16.

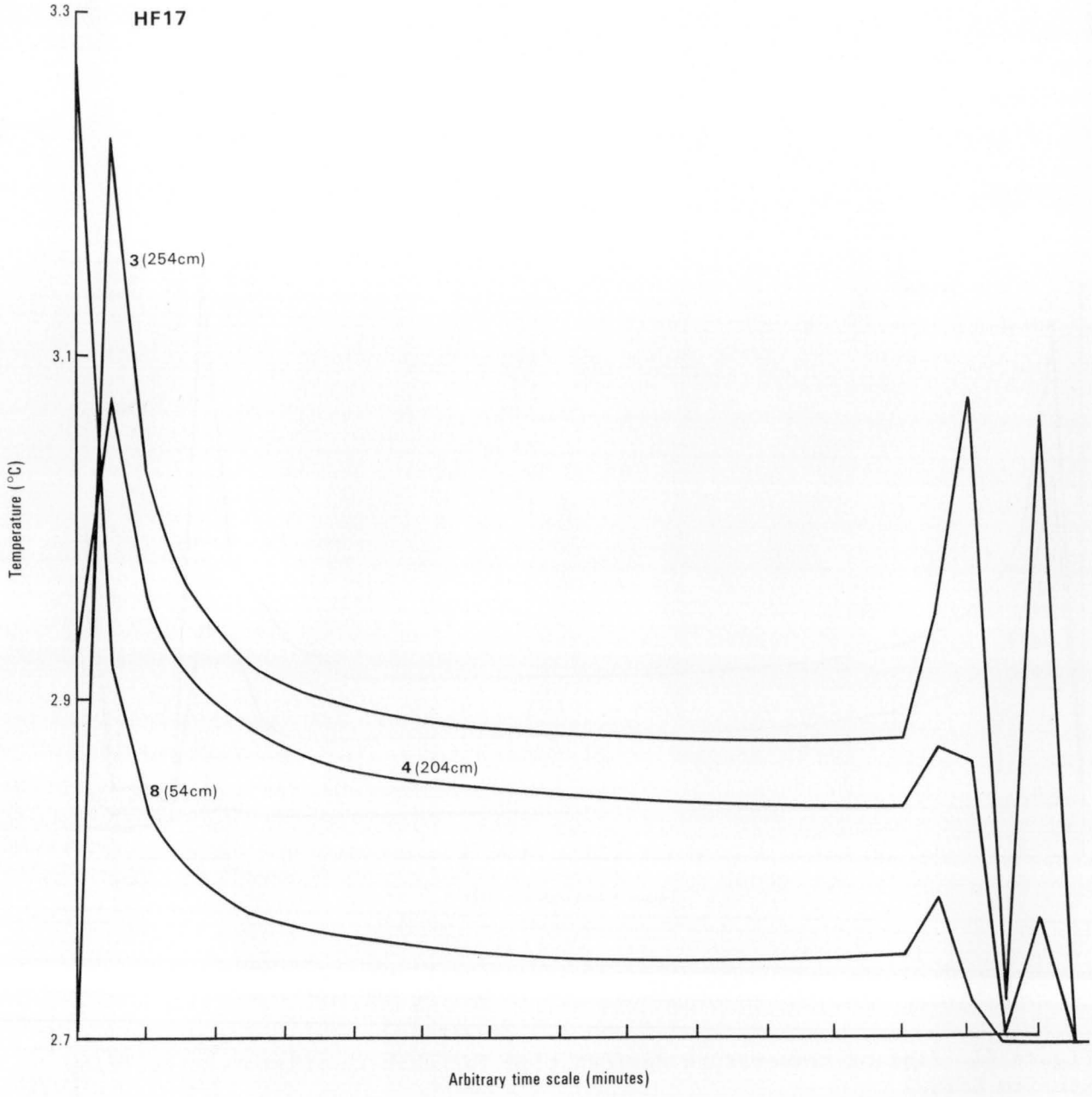

Figure 62: Plot of temperature against time for each thermistor at heatflow station HF17.

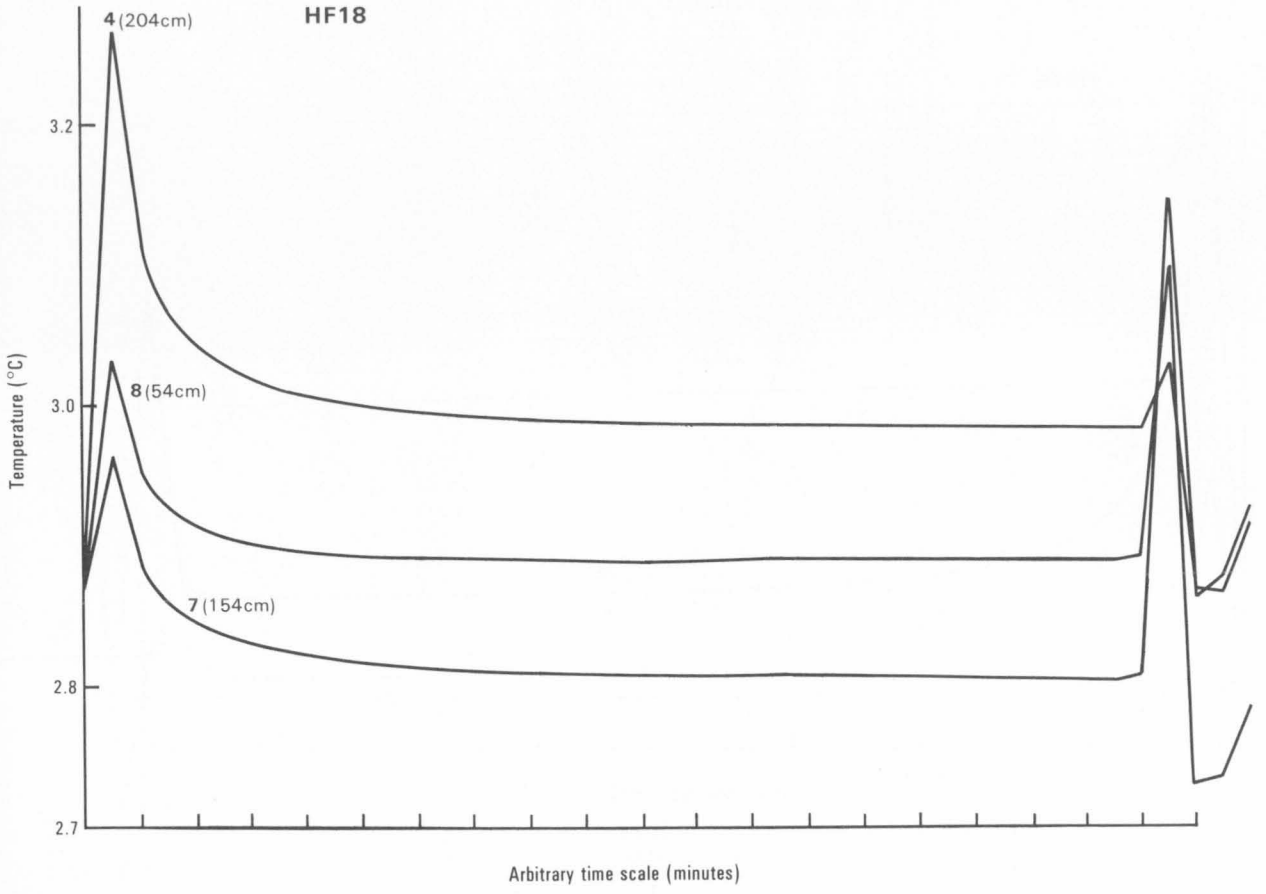

Figure 63: Plot of temperature against time for each thermistor at heatflow station HF18.

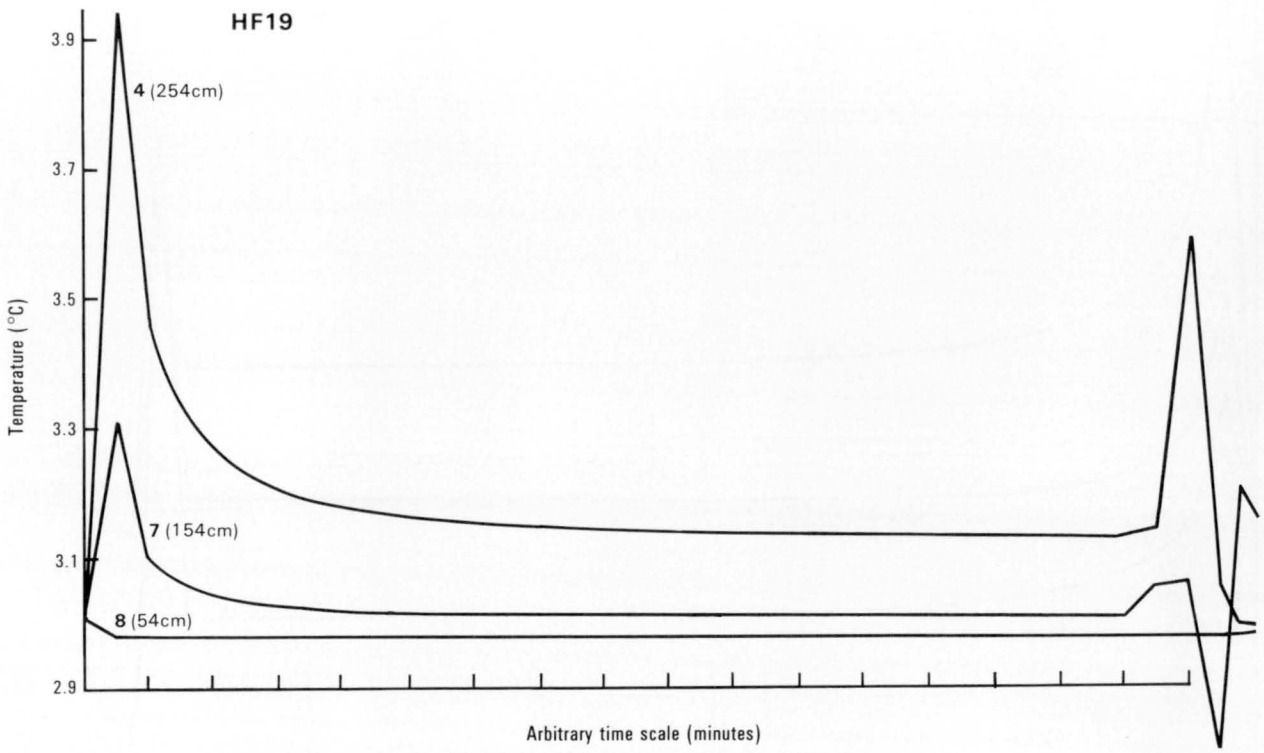

Figure 64: Plot of temperature against time for each thermistor at heatflow station HF19.

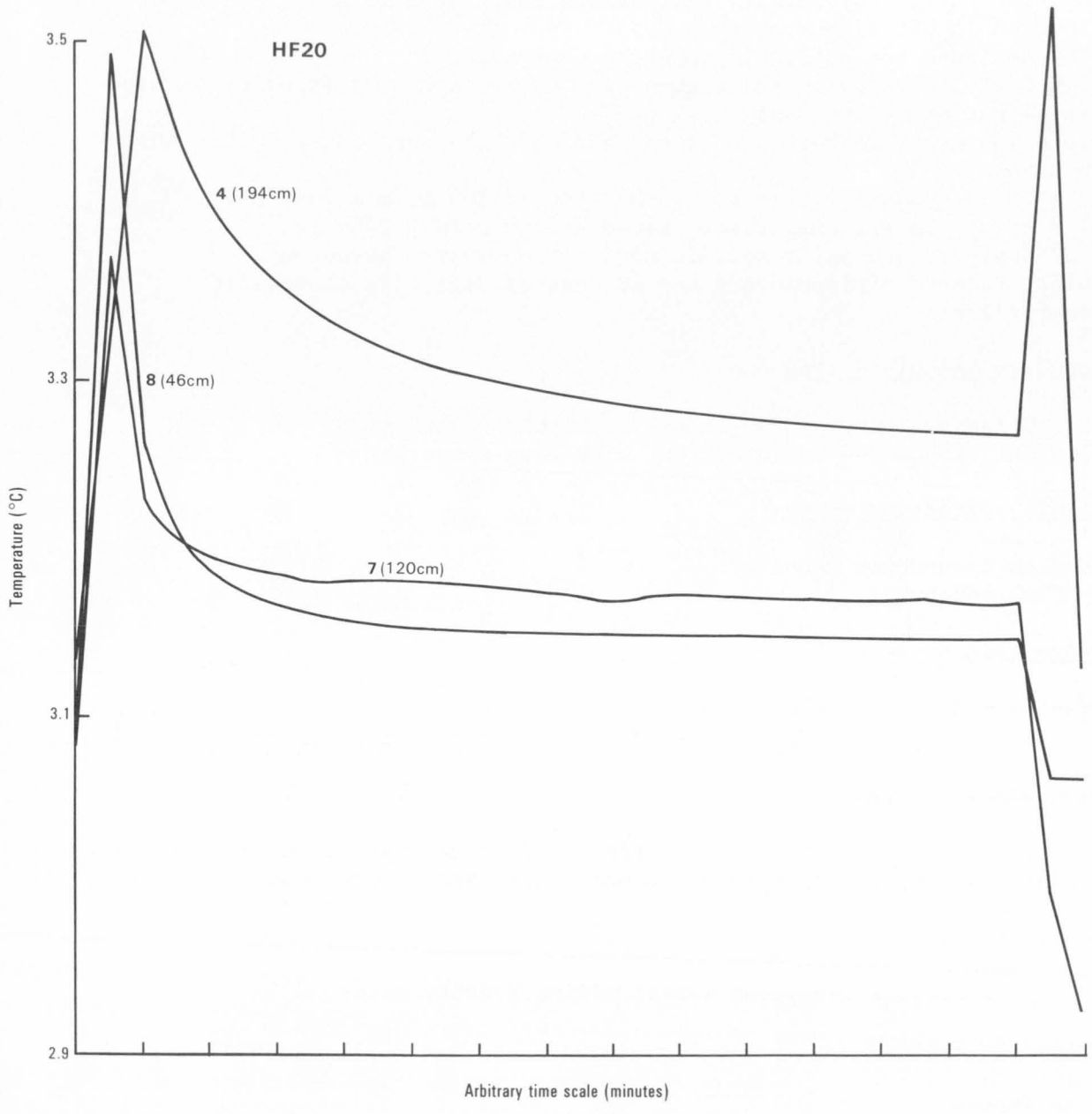

Figure 65: Plot of temperature against time for each thermistor at heatflow station HF20.

APPENDIX K: Equipment utilised

GEOPHYSICAL

Primary Seismic System

- 2400 m Teledyne hydrophone streamer with 48 x 50 m groups
- Syntron RCL-2 individually addressable cable levellers
- 1600 cu in GSI airgun array
- BMR designed and built airgun array controller
- 3 x BOLT 1500C 500 cu in airguns with wave-shape kits (single gun used when airgun array is down)
- Teledyne gun signature phones and gun depth sensors and I/O SS-8 shot sensors
- 3 x Price A-300 compressors, each rated at 300 scfm @ 2000 psi
- 1 x Price AGM W-2 compressor, rated at 200 scfm @ 2000 psi
- BMR-designed and built seismic acquisition system based on Hewlett-Packard minicomputers and 48-channel digitally controlled preamp/filters

Secondary Seismic System

- 2 x Teledyne 28420 single-channel hydrophone streamers
- 1 x BOLT 1500C 100 cu in airgun, with wave-shape kit

Seismic Refraction System

- Reftek-6 sonobuoy receiver
- Reftek sonobuoys

Bathymetric Systems

- Raytheon deep-sea echo-sounder; 2 kW maximum output at 3.5 kHz
- Raytheon deep-sea echo-sounder; 2 kW maximum output at 12 kHz

Magnetometer System

- 2 x Geometrics G801/803 proton precession magnetometers; may be used a standard single-sensor cable or in horizontal gradiometer configuration

Gravity Meter System

- 1 x Bodenseewerk Geosystem KSS-31 marine gravity meter

Navigation Systems

Prime System

- Magnavox MX1107RS dual channel satellite receiver
- Magnavox MX610D dual axis sonar doppler speed log
- Arma-Brown SGB-1000 gyro-compass

Secondary System

- Magnavox MX1142 single channel satellite receiver
- Raytheon DSN450 dual-axis sonar doppler speed log
- Robertson gyro-compass

GPS Navigation System

- 1 x Magnavox T-Set GPS navigator

Radio Navigation

- DECCA HIFIX-6

Data Acquisition System

- data acquisition system built around Hewlett-Packard 2113 E-Series minicomputer, with tape drives, disc drives, 12" and 36" plotters, line printers, and interactive terminals

Heat-flow Equipment

- 1 x Nichiyu Giken Kogyo NTS-11AU thermal gradient probe
- needle-type thermal conductivity measuring equipment

GEOLOGICAL

- 1 x deep-sea geological winch containing 10000 m of 18 mm wire
- 1 x hydrographic winch containing 4000 m of 6 mm wire
- piston or gravity corers; maximum barrel length 10 m
- chain dredges

APPENDIX L: DAS channels recorded

The following is a list of the channel allocations for the non-seismic data for the Southern Margin 1 and 2 cruises.

Main Data

The main data is saved on magnetic tape every 60 seconds in blocks of 128 X 6 floating point words.

1 - Clock (Survey and Day Number)
2 - Acquisition time (GMT) from computer clock
3 - Master clock time at acquisition
4 - Latitude, best estimate (Radians)
5 - Longitude, best estimate (Radians)
6 - Speed, best estimate (knots)
7 - Heading, best estimate (degrees)
8 - Magnetometer no. 1
9 - Magnetometer no. 2
10 - Depth no. 1; 3.5 kHz
11 - Depth no. 2; 12 kHz
12 - F/A Magnavox sonar-doppler (3920.4 counts/nm)
13 - P/S Magnavox sonar-doppler (3920.4 counts/nm)
14 - F/A Raytheon sonar-doppler (193.5 counts/nm)
15 - P/S Raytheon sonar-doppler (193.5 counts/nm)
16 - Paddle log (approx 7000 counts/nm)
17 - not used
18 - Instrument room gyro (degrees)
19 - Bridge gyro (degrees)
20 - not used
21 - not used
22 - not used
23 - not used
24 - not used
25 - Hifix Fine A (centilanes)
26 - Hifix Fine B (centilanes)
27 - Hifix Fine C (centilanes)
28 - Hifix Coarse A (centilanes)
29 - Hifix Coarse B (centilanes)
30 - Hifix Coarse C (centilanes)
31 - 40 - not used
41 - T-SET ; number of satellites and satellite numbers in constellation
42 - T-SET time (GMT seconds)
43 - T-SET Dilution of Precision
44 - T-SET latitude (radians)
45 - T-SET longitude (radians)
46 - T-SET height above geoid (metres)
47 - T-SET speed (knots X 10)
48 - T-SET course (degrees X 10)
49 - T-SET frequency bias
50 - T-SET GMT (.HHMMSS)
51 - Latitude, calc. from Magnavox Sonar-Doppler & A.B. gyro
52 - Longitude, calc. from Magnavox Sonar-Doppler & A.B. gyro
53 - Speed calc. from Magnavox sonar doppler & A.B. gyro

54 - Course calc. from Magnavox sonar doppler & A. B. gyro
55 - Latitude, calc. from Raytheon Sonar-Doppler & bridge gyro
56 - Longitude, calc. from Raytheon Sonar-Doppler & bridge gyro
57 - Speed calc. from Raytheon sonar doppler & bridge gyro
58 - Course calc. from Raytheon sonar doppler & bridge gyro
59 - Latitude, calc. from paddle log & A.B. gyro
60 - Longitude, calc. from paddle log & A.B. gyro
61 - Speed calc. from paddle log
62 - Course calc. from A.B. gyro
63 - Latitude, radio-nav
64 - Longitude, radio-nav
65 - Speed from radio-nav
66 - Course from radio-nav
67 - GMT from Magnavox MX1107 sat nav (secs)
68 - Dead Reckoned Time from MX1107 (secs)
69 - Latitude (radians) MX1107
70 - Longitude (radians) MX1107
71 - Speed (knots) MX1107
72 - Heading (degrees) MX1107
73 - GMT from Magnavox MX1142 sat nav
74 - Dead Reckoned Time from MX1142
75 - Latitude (radians) MX1142
76 - Longitude (radians) MX1142
77 - Speed (knots) MX1142
78 - Heading (degrees) MX1142
79 - Gravity (mGal * 100)
80 - ACX (m/s/s * 10000)
81 - ACY (m/s/s * 10000)
82 - Sea state (N/A)
83 - AGRF magnetic anomaly no. 1
84 - AGRF magnetic anomaly no. 2
85 - Magnetics difference (gradiometer)

The T-SET channel 41, which holds the number and numbers of the satellites in the current constellation, has data packed as follows. The units of the value in the channel gives the number of satellites and the remainder gives a bit representation of the satellite number. For example; 1602 would imply 2 satellites (the units) leaving 160 which indicates satellites 5 and 7 (bits 5 and 7 on).

Transit Satellite Fixes

The transit satellite fix information from both the MX1107 and the MX1142 are saved, in blocks of 20 floating point words, when it becomes available. The data from each navigator is in a similar format, each being identified by the first word.

1 - 1107 or 1142
2 - Day number (1107) or dat2 (1142)
3 - GMT
4 - Latitude (radians)
5 - Longitude(radians)
6 - Used Flag (0 = not used; 1 = used)
7 - Elevation (degrees)
8 - Iterations

9 - Doppler counts
10 - Distance from DR (naut miles)
11 - Direction from DR (degrees)
12 - Satellite number
13 - Antenna height (metres)
14 - 20 - Doppler spread flags (1107 only)

The raw satellite data from the MX1107 transit satellite receiver is saved every 2 minutes during each satellite pass as a block of 600 single words. These data are saved in the Magnavox 702 emulation mode. The first 4 words in each block (2 floating point words) identify the block, 702, and the start time of the block.

DATE DUE

[illegible]		

RAECO

R 88/21457 Cat. No. 8521527

9 780644 087193